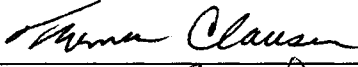
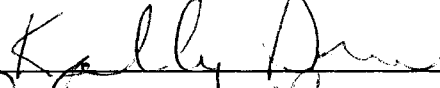




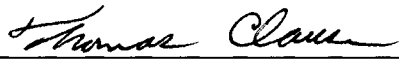
**CULTURABILITY, TEMPORAL CHANGE, PHYLOGENETIC ANALYSIS,  
AND YIELD OF MICROBIAL COMMUNITIES IN A SUBARCTIC LAKE –  
HARDING LAKE**

**By**

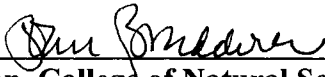
**Xiaoming Zhao**

**RECOMMENDED:**

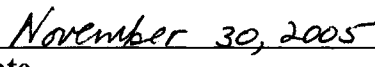
  
\_\_\_\_\_  
  
\_\_\_\_\_  
  
\_\_\_\_\_  
  
\_\_\_\_\_  
**Advisory Committee Chair**

  
\_\_\_\_\_  
**Chair, Department of Chemistry and Biochemistry**

**APPROVED:**

  
\_\_\_\_\_  
**Dean, College of Natural Science and Mathematics**

  
\_\_\_\_\_  
**Dean of Graduate School**

  
\_\_\_\_\_  
**Date**



**CULTURABILITY, TEMPORAL CHANGE, PHYLOGENETIC ANALYSIS,  
AND YIELD OF BACTERIAL COMMUNITIES IN A SUBARCTIC LAKE –  
HARDING LAKE**

**A  
THESIS**

**Presented to the Faculty  
of the University of Alaska Fairbanks**

**in Partial Fulfillment of the Requirements  
for the Degree of**

**DOCTOR OF PHILOSOPHY**

**By**

**Xiaoming Zhao, M.S.**

**Fairbanks, Alaska**

**December 2005**

UMI Number: 3206056

Copyright 2006 by  
Zhao, Xiaoming

All rights reserved.

### INFORMATION TO USERS

The quality of this reproduction is dependent upon the quality of the copy submitted. Broken or indistinct print, colored or poor quality illustrations and photographs, print bleed-through, substandard margins, and improper alignment can adversely affect reproduction.

In the unlikely event that the author did not send a complete manuscript and there are missing pages, these will be noted. Also, if unauthorized copyright material had to be removed, a note will indicate the deletion.

**UMI**<sup>®</sup>

---

UMI Microform 3206056

Copyright 2006 by ProQuest Information and Learning Company.

All rights reserved. This microform edition is protected against unauthorized copying under Title 17, United States Code.

ProQuest Information and Learning Company  
300 North Zeeb Road  
P.O. Box 1346  
Ann Arbor, MI 48106-1346

## ABSTRACT

Heterotrophic bacteria, adapted to small concentrations of substrate, are a main component of the microbial flywheel. However, understandings of their activity, isolation, genetics, and nutrition are restricted to the large, easily isolated and culturable bacteria. By using the dilution culture method, apparent culturabilities could approach 10% in unamended lake water and were inversely proportional to the number of cells inoculated from mixed species in a natural environment from Harding Lake. Substrate additions could not improve bacterial culturability in the dilution cultures.

Comparative sequence analyses of 16S rDNA genes showed that all bacterial species have similar lengths in the phylogenetic tree, suggesting similar evolution rates. These indicated close relationships among the six bacterial divisions:  $\alpha$ -proteobacteria,  $\beta$ -proteobacteria,  $\gamma$ -proteobacteria, cytophaga/flexibacter/bacteriodes, acidobacteria, and cyanobacteria. Possible reasons include that metabolic enzymes of these bacteria were modified to adapt to low temperatures from tropical temperatures in arctic areas at the same time. These findings may provide insight into the recent evolution of the bacteria in near polar freshwater. Moreover, a high abundance of  $\alpha$ -proteobacteria and  $\gamma$ -proteobacteria was found in Harding Lake, suggesting high growth rates of these bacteria in the freshwater region. This is consistent with a rapid continuous shift in the distribution of dominant species observed in Harding Lake, according to the TRFLP, DGGE, and flow cytometry data.

Our results also suggested that input of dissolved organic matter derived from terrestrial plants and soils, introduction of terrestrial bacteria, and bacteria themselves led to the bacterial species shifts associated with the seasonal change.

Bacterial growth yield is used to measure this carbon conversion efficiency. However, bacterial growth yields have been seriously underestimated in previous studies. Our *in situ* values for bacterial growth yield from an amino acid mix were actually closer to 50% and 70% in active systems by using a modified, sensitive and accurate method and increased with the increase of temperature between 1°C and 6°C.

**TABLE OF CONTENTS**

	Page
Signature Page	i
Title Page	ii
Abstract	iii
Table of Contents	v
List of Figures	viii
List of Tables	x
List of Appendices	xi
List of Abbreviations	xiii
Acknowledgements	xiv
<b>Chapter 1: Introduction</b>	<b>1</b>
<b>Chapter 2: Materials and Methods</b>	<b>9</b>
2.1 Sample collections	9
2.2 Bacterial processing and extraction of DNA from dilution cultures	9
2.3 Bacterial processing from whole lake water	10
2.4 Bacterial processing and extraction of DNA of lake water with freeze-and-thaw	10
2.5 Extraction of DNA from whole lake water	10
2.6 TRFLP	12
2.7 DGGE	13

	Page
2.8 Culturability's determination	14
2.9 Clone construction and screening	16
2.10 Yield measurements	18
2.11 Flow cytometry	19
2.12 Fluorescence microscopy	19
<b>Chapter 3: Results</b>	<b>21</b>
3.1 Bacterial culturabilities	21
3.2 Bacterial species changes	29
3.3 Bacterioplankton seasonal properties	32
3.4 Effect of temperature on cell yield	34
<b>Chapter 4: Discussion</b>	<b>35</b>
4.1 Bacterial culturabilities	35
4.2 Bacterial species changes	39
4.3 Effect of temperature on bacterial growth yield	43
4.4 Bacterioplankton seasonal properties and multi-substrate use	44
4.5 Experimental bias and future work	46
<b>Chapter 5: Conclusions</b>	<b>49</b>



**References**

51

**Appendices**

61

## LIST OF FIGURES

	Page
Figure 1.1. Microbial flywheel with bacteria as a chief component in the recycling of mineral nutrients for continued aquatic productivity.	1
Figure 1.2. Cytoarchitectural model of nutrient kinetics.	3
Figure 1.3. Location of Harding Lake in Alaska.	7
Figure 3.1. Fluorescence images of Harding Lake bacteria stained with DAPI.	21
Figure 3.2. Culturability changes with different inoculum sizes.	22
Figure 3.3. Phylogenetics and TRFLP of 16S rDNA of Harding Lake bacteria (Oct. 2004).	25
Figure 3.4. TRFLP of Harding Lake bacteria and similarity value comparisons.	26
Figure 3.5. DGGEs of three seasons and phylogenetic analysis of dominant species.	27
Figure 3.6. Flow cytometry profiles of DNA and biomass of Harding Lake bacteria over three seasons in 2001.	28
Figure 3.7. Bacterial genomic DNA and amplified 16S rDNA from the whole Lake water.	30
Figure 3.8. Fragments of the amplified human wild type p53 gene and mutant DNA.	31
Figure 3.9. Annual cycle of Harding Lake.	33
Figure 3.10. The reciprocal of yield to reciprocal of absolute temperature.	34
Figure A.1. Cytoarchitectural model of nutrient kinetics.	94
Figure A.2. Monod (A and C) and affinity (B and D) plots of leucine uptake from Resurrection Bay seawater at a 10-m depth in Thumb Cove during June.	95

Figure A.3. Uptake of [ $^{14}\text{C}$ ]leucine by “ <i>M. arcticus</i> ” in the presence of glutamate.	96
Figure A.4. Kinetics of alanine uptake by “ <i>M. arcticus</i> ” to 10 $\mu\text{g/liter}$ .	97
Figure D.1. Thermal cycling conditions for PCR amplification.	115

**LIST OF TABLES**

	Page
Table 3.1. Top BLAST Matches of 16S rDNA sequences from 13 bacterial isolate sequences.	23
Table 3.2. Bacterial species from two sets of extinction cultures untreated and treated with glucose and amino acid mix respectively.	28
Table A.1. Nomenclature.	98
Table A.2. Specific affinities for bacterioplankton in Gulf of Alaska coastal water.	99
Table A.3. Effect of cosubstrates and inhibitors on amino acid uptake by <i>Marinobacter arcticus</i> .	100
Table A.4. Proportional change in kinetic parameters for whole cells by quantitative change in isolated cytoarchitectural properties calculated as an effectiveness factor <sup>a</sup> .	101
Table D.1. Reaction Volumes and Final Concentrations of the PCR Components.	114

## LIST OF APPENDICES

	Page
Appendix A: The Experimental and Theoretical Bases of Specific Affinity, a Cytoarchitecture-Based Formulation of Nutrient Collection to Supersede the Michaelis-Menten Paradigm of Microbial Kinetics	61
Appendix B: The Effect of Temperature on Nutrient Limited Cell Yield	111
Appendix C: Annual Dynamic of Microbial Processes in a Near-arctic Lake	112
Appendix D: PCR Protocol with Qiagen PCR Core Systems	114
Appendix E: Purification of Genomic DNA from Bacteria with Qiagen Tissue Kit	116
Appendix F: Purification of PCR Products with Amicon Microcon-PCR Centrifugal Filter Devices	118
Appendix G: DGGE Protocol with the Dcode™ System and Model 475 Gradient Delivery System	119
Appendix H: DNA Gel Purification Protocol with Bio-Rad Quantum Prep™ ‘N Squeeze DNA Gel Extraction Spin Columns	129
Appendix I: pGEM-T Easy Vector Multiple Cloning Sequences	130
Appendix J: pGEM-T Easy Vector Map and Sequence Reference Points	131
Appendix K: Protocol for Ligations Using the pGEM®-T Easy Vectors	132
Appendix L: Protocol for Transformation Using pGEM®-T Easy Vector Ligation Reactions	133

Appendix M: Plasmid Purification with Promega Vac-Man Laboratory Vacuum Manifold and Wizard Plus Minipreps DNA Purification System	135
Appendix N: Protocol for Culturability Experiment 1	137
Appendix O: Protocol for Culturability Experiment 2	140
Appendix P: Protocol for Culturability Experiment 3 with Species Distribution	143
Appendix Q: ABI Internal DNA Standard GeneScan TAMRA 2500 and GeneScan ROX 2500	147
Appendix R: The Image from ABI 373XL DNA Sequencer	148
Appendix S: Flow Cytometry Cytographs of Positive Dilution Culture	149
Appendix T: Electropherograms of the 5' T-RFLP of <i>Msp</i> I-digested bacterial 16S rDNAs from Positive Dilution Cultures	150
Appendix U: The Quantification of Some Purified Recombinant Plasmid DNA by NanoDrop ND-1000 Spectrophotometer	151
Appendix V: ABI 3100 Genetic Analyzer Sequencing of Uncultured Bacterium Clone KM94	152

**LIST OF ABBREVIATIONS**

TRFLP Terminal Restriction Fragment Length Polymorphism

DGGE Denaturing Gradient Gel Electrophoresis

## ACKNOWLEDGEMENTS

I am grateful to my advisory committee members, Dr. Don Button, Dr. Thomas Clausen, Dr. John Keller, and Dr. Kelly Drew for their direction of my research and dissertation. I am especially grateful to my major advisor Dr. Don Button for his patience and his scientific guidance.

I would like to thank my wife Dr. Huiwen Zhao and my son Ran Zhao for their smiles, encouragement, and love. I would like to thank my parents, my parents-in-law, my older brother, my younger sister, and my uncle for their continual support and taking care of my son.

I would like to thank Garret Perney, Doug Macintosh, and Elizabeth Gustafson for helping me collect samples, and data. I would like to thank Betsy Roberson for offering the annual cycle of Harding Lake data. I would like to thank Dr. Peter Gay, Dr. Lee Taylor, and the Core lab for technical assistance.

I am grateful to the Department of Chemistry and Biochemistry, the College of Natural Science and Mathematics, and the Graduate School at UAF. I would like to thank Sheila Chapin, Emily Reiter, and Marlys Schneider, for what they have done for me.

I would like to thank Carrie Aldrich and other tutors at the Writing Center for helping me with my dissertation.



## Chapter 1

### Introduction

Heterotrophic aquatic bacteria, adapted to small concentrations of substrate, are a main component of a microbial “flywheel” system (Strom 2000), which provides a capacity to supply minerals on demand while most of its members cycle in biomass over time (Figure 1.1). These bacteria grow on low concentrations of nutrients (Button et al. 1993) and constitute about half the biomass in aquatic systems (Button et al. 1996).

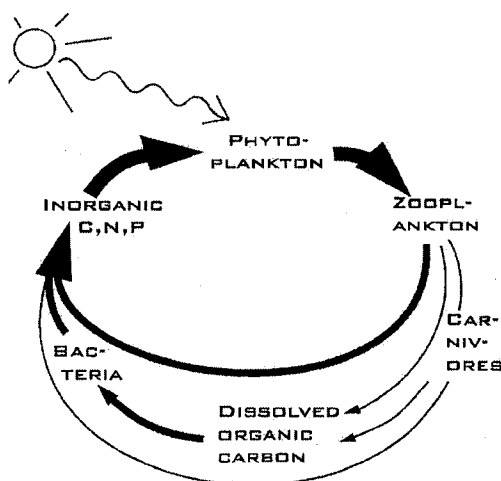


Figure 1.1. Microbial flywheel with bacteria as a chief component in the recycling of mineral nutrients for continued aquatic productivity. While most members cycle in biomass over time, bacteria cycle in activity providing a ready capacity to supply minerals on demand.

They take advantage of the organic matter from primary production to sustain food webs in aquatic systems (Williams 1981, and Taylor 1982), supply minerals to phytoplankton from spent biochemicals, contribute to secondary productivity (Ducklow et al. 1995), affect system depuration (Yoch 2002, and Scarrett et al. 2000), reduce the concentrations of dissolved organics, produce major quantities of carbon dioxide in the atmosphere, and help control other climate affecting greenhouse gases. Because of their importance, the heterotrophic bacteria in marine systems have been well studied during past decades. However, bacteria in subarctic freshwater systems have been studied far less than those in marine environments.

One of the problems of understanding this mostly unseen but major component of our environment is difficulty in isolation (Watanabe et al. 2000). While heterotrophic bacteria often dominate planktonic biomass in natural aquatic systems (Button et al. 1996), their culturabilities are often lower than 0.25% (Amann et al. 1995). However, the viable count method and autoradiography have shown that 39% to 76% of the bacteria are metabolically active (Karner et al. 1997, and Kogure et al. 1979). Understanding of activity, isolation, genetics, and nutrition was obtained only for the large, easily isolated and culturable bacteria. Smaller bacteria, which utilize very dilute nutrients from the environment, cannot be isolated and cultured. They are resistant to the classic isolation and cultivation method, which allows bacteria to grow on agar with added substrate. Therefore, improvement of their culturability has been a challenging issue, encouraging scientists to search for more efficient isolation and cultivation approaches.

One approach for addressing this problem is the dilution culture method. Dilution culture, produced by diluting an ambient population to near extinction, is an efficient method for growing the typical oligobacteria in natural aquatic systems. Its advantage is that abundant bacteria are selected rather than nutrient-tolerant ones. Moreover, it removes and minimizes the influence of phytoplankton and grazers on bacterial communities. This method has been successfully applied to the investigation of seawater in theory and laboratory (Button 2001, Button et al. 1993, and Quang et al. 1998). The novel isolation technique, along with kinetic theory based on organism cytoarchitecture (Button et al. 2004, and Figure 1.2), offers the possibility for advancement.

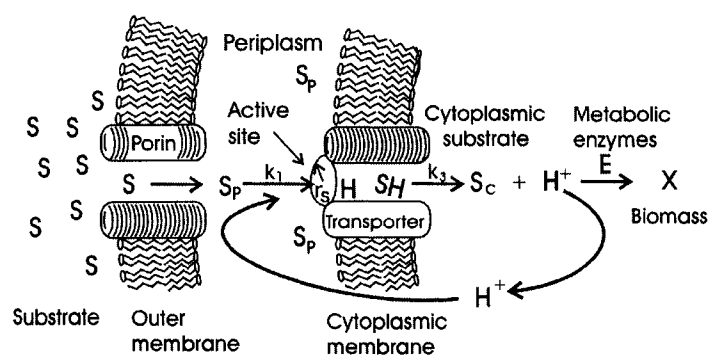


Figure 1.2. Cytoarchitectural model of nutrient kinetics. Ambient nutrient  $S$  diffuses through a porin to periplasmic concentration ( $[S_p]$ ), where it combines with a proton-empowered permease having an active-site radius of  $r_s$ . Transport produces  $[S_c]$  that generates both a proton potential and a concentration-driving force that facilitates substrate flow through an enzyme sequence (E) to produce cell material (X) (Button et al. 2004).

In addition, sequencing from bulk environmental and medium DNA has provided important phylogenetic and metabolic information. A study reports that the members of the SAR11 group are a deeply branching cluster of  $\alpha$ -proteobacteria. These bacteria have less than 82% sequence similarity to cultivated members of  $\alpha$ -proteobacteria (by comparison of 16S rDNA clone sequences), and are inhibited by addition of the supplement of dilute proteose peptone in preserved cell cultures (Rappe et al. 2002). Diversity studies using culture-independent methods have strongly expanded the knowledge about the phylogenetic composition of freshwater bacterial communities. In a comparative study, Zwart et al. (2002) have identified 34 putative phylogenetic clusters of bacteria, which contain typical freshwater inhabitants. These putative freshwater bacteria consist of  $\alpha$ ,  $\beta$ , and  $\gamma$ -proteobacteria, cytophaga-flavobacterium-bacteroides, cyanobacteria, actinobacteria, and verrucomicrobia. The 16S rDNA clone sequencing and phylogenetic analyses have also revealed that bacterial species shift with the seasonal change in organic matter source in an Arctic lake (Crump et al. 2003). All of these studies have used random cloning of 16S rDNA genes. These phylogenetic studies have helped us to have a better understanding of nutrient and other condition's influence on bacterial communities in aquatic systems and laboratory media.

Aquatic systems contain a variety of dissolved organic matter derived from terrestrial plants, soils, phytoplankton, aquatic plants, algae and other aquatic species (Thurman 1985). Together with phytoplankton blooms (Riemann et al. 2001),

temperature (HaldaAlija et al. 2001), and signal molecules (Bruns et al. 2002), the availability of nutrients changes the bacterioplankton community composition in these aquatic systems (Hofle 1992). For example, the results from lake and creek field studies reveal that the nutrient composition of lakes and creeks affects the structure of the bacterial community (Crump et al. 2003, HaldaAlija et al. 2001, and Lindstrom 2000). However, investigators have never employed multiple approaches together to detect and confirm seasonal bacterioplankton composition change in near Arctic freshwaters. Moreover, little is known about the relationship of bacterial species composition shifts and dissolved organic compounds in the freshwaters of these regions.

However, molecular ecological approaches, such as terminal restriction fragment length polymorphism (TRFLP) (Scala et al. 2001, and Dunbar et al. 2001), denaturing gradient gel electrophoresis (DGGE) (Muyzer et al. 1993), fluorescence microscopy (Button and Robertson 1993), and recombinant DNA techniques (Dunbar et al. 1999), allow us to investigate the dependence of microbial populations on seasonal changes and dissolved organic matter source, in spite of the limitations of culturability and species identification.

Lastly, bacterial growth yield is used to measure carbon conversion efficiency, which is defined as the ratio of bacterial production to substrate consumption. In natural aquatic systems, bacteria use large amounts of dissolved organic matter to gain their own biomass for maintaining activities, and then release carbon dioxide to the air (Figure 1.2).

The carbon conversion efficiency value can be estimated from carbon conversion in organics labeled with an isotope and unlabeled organics. Bacterial growth efficiency values reported for estuarine and coastal waters were 18 and 11%, respectively (Ram et al. 2003). A bacterial growth yield of 16% was determined in a shallow and temperate lake in Austria (Reitner et al. 1999). de Giorgio et al. (1997) reported that bacterial growth efficiency values in most freshwater and marine systems are generally below 40%, most often between 5% and 30%. Most studies give a lower bacterial yield value. In fact, carbon conversion efficiency of 60% for bacterial growth is an accepted value (Calow 1977). Therefore, bacterial secondary productivity and bacterial growth yield may have been seriously underestimated in previous studies. The conversion efficiency of the substrate cannot accurately reflect carbon and energy flow in aquatic systems and may be incompatible with availability of nutrient resources on complex natural substrates. This results in a problem with understanding nutrient flux in natural environments. However, Button and his colleagues (1981) report a sensitive and accurate method for measuring bacterial kinetics based on the rate of  $^{14}\text{CO}_2$  recovery from radioactive dissolved substrate. This offers the possibility for accurately measuring the bacterial growth yield in near Arctic lakes.

Harding Lake lies in Interior Alaska, next to the Tanana River and the Tanana-Yukon uplands (Figure 1.3). A meltwater runoff, estimated to be 20 - 30% of the annual snowfall, is measured each year, and there is an obvious flow during snowmelt or heavy rainfall in spring and late summer (LaPerriere 2003).

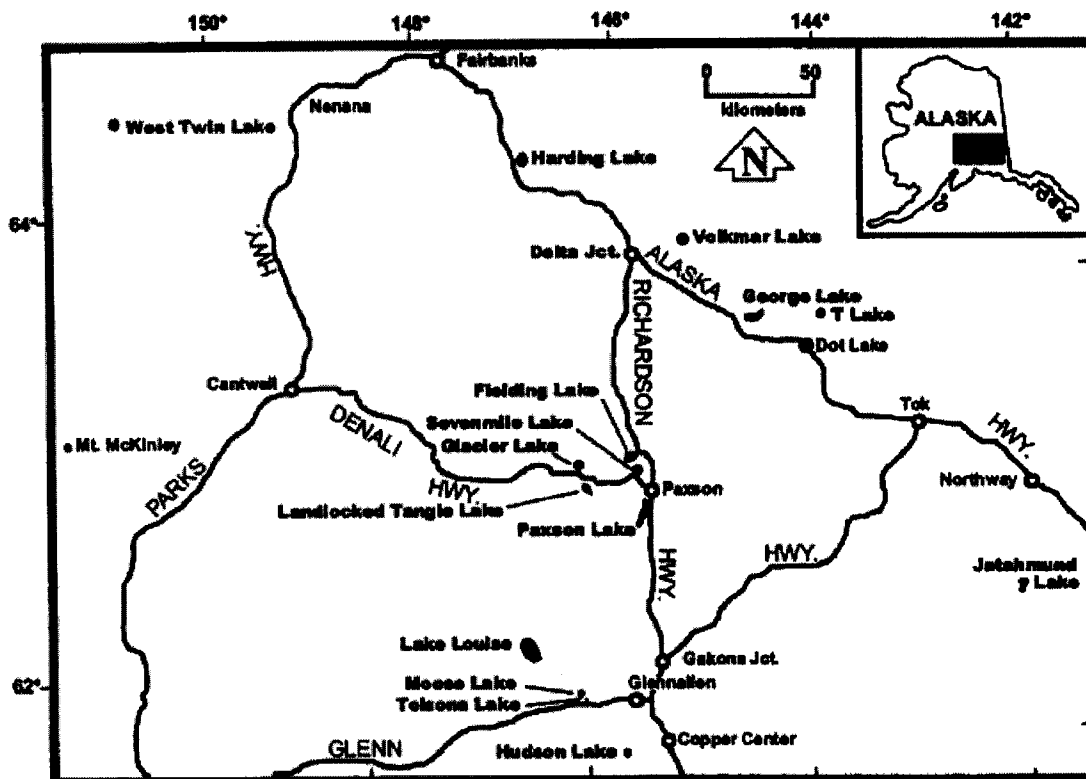


Figure 1.3. Location of Harding Lake in Alaska (LaPerriere 2003).

To answer questions of how the bacterial populations in high-latitude lakes change with seasonal change while maintaining a rather constant biomass, whether the dilution culture procedure developed for isolation and culturability determinations in seawater can be applied to near Arctic lakes, and what the accurate carbon conversion efficiency is in near Arctic freshwater systems, we used multiple approaches, such as TRFLP, DGGE, flow cytometry, epifluorescence microscopy, cloning, and isotopic techniques. The results suggest an interaction between bacterial populations and

dissolved organic matter in Harding Lake, a subarctic lake. The dilution culture protocol used for seawater isolation and culturability determinations worked for freshwater as well, and apparent culturabilities could approach 10% in unamended lake water. Based on our method, our *in situ* values for cell yield from an amino acid mix were actually closer to 50% and 70% in active systems with linear kinetics. These results will lead to improved knowledge for exploring subarctic freshwater environments, which are among the least understood and perhaps therefore not optimally managed.

In this dissertation, the materials and the methods are introduced in Chapter 2. The experimental results are described in Chapter 3. A discussion of these results is found in Chapter 4. Appendix A is a published paper (Button et al. 2004), in which I was a co-author. In this paper, a theory for solute uptake by whole cells was derived with a focus on the ability of oligobacteria to sequester nutrients. It provided a general relationship that was used to obtain the kinetic constants for *in situ* marine populations in the presence of naturally occurring substrates. Calculations demonstrated that most oligobacteria in the environment must use multiple substrates simultaneously to attain sufficient energy and material for growth, a requirement consistent with communities largely comprising few species. I have contributed by detecting the number of dominant species in samples using terminal restriction fragment length polymorphism. In this dissertation, detailed protocols, supplementary data, and two abstracts of manuscript drafts resulting from our work are also presented in appendixes.



## **Chapter 2**

### **Materials and Methods**

#### **2.1 Sample collections**

Harding Lake lies in Interior Alaska, next to the Tanana River and the Tanana-Yukon uplands. Different volumes of samples were collected in April 2002, May 2002 and October 2004 for the culturability experiment of dilution cultures; in winter (January), spring (April) and summer (June) 2001 for species change detection of whole lake waters; and in April 2004 and February 2005 for bacterial yield measurement. All February, April, and May samples were taken from 1.5 meter below the upper surface of the ice while the June and October samples were from the lake water surface. Within 3 hours samples were trucked to the lab at the University of Alaska Fairbanks in 10-liter or 20-liter carboys in an insulated box.

#### **2.2 Bacterial processing and extraction of DNA from dilution cultures**

Nine milliliters of positive dilution cultures scored by flow cytometry and epifluorescence microscopy were put into Beckman Ultra-clear centrifuge tubes. They were spun in the Beckman L8 70M ultracentrifuge at 36,000 rpm (SW40 rotor) at 4°C for 60 minutes. The supernatants were discarded and the pellets were retained in the test tubes. The bacterial cells were lysed by freeze-thaw cycles (-20°C for 5 minutes, room temperature for 5 minutes, 5 cycles). The lysed cells (16S rDNA templates) were immediately frozen and stored at - 20°C until further processing in the laboratory.

### **2.3 Bacterial processing from whole lake water**

Ten liters of whole lake waters collected in winter, spring and summer in 2001 were filtered through GF/C filters (Whatman) to remove larger particles and phytoplankton respectively. Subsequently, bacteria were concentrated onto 0.2-micron polyester filters (Poretics). The filters were cut into small pieces, about 0.5cm x 0.5cm. They were immediately frozen and stored at - 20°C until further processing in the laboratory.

### **2.4 Bacterial processing and extraction of DNA of lake water with freeze-and-thaw**

Nine milliliters of the whole lake waters from 2004 October were put into Beckman Ultra-clear centrifuge tubes. They were spun in the Beckman L8 70M ultracentrifuge at 36,000 rpm (SW40 rotor) at 4°C for 60 minutes. The supernatants were discarded and the pellets were retained in the test tubes. The bacterial cells were lysed by freeze-thaw cycles (-20°C for 5 minutes, room temperature for 5 minutes, 5 cycles). The lysed cells (16S rDNA templates) were immediately frozen and stored at - 20°C until further processing in the laboratory.

### **2.5 Extraction of DNA from whole lake water**

DNA was extracted from the whole lake waters collected in 2001 according to the DNeasy Tissue Kit manual (Qiagen). The samples were lysed in 200 µl of lysis buffer (20 mM Tris-Cl, pH 8.0, 2 mM EDTA, 1.2% Triton X-100, 20 mg/ml lysozyme). Twenty

micro liters of Proteinase K (20 mg/ml), 4  $\mu$ l of RNase A (100 mg/ml), and 200  $\mu$ l of Buffer AL were added into the samples. They were mixed immediately by vortexing and incubated at 70°C for 10 minutes. 200  $\mu$ l of 100% ethanol was added to each sample and mixed thoroughly by vortexing. The mixtures were pipetted into the DNeasy mini column sitting in a 2-ml collection to bind the DNA and were then centrifuged at 8000 rpm (6000 g) in an Eppendorf 5414 centrifuge for 1 minute. The filtrates and the collection tubes were discarded. The DNeasy mini columns were placed in new 2-ml collection tubes followed by adding 500  $\mu$ l of Buffer AW1 and centrifuged for 1 minute at 8000 rpm (6000 g). The filtrates and the collection tubes were discarded. The DNeasy mini columns were placed in new 2-ml collection tubes followed by adding 500  $\mu$ l of Buffer AW2 and centrifuged for 3 minutes at 14,000 rpm to dry the DNeasy membranes. The flow-through and the collection tubes were discarded. The DNeasy mini columns were placed in clean 1.5-ml microcentrifuge test tubes followed by adding 100  $\mu$ l of Buffer AE directly onto the DNeasy membranes and incubated at room temperature for 1 minute. The columns were centrifuged for 1 minute at 8000 rpm (6000 g) to elute them, followed by adding 100  $\mu$ l of Buffer AE directly onto the same DNeasy membranes to elute the DNAs. Then they were incubated at room temperature for 1 minute and centrifuged for 1 minute at 8000 rpm (6000 g) to collect the DNA filtrates. The bands of bacterial genomic DNA obtained from the whole lake waters were run on 1.0% agarose gel, stained with SYBR Green I. A photograph was taken under a transilluminator. The extracted DNA samples (16S rDNA templates) were immediately frozen and stored at -20°C until further processing in the laboratory.

## 2.6 TRFLP

16S rDNA templates from the whole lake water or positive dilution cultures were amplified with forward primer (5'-GTTTGATCCTGGCTCAG-3') fluorescently labeled with 6-FAM (6-carboxyfluorescein) and backward (5'-ACGGTTACCTTGTTACGACTT-3') (Qiagen). PCR amplification began with a 2-minute denaturation at 95°C; this was followed by 30 cycles of 95°C for 1 minute, 50°C for 1 minute, and 72°C for 1.5 minute. The final cycle was extended at 72°C for 5 min. After purification with Amicon Microcon-PCR Centrifugal Filter Devices (Millipore), DNA was digested with the restriction endonuclease *Msp* I or *Rsa* I (Promega). The digestion was carried out in a total volume of 20 µl for 4 hours at 37°C. For species change detection of the whole lake waters, 1.0 µl of the digested amplicons were mixed with 14.4 µl of formamide and 0.6 µl of an internal DNA standard (GeneScan 2500 TAMRA, Applied Biosystems). The mixtures were denatured at 95°C for 2 minutes. Electrophoresis on a polyacrylamide gel was then performed using ABI373 XL DNA sequencer. After electrophoresis, the sizes of the 5'-terminal restriction fragments and the intensities of their fluorescence emission signals were calculated and analyzed by the GeneScan 3.1 and Genotyper (Applied Biosystems). For the culturability experiment of dilution cultures, 0.6 µl of the digested amplicons were mixed with 9.5 µl of formamide and 0.6 µl of an internal DNA standard (GeneScan 2500 ROX, Applied Biosystems). The mixtures were denatured at 95°C for 2 minute. Electrophoresis on a polyacrylamide gel was then performed using ABI3100 Genetic Analyzer. After electrophoresis, the sizes of

the 5'-terminal restriction fragments and the intensities of their fluorescence emission signals were calculated and analyzed by the GeneMapper (Applied Biosystems). This permitted the comparison of TRFLP community fingerprint patterns obtained from the lake waters of the different seasons for similarities and dissimilarities. For making comparisons between TRFLP profiles from different seasons, pairwise similarity values were calculated by using Sorenson's index:  $C_s = 2j_N / (a_N + b_N)$ , where  $j$  is the number of common species in samples A and B,  $a_N$  is the number of species in sample A, and  $b_N$  is the number of species in sample B. A similarity value of 1 indicates that species profiles are identical, and a similarity value of 0 indicates that no species are shared.

## 2.7 DGGE

To test the accuracy of DGGE, the human wild type p53 gene and the mutant DNA were first amplified and then run on DGGE gel with a denaturing gradient of 25 - 65% according to the manufacture's instruction (Bio-Rad). The electrophoresis was run at 60°C for 15 h at 75 volts. The gel was stained for 20 min with 0.5 liter of H<sub>2</sub>O containing 50 µl of 10 mg/ml ethidium-bromide after electrophoresis. The DGGE gel was photographed with a Typhoon 9200. 16S rRNA gene templates from the whole lake waters were amplified with GC clamp-forward primer (5'-GC-clamp-CACAAGCGGTGGAGCATGTGG-3') and backward primer (5'-GCCCGGGAACGTATTCACCG-3') (Qiagen). A touchdown PCR was employed as follows: the annealing temperature was initially set at 66°C and was then decreased by 0.5°C every cycle until it was 56°C. Ten additional cycles were run at 56°C. Denaturing

was performed at 95°C for 1 min, and extension was performed at 72°C for 2 min. The final extension step was 5 minutes at 72°C. PCR products were loaded onto a 6.5% polyacrylamide gel in 1× buffer (40 mM Tris, 20 mM acetic acid, and 1 mM EDTA, pH 8.3) with a denaturing gradient ranging from 25 to 65%. The electrophoresis was run at 60°C for 15 h at 75 volts. The gel was stained for 20 min with 0.5 liter of H<sub>2</sub>O containing 50 µl of 10 mg/ml ethidium-bromide after electrophoresis. The DGGE gel was photographed with a Typhoon 9200. Bands in the DGGE gel of 16S rRNA fragments were excised with a razor blade. The DNA was purified and retrieved from the Quantum Prep™ ‘N Squeeze DNA Gel Extraction Spin Columns (Bio-Rad). The sequence analysis of selected clones was employed on an ABI3100 Genetic Analyzer with forward (5'-GCACAAGCGGTGGAGCATGTGG-3') and backward (5'-GCCCGGGAACGTATTCACCG-3'). The dye terminator cycle-sequencing reactions were used according to the manufacturer's guidelines. The sequences were compared with similar sequences of reference organisms by performing a BLAST search. Phylogenetic analyses were accomplished with the Mega 2.1 software.

## **2.8 Culturability's determination**

Lake surface waters were collected into 20-liter carboys in an insulated box in April 2002, May 2002 and October 2004 at Harding Lake and immediately shipped to the laboratory. Culture tubes were soaked with lake water and the growth media were prepared by collecting the lake water from the sites, filtering it with 0.2 µm polyester filters, and autoclaving it. Culture tubes were cleaned, fired, closed with caps lined with

acid-washed Teflon to reduce accumulation of organic compounds from the air, and filled with 50 ml of the autoclaved growth medium. The bacterial population counts were done with epifluorescence microscopy and corrected later with flow cytometry for more accurate evaluation. The samples were diluted to known values with the unamended growth media and the mixtures were incubated at ambient temperatures with agitation and observation over several months. Statistically, the calculated inoculum sizes were between 3.2 and 604 cells per tube with 10 tubes at each dilution level. Three sets of dilution cultures from lake waters (April 2002, May 2002, and October 2004) were incubated at 5°C, 8°C and 12°C respectively, without addition of substrate. The fourth set of dilution cultures was incubated at 12°C, with the addition of the glucose and amino acid mixtures. During incubation, the glucose and amino acid mixtures (0.5 µg glucose and amino acid/50ml culture, 1.25 µg glucose and amino acid/50ml culture, 2.5 µg/glucose and amino acid/50ml culture, and 5.0 µg/glucose and amino acid/50ml culture) were added into the cultures at day 1, day 7, day 14 and day 21 respectively. Examinations for developing population were done after 4-week incubation. When evaluated using microscopy and flow cytometry, the tubes were scored positive if there was a substantial number of bacteria ( $3.9 \times 10^4$  cells/ml). The positive cultures were subsequently processed and TRFLPs were run for determining the number of bacterial species. Growth rates were calculated from the change in cell population over time.

Culturabilities ( $V$ ) were calculated from equation (1) extended to account for ability to identify different species. It is assumed that these species  $X_i$  are distributed as a

binomial ( $N, p$ ) where  $p = 1 - \exp(-aV/N)$ ,  $a$  is the number of organisms added to each potential culture,  $Y$  is the number of species that arise, and  $N$  is the total number of species in the inoculum. The maximum likelihood estimate of  $p$  is  $p = Y/nN$  to give a maximum likelihood of  $V$  as

$$V = -N/a \ln(1 - Y/nN) \quad (1)$$

The standard deviation of  $p$  is  $se(p) = \{p(1-p)/nN\}^{1/2}$  to give the standard deviation of  $V$  as

$$se(V) = [N/a(1-p)] se(p) \quad (2)$$

The identification of bacterial species in the whole lake water of 12°C and all the positive dilution cultures were fulfilled by 16S rDNA clone construction and sequencing.

## 2.9 Clone construction and screening

PCR were performed on 50- $\mu$ l reaction mixtures (25 mM MgCl<sub>2</sub>, 10 mM each of PCR nucleotide mix, 10x reaction buffer, 5 units of thermophilic *Taq* DNA polymerase) for each DNA sample, using forward primer (5'-GTTTGATCCTGGCTCAG-3') and backward primer (5'-ACGGTTACCTTGTTACGACTT-3') (Alm et al. 1996, and Vetriani et al. 1999) [Promega]. PCR amplification began with a 2-minute denaturation at 95°C; this was followed by 30 cycles of 95°C for 1 minute, 56°C for 1 minute, and 72°C



for 2 minutes. The final cycle was extended at 72°C for 5 minutes. PCR cycles were stopped while the product concentration was still increasing exponentially. PCR products were purified with Amicon Microcon-PCR Centrifugal Filter Devices (Millipore) in accordance with the manufacturer's instructions. PCR products were ligated into the pGEM-T Easy Vector (Promega) and used to transform JM109 competent cells (Promega) in accordance with the manufacturer's instructions. The transformed cells were plated on Luria-Bertani (LB) agar plates containing 100 µg of ampicillin ml<sup>-1</sup>, 80 µg of X-Gal (5-bromo-4-chloro-3-indolyl-β-D-galactopyranoside) ml<sup>-1</sup>, and 0.5 mM IPTG (isopropyl-β-D-thiogalactopyranoside) as recommended by the manufacturer and incubated overnight at 37°C. Thirty positive colonies were picked and frozen in a LB broth with glycerol at -70°C. Recombinant plasmid DNA was purified with a Vac-Man Laboratory Vacuum Manifold and Wizard Plus Minipreps DNA Purification System (Promega) and quantified with a NanoDrop ND-1000 spectrophotometer and ND-1000 V3.1.0 software. The recombinant plasmid DNA was then sequenced according to the direction of insertion by using an ABI 3100 Genetic Analyzer (Applied Biosystems) and a BigDye terminator cycle sequencing kit (Applied Biosystems) at the Core Lab of UAF. All the sequences were compared with similar sequences of reference organisms by performing a BLAST search. The sequences were analyzed with Sequencher 4.5 and BioEdit 7.0.5.2. Phylogenetic trees were constructed by the neighbor-joining method with the CLUSTAL X software package.

## 2.10 Yield measurements

The 1°C (February 2005), 4°C (April 2004) and 6°C (May 2005) water samples were collected from Harding Lake. The samples were immediately shipped to the laboratory in insulated carboys within 3 hours of collection. Forty microliters of isotopic amino acid mixture (Amersham Bioscience, CFB 104, L-[U-<sup>14</sup>C] amino acid mixture, 1.85 MBq (U indicates uniformly labeled), totaling 50 µCi, were added to 400ml of the lake water, incubated at 1°C, 4°C and 6°C respectively, and shaken at certain intervals. Samples were preserved with 37% formalin to 3% v/v and populations stained with 50 µl of DAPI (0.5 mg/ml) in 1 ml of Triton-100 (5%) for determination using an epifluorescence microscope. At these intervals samples were filtered through 0.1 µm pore size polycarbonate filters, and the radioactivity retained determined by scintillation counter. Metabolic <sup>14</sup>CO<sub>2</sub> was determined by acidification of 50ml subsamples with 1N H<sub>2</sub>SO<sub>4</sub> to pH 3.4-3.5. The liberated <sup>14</sup>CO<sub>2</sub> was swept through and collected in a collection train containing scintillation fluid (the ratio: phenethylamine 270 ml, methanol 270 ml, toluene 461 ml, omnifluor 51 g) with a 0.5 liter/min flow of nitrogen for 30 minutes. The bacteria were filtered on the filters at the certain intervals. A water blank was run without bacteria under the same conditions as the sample above. <sup>14</sup>CO<sub>2</sub> released and labeled amino acid taken up by bacteria were collected at the different times and their radioactivities were determined by scintillation spectrometry at specified times. Cell yields were calculated from the ratio of cell material to <sup>14</sup>CO<sub>2</sub> plus filter count. These calculations assumed that the added tracer substrate does not contribute to saturation, the isotopic substrate was used with efficiency similar to that in the natural system, and that

the main metabolic products were cell material and energy for which carbon dioxide was a surrogate.

### **2.11 Flow cytometry**

Cell population, mass and DNA content were determined by flow cytometry. Samples were preserved with formaldehyde at 0.5% with refrigeration to conserve the light scatter and DAPI-DNA fluorescence properties of aquatic heterotrophic bacteria for many months without detectable change. Cell mass was from forward light scatter intensity according to the Rayleigh-Gans theory as applied to low-refractive index particles, verified by Coulter Counter sizing and corrected for bound formaldehyde. DNA was analyzed by DAPI-DNA fluorescence with under staining conditions that minimize non-specific fluorescence. Populations were taken from the values of appropriate mass and fluorescence in analyzed volumes determined by the number of internal standard fluorescent beads as determined by Coulter Counter.

### **2.12 Fluorescence microscopy**

50  $\mu$ l of the DNA-binding dye 4',6-diamidino-2-phenylindole (DAPI) (0.5 mg/ml) were added to 1ml of Triton-100 (5%) followed by filtering with 0.2 micron black filters. The filtered dye solutions (66 $\mu$ l) were added to 3 ml of the lake waters or dilution cultures. Samples or cultures were stained for 45 minutes to 1 hour and slides were made. Populations were determined by Leitz Dialux 20 EB Fluorescence

Microscope. In addition, the sizes of bacteria in Harding Lake were measured using Zeiss Laser Scanning Confocal Microscope LSM510 2.8.

## Chapter 3

### Results

#### 3.1 Bacterial culturabilities

Bacteria-containing water samples were diluted to a few bacteria and inoculated into filtered autoclaved lake water. Most of these bacteria from Harding Lake were smaller than 1  $\mu\text{m}$  in length under the scanning confocal microscope (Figure 3.1).



Figure 3.1. Fluorescence images of Harding Lake bacteria stained with DAPI. Bacteria from Harding Lake were smaller than 1  $\mu\text{m}$  under the confocal microscope. Scale bar, 1  $\mu\text{m}$ .

Dilution cultures were perpetuated for extended periods in unamended, filtered and autoclaved lake water. Therefore, the dilution culture protocol previously used for seawater isolation and culturability determinations worked for freshwater as well. About

22% of the incubated cultures were visible by flow cytometry and epifluorescence microscopy within 4 weeks. Using the dilution culture protocol, culturability was inversely proportional to the number of cells inoculated from mixed species in Harding Lake according to populations detected by epifluorescence microscopy, flow cytometry, and TRFLP (Figure 3.2).

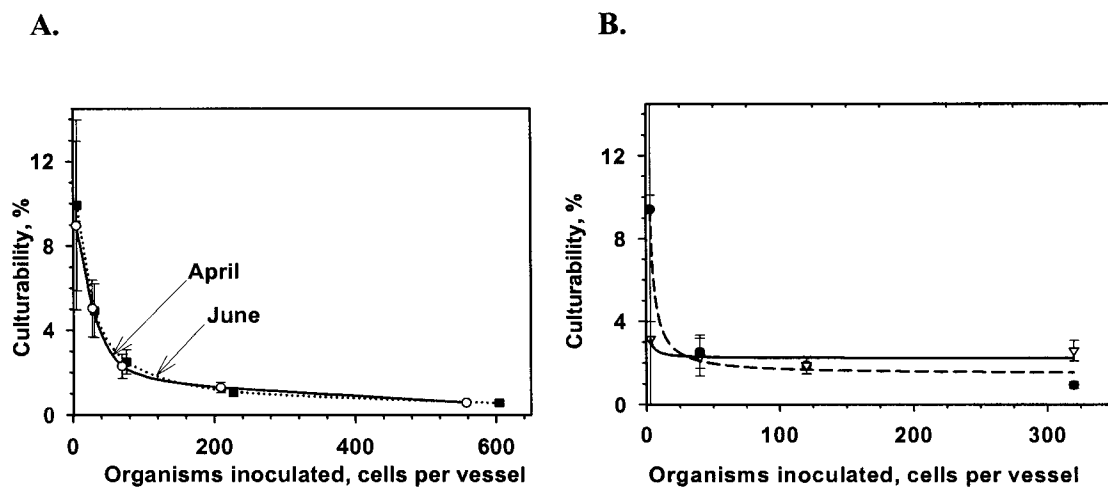


Figure 3.2. Culturability changes with different inoculum sizes. A: culturability was inversely proportional to the number of cells inoculated from mixed species in Harding Lake, without any substrate addition (April and June 2002). B: culturability was inversely proportional to the number of cells inoculated from mixed species in Harding Lake, without any substrate addition (dash line) and was not improved with the addition of glucose and the amino acid mix (solid line) (Oct. 2004).

However, apparent culturability approached 10% in unamended lake water (Figure 3.2). Further, substrate addition could not improve culturability at the small

inoculum's size (smaller than 40 cells); there was no obvious improvement of culturability with the addition of glucose and the amino acid mix (Figure 3.2A). To provide a more suitable nutritional environment, dilution cultures were dialyzed against a seawater community in dialysis bags. However, most uninoculated controls developed populations due to membrane failure.

The bacterial community structure was analyzed by using the clone library method. A clone library was constructed and 13 clones among the 30 positive colonies were sequenced from 5' end of the 16S rDNA-PCR products from the sample collected in October of 2004. The partial 16S rDNA sequences were then submitted separately to BLAST. The sequences and the species names of the 13 clones are shown in Table 3.1.

Table 3.1. Top BLAST matches of 16S rDNA sequences from 13 bacterial isolates.

Isolate number	Sequence size (bp)	Top match	Mismatches (bp)
1	592	<i>Flexibacter canadensis</i> IFO 15130	6
2	580	<i>Methylophilus methylotrophus</i>	12
3	573	<i>Polynucleobacter necessarius</i>	0
4	567	<i>Flexibacter sancti</i> IFO 16034	0
5	585	<i>Acidocella</i> sp. NO-12	0
6	584	<i>Sphingomonas capsulata</i>	0
7	567	<i>Chromatium okenii</i>	0
8	570	<i>Thiocystis gelatinosa</i>	0
9	592	<i>Azoarcus evansii</i>	6
10	590	Unidentified cyanobacterium clone LD9	0
11	585	<i>Pseudomonas syringae</i>	0
12	589	<i>Acidobacterium capsulatum</i>	0
13	560	Uncultured bacterium clone KM94	0

The cloned 16S rDNA sequences together with phylogenetic analysis suggested that the dominant bacterial composition from three seasons was mainly  $\alpha$ -proteobacteria-,

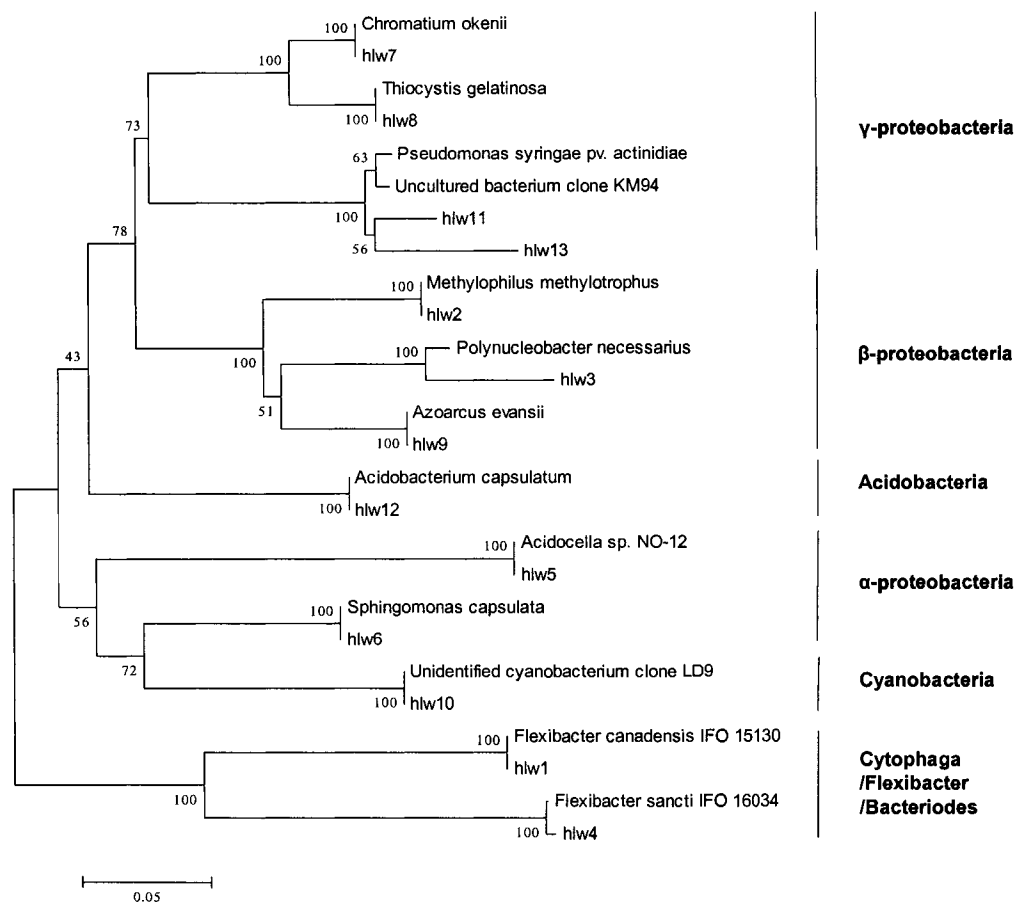
$\beta$ -proteobacteria-,  $\gamma$ -proteobacteria-, cytophaga/flexibacter/bacteriodes-, acidobacteria-, and cyanobacteria-related phlotypes. All of them have at least 90% similarity (Figure 3.3A). However, only a small number of bacterial species were found in Harding Lake in the fall of 2004 by using TRFLP (Figure 3.3B) and clone library construction (Figure 3.3A). A possible reason for detecting a small number of species is that the TRFLP method based on 16Sr DNA was not sensitive enough to quantify all the species in Harding Lake. In addition, the analysis of only 13 clones could not properly reveal the bacterial diversity in Harding Lake because there were no duplicated sequences from the cloned isolates. Similarly, the data acquired in 2001 (Figure 3.4, Figure 3.5A, and Figure 3.6) also could not indicate the bacterial diversity in Harding Lake.

The influence of substrate on the culturability of freshwater bacterioplankton was studied. Many species could not grow in the dilution cultures after a 4-week incubation. *Polynucleobacter necessarius*, *Azoarcus evansii*, *Chromatium okenii*, and *Thiocystis gelatinosa* could not grow in the dilution cultures. This differs from the species in the whole lake water (Table 3.2, and Figure 3.3A). However, *Flexibacter sancti* survived in the two cultures containing 320 cells without the addition of substrate but not in the cultures treated with glucose and the amino acid mix (Table 3.2). Glucose and the amino acid mixture at the high concentration might exert inhibitory effects on *Flexibacter sancti*.



Figure 3.3. Phylogenetics and TRFLP of 16S rDNA of Harding Lake bacteria (Oct. 2004). A. Phylogenetic analysis of thirteen 16S rDNA clones from Harding Lake indicated a lower microbial community composition and close relationships among six divisions. Divisions are indicated by vertical lines at the right of the tree. The number between each two branches indicates a confidence level supporting the relationship. Scale bar corresponds to 0.05 substitutions per nucleotide position. B. T-RFLP of *Msp* I-digested 16S rDNA from Harding Lake bacteria in the fall of 2004. X axis is DNA intensity. Y axis is DNA length, base pairs.

A.



B.

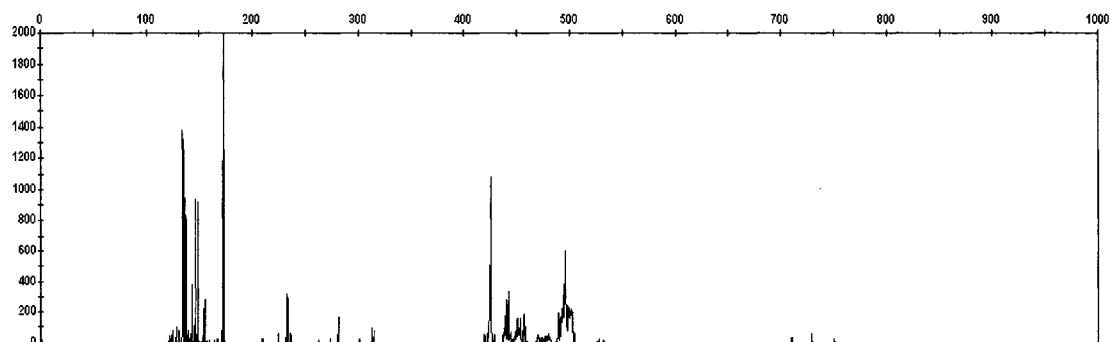
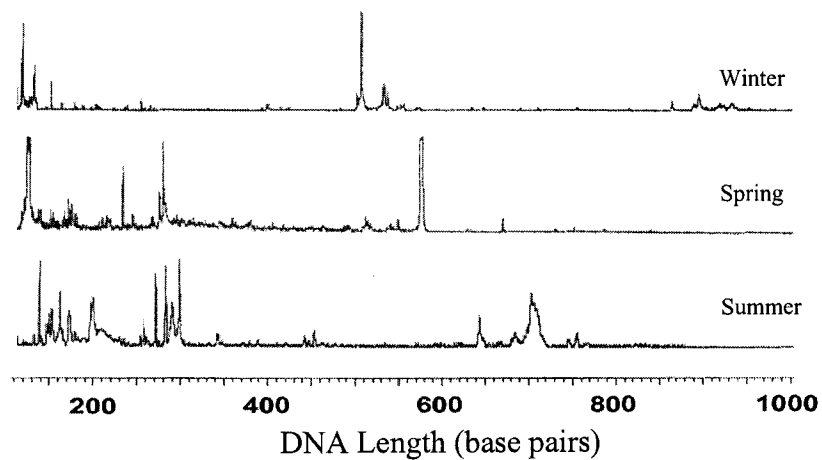
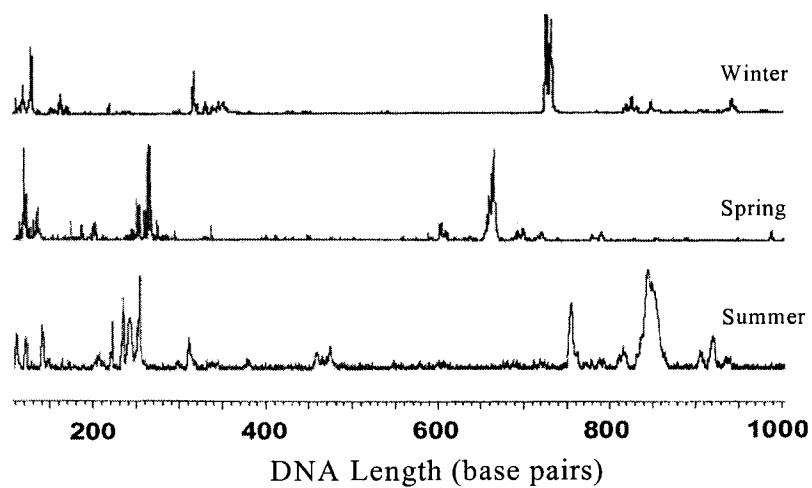


Figure 3.4. TRFLP of Harding Lake bacteria and similarity value comparisons. A: electropherograms of 5' T-RFLP of *Msp* I-digested 16S rDNA from Harding Lake bacteria with the seasonal change in 2001. B: electropherograms of 5' T-RFLP of *Rsa* I-digested 16S rDNA from Harding Lake bacteria with the seasonal change in 2001. C: similarity value comparisons from TRFLP profiles of 16S rDNA of Harding Lake bacteria of the three seasons in 2001. Win.: winter sample; Spr.: spring sample; Sum.: summer sample.

A.



B.



C.

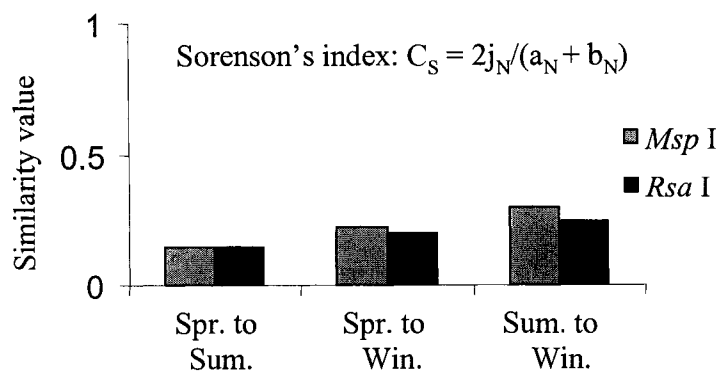
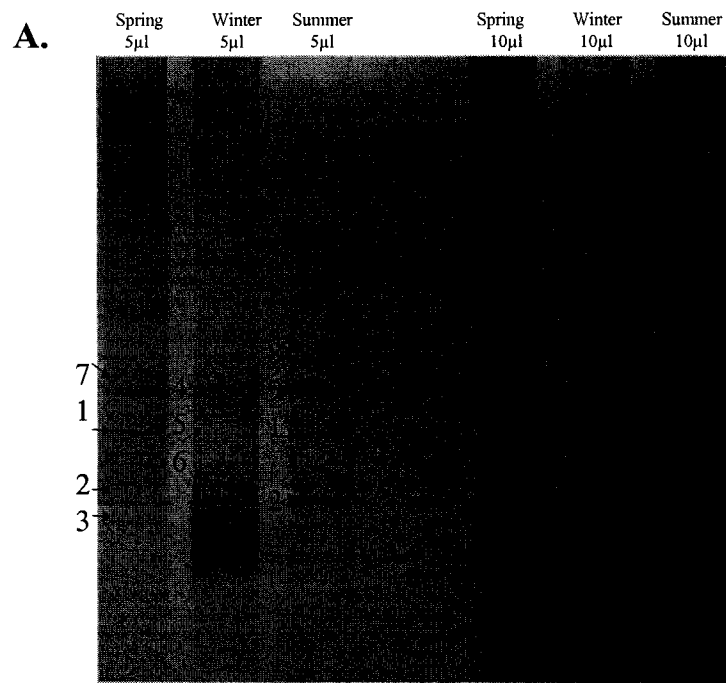
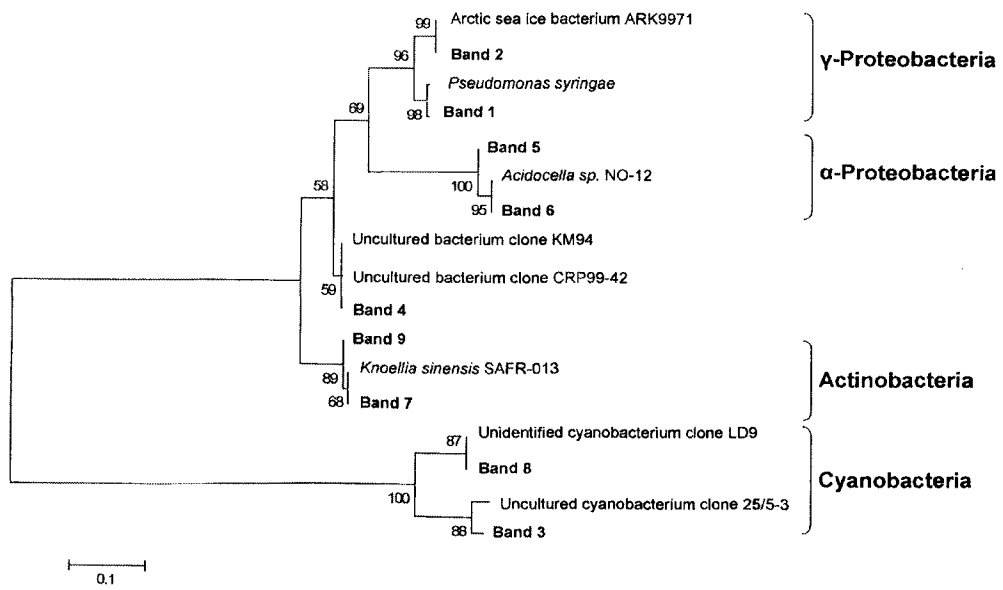


Figure 3.5. DGGEs of three seasons and phylogenetic analysis of dominant species. A: DGGE profiles of partial 16S rDNA of Harding Lake bacteria in three seasons. B: phylogenetic analysis of sequences derived from partial 16S rDNA sequences of some dominant bacteria in three seasons. Each band indicates one species and the same band number indicates the same species. Band 1, 2, 3, and 7: spring species sequenced; Band 4, 5, and 6: winter species sequenced; Band 1, 2, 3, 8, and 9: summer species sequenced. Divisions are indicated by brackets at the right of the tree. Scale bar corresponds to 0.1 substitutions per nucleotide position.



**B.**



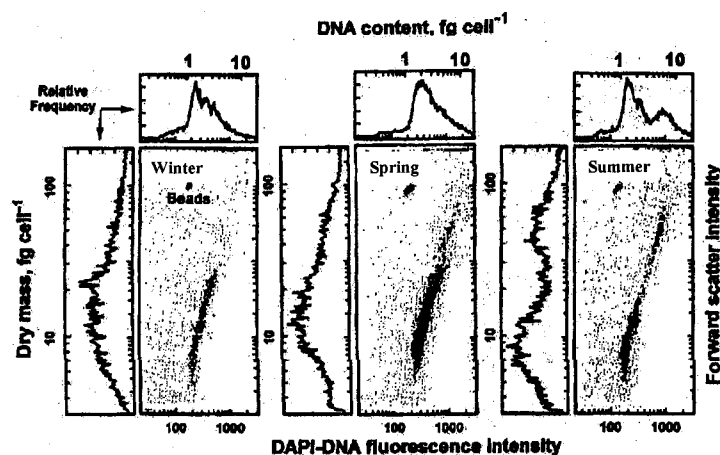


Figure 3.6. Flow cytometry profiles of DNA and biomass of Harding Lake bacteria over three seasons in 2001. The larger cells having more DNA obviously appeared in summer.

Table 3.2. Bacterial species from two sets of extinction cultures untreated and treated with glucose and amino acid mix. *Polynucleobacter necessarius*, *Azoarcus evansii*, *Chromatium okenii*, *Thiocystis gelatinosa* could not grow in the dilution cultures by comparing with the species in the whole lake water (Figure 3.3A).

With Glucose and Amino Acid Mix			Without Glucose and Amino Acid Mix		
Cells	Referring culture	Species designation	Cells	Referring culture	Species designation
			0	Y8	<i>Sphingomonas capsulata</i>
3.2	O2	Unidentified cyanobacterium clone LD9	3.2	S4	<i>Sphingomonas capsulata</i>
40	P5	<i>Acidobacterium capsulatum</i>	40	T5	<i>Acidocella</i> sp. NO-12
	P8	<i>Acidobacterium capsulatum</i>		T7	Unidentified cyanobacterium clone LD9
120	Q2	<i>Pseudomonas syringae</i> pv. <i>actinidiae</i>	120	U2	Unidentified cyanobacterium clone LD9
	Q3	<i>Pseudomonas syringae</i> pv. <i>actinidiae</i>		U3	<i>Acidobacterium capsulatum</i>
	Q4	<i>Methylophilus methylotrophus</i>			<i>Pseudomonas syringae</i> pv. <i>actinidiae</i>
	Q7	<i>Sphingomonas capsulata</i>			<i>Acidobacterium capsulatum</i>
				U4	Unidentified cyanobacterium clone LD9
320	R2	<i>Methylophilus methylotrophus</i>	320	V4	<i>Acidocella</i> sp. NO-12
	R3	<i>Methylophilus methylotrophus</i>			<i>Flexibacter sancti</i> IFO 16034
		<i>Acidobacterium capsulatum</i>			Unidentified cyanobacterium clone LD9
	R5	<i>Acidocella</i> sp. NO-12		V6	<i>Acidobacterium capsulatum</i>
	R8	<i>Acidobacterium capsulatum</i>		V7	<i>Flexibacter sancti</i> IFO 16034
					<i>Acidocella</i> sp. NO-12

### 3.2 Bacterial species changes

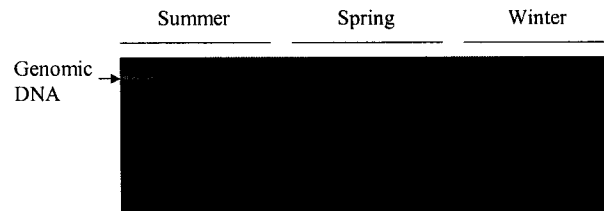
The samples collected in winter, spring, and summer in 2001 were assayed by TRFLP, DGGE, and flow cytometry. Analyses of the bacterial 16S rRNA gene fragments on TRFLP and DGGE gels, and the DNA and biomass distributions with flow cytometry were performed to examine the shifts of Harding Lake bacterial communities over the seasons. The bacterial communities appeared to be different from winter to summer.

The bacterial genomic DNAs were extracted from the samples collected in the three seasons; all bacterial genomic DNAs from these samples were detected on 1.5% agarose gel stained with 1.0  $\mu\text{g}/\mu\text{l}$  of ethidium bromide (Figure 3.7A). They were successfully amplified and their PCR bands of about 1500 base pairs were detected on 1.0% agarose gel stained with 1.0  $\mu\text{g}/\mu\text{l}$  of ethidium bromide (Figure 3.7B). These guaranteed the validity of TRFLP. TRFLP fingerprinting under nondenaturing conditions was tested with bacteria isolated from Harding Lake and digested with *Msp* I or *Rsa* I. The peaks of the TRFLP profiles of three seasons seldom coincided with each other (Figure 3.4A and B). Pair-wise similarity values were calculated to compare the three samples of the three seasons by using Sorenson's index,  $C_s = 2j_N/(a_N+b_N)$ , a pair-wise similarity coefficient. The similarity value for the winter sample to the spring sample was slightly higher than for the spring sample to the summer sample (0.22 compared to 0.17 with *Msp* I, and 0.20 compared to 0.17 with *Rsa* I) while the similarity value for the winter sample to the summer sample was highest (0.30 with *Msp* I and 0.26 with *Rsa* I). All the similarities were lower than 0.4 and differed for the different seasonal types



(Figure 3.4C). Consequently, there were obvious temporal differences in bacterial community compositions. Each peak indicates one bacterial species.

**A.**



**B.**

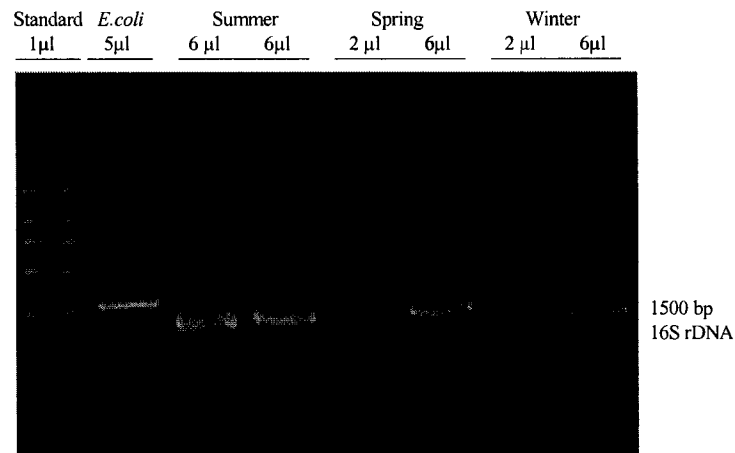


Figure 3.7. Bacterial genomic DNA and amplified 16S rDNA from the whole lake water.

A: bacterial genomic DNA obtained from the whole lake water in three seasons in 2001, stained with SYBR Green I. B: amplified 16S rDNA obtained from the whole lake bacteria in three seasons in 2001, stained with SYBR Green I.

The efficiency of DGGE was tested with wild-type and mutant p53 genes. Amplified 191 bp fragments of wild-type and mutant p53 genes were detected on 1.5% agarose gel (Figure 3.8A) and were successfully separated on 6.5% polyacrylamide gel with a denaturing gradient of 25 to 65% (Figure 3.8B).

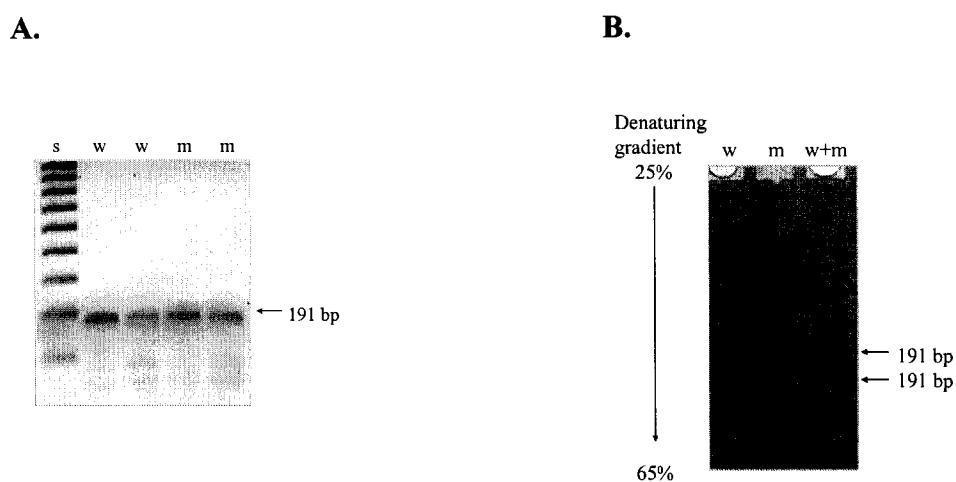


Figure 3.8. Fragments of the amplified human wild type p53 gene and mutant DNA. A: fragments of the amplified human wild type p53 gene and mutant DNA on 1.5% agarose gel stained 1.0  $\mu\text{g}/\text{ml}$  of ethidium bromide. B: fragments of the amplified human wild type p53 gene and mutant DNA on 6.5% polyacrylamide gel with a denaturing gradient of 25 to 65%, stained 1.0  $\mu\text{g}/\text{ml}$  of ethidium bromide. w: wild-type gene; m: mutant DNA; s: Bio-Rad 100 bp Texas Red Ruler; w+m: wild-type gene and mutant DNA.

The DGGE profiles of the bacterial communities for three seasons of Harding Lake water are shown in Figure 3.7A. DGGE bands were observed in the profiles. The

DGGE profiles from the three seasons were different and the DGGE bands seldom coincided by comparing the three profiles. Sequencing of 9 16S rDNA DGGE bands together with phylogenetic analysis suggested that the dominant bacterial composition from three seasons was mainly four bacterial divisions:  $\alpha$ -proteobacteria,  $\gamma$ -proteobacteria, cyanobacteria, and actinobacteria, having at least 95% similarity (Figure 3.5B).

The results of TRFLP and DGGE were also confirmed by the data acquired with flow cytometry. The results indicated that the shifts in the bacterial populations took place with the seasonal change. The change in the dominant bacterial species from winter to spring was obvious with the appearance of larger cells having more DNA in summer (Figure 3.6).

### **3.3 Bacterioplankton seasonal properties**

Large changes in bacterial properties and activities were found to correlate with the annual temperature cycle in Harding Lake (Figure 3.9). Changes quantified include productivity, bacterial population, DNA/organism, dry mass/organism, frequency of large to small DNA-content cells, the ratio of large to small mass cells, the concentration of dissolved free amino acids, the uptake rate of mixed amino acids, and specific affinity for them. The bacterial content of Harding Lake water was relatively constant over the seasons (Figure 3.9B). The nutrient uptake rate was very small (Figure 3.9G). The specific affinities for amino acids were only 20 to 1500 L/g-cells hr, winter to summer

(Figure 3.9H). Bacterial growth rate was calculated from one positive dilution culture in which 3.2 cells inoculated in 50-ml autoclaved lake water grew into  $1.6 \times 10^6$  cells per ml with 3 species after a 4-week incubation; the rate value is  $0.0045 \text{ hr}^{-1}$ .

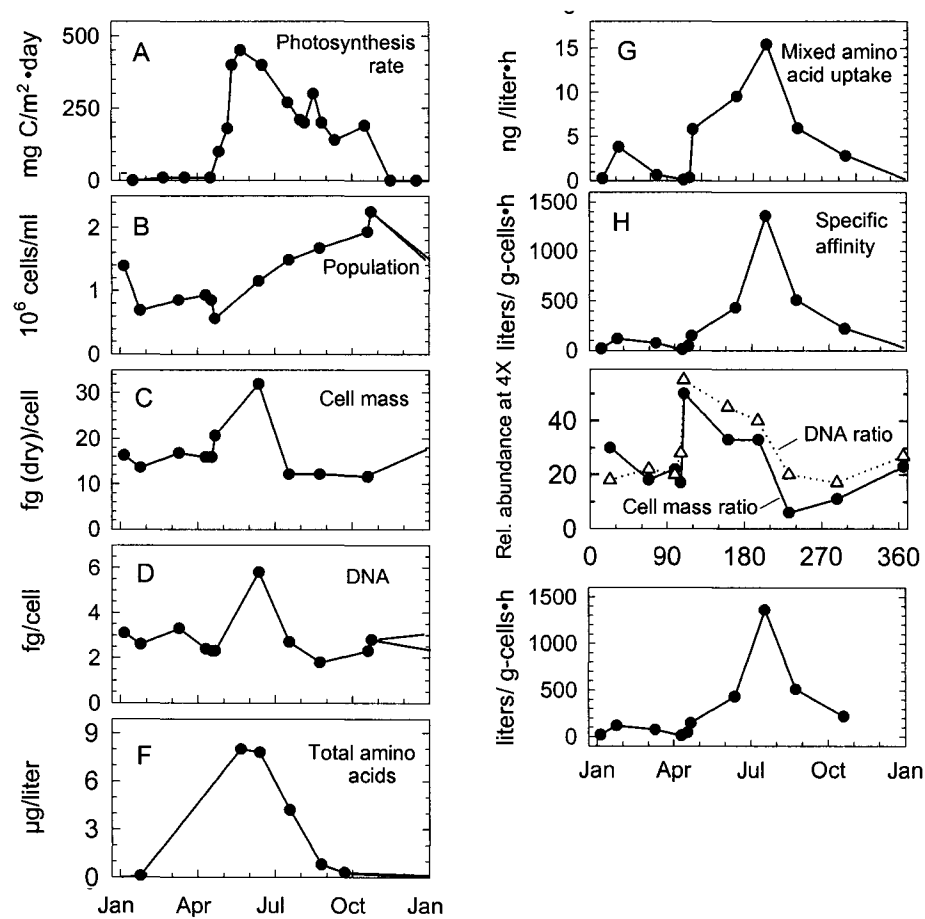


Figure 3.9. Annual cycle of Harding Lake.

### 3.4 Effect of temperature on cell yield

Samples were collected from Harding Lake near Fairbanks Alaska in insulated 10-liter carboys, and transported to the laboratory without perceptible temperature change. Incubations were begun within 3 hours in the laboratory at *in situ* temperatures. Cell yields were computed from filter and evolved CO<sub>2</sub> radioactivity. In colder temperatures, 1°C vs 6°C, incubations were extended from about 4 to 24 hours to increase sensitivity. This period is still short enough to minimize the effect of changing biomass due to growth on the rate of uptake, as supported by linear rates. As shown in Figure 3.10, there was a progressive increase in cell yield with *in situ* temperature.

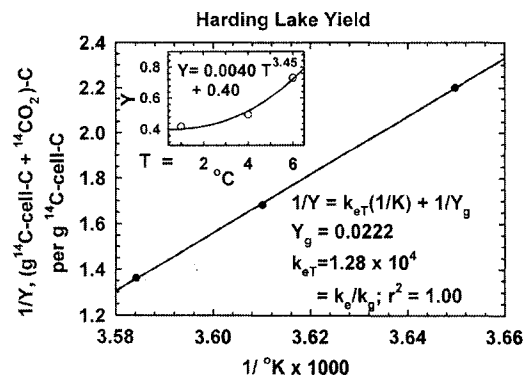


Figure 3.10. The reciprocal of yield to reciprocal of absolute temperature.

## Chapter 4

### Discussion

#### 4.1 Bacterial culturabilities

By using traditional techniques, typical bacterial species in aquatic systems have been cultured in laboratories, however, the majority of bacteria cannot be cultured (Jaspers et al. 2001). Dilution culture, combined with flow cytometry and epifluorescence microscopy, which have high sensitivity and resolution, have been successfully employed for seawater isolation and culturability determinations (Button et al. 1993, and Quang et al. 1998). The current project showed that the dilution culture protocol that had been used for the seawater isolation and culturability determinations also worked for freshwater bacteria. Sterile freshwater in this study was capable of supporting more than  $10^6$  cells per ml, which is consistent with seawater capability (Button et al. 1993). We used sterilized freshwater partitioned against raw lake water through membrane to provide an effective nutritional environment, but the experiments failed because cellulose dialysis bags were microbiologically unstable. However, by using our protocol, we improved the culturability value to 10% at the small inoculum sizes in unamended lake water (Figure 3.2), instead of the reported lower values (Amann et al. 1995); the culturabilities obtained represented at least a 100-fold improvement over conventional agar plate techniques.

Apparent culturabilities were inversely proportional to the number of cells inoculated from mixed species in a natural environment from Harding Lake (Figure 3.2),

suggesting inhibitory interactions. The possible mechanisms for decreased culturability include oxidative stress damage that prevents cell growth (Walker 1996), and lack of cell-to-cell communication in the laboratory media (Barer et al. 1999). For example, bacteria in laboratory cultures are exposed to lethal chemical or physical agents or conditions, such as a high concentration of substrate (Bartscht et al. 1999), which damage DNA or interfere with DNA replication. Therefore, most of the bacteria are injured and not able to recover. Physiological activities of bacteria are also influenced by potent signaling molecules, such as post-translationally processed peptides (Kleerebezem et al. 1997), and N-acyl homoserine lactones (Swift et al. 1996). Dilution cultures in this study did not offer these bacteria the same concentration of signaling molecules in each diluted laboratory medium as the lake environment. Therefore, decreased cell-to-cell communication causes cell death and decreased culturability. When compared to the phylogenetic tree of the whole lake species, a large portion of the bacteria in the dilution cultures could not grow (Table 3.2, and Figure 3.3A), possibly due to changes in environmental factors and inappropriate incubations. Thus, bacteria competed for the substrates in the limited nutrient environment, leading to a small number of surviving species (Figure 3.3). Culturability is inversely proportional to the number of cells inoculated from the mixed species, which is consistent with the antagonistic effect and quorum sensing (Kleerebezem et al. 1997, Srinivasan et al. 1998, Barer et al. 1999, and Swift et al. 1996).

Prior to the bacterial species sequence analysis carried out in this study, we quantified plasmid DNA. The results indicated that all the DNA met with the 0.1  $\mu\text{g}/\mu\text{l}$  concentration requirement for cycle sequencing. Then thirteen species were cloned based on 16S rDNA (Figure 3.3A). We could not conclude that there was a small number of species in Harding Lake because there were no duplicated sequences from cloned isolates. In fact, we hypothesize that there were far more than 13 species in Harding Lake.

To test the influence of extra substrates on the growth of Harding Lake bacteria, we amended an amino acid mix and glucose into the cultures at one-week intervals. The amendments could not stimulate a higher population and in fact inhibited the growth of bacteria at the small inoculum size (Figure 3.2A and B). The amino acid amendment caused a reduction of bacterial community diversity, which is consistent with the report by Hofle (1992). *Flexibacter sancti* could not grow in the cultures treated with glucose and the amino acid mix (Table 3.2), possibly suggesting an inhibitory role for glucose and amino acids to this species. Growing cultures should deplete ambient substrates, yet substrate additions caused inhibition of most typical species and resulted in an obvious decrease of bacterial species.

Comparative sequence analyses of 16S rDNA genes showed that all these bacterial species have similar length in the phylogenetic tree (Figure 3.3A), suggesting similar evolution rates. They have a high sequence similarity. These indicated close



relationships among the six bacterial divisions:  $\alpha$ -proteobacteria,  $\beta$ -proteobacteria,  $\gamma$ -proteobacteria, cytophaga/flexibacter/bacteriodes, acidobacteria, and cyanobacteria having at least 90% similarity (Figure 3.3A). The result was consistent in the DGGE analysis of lake water collected in 2001 (Figure 3.5B). One possible reason is that the metabolic enzymes of these bacteria have evolved to adapt to low temperatures from tropical temperatures in the arctic area at the same time. These findings may provide insight into the recent evolution of the bacteria in sub-Arctic freshwaters. Additionally, high abundances of  $\alpha$ -proteobacteria and  $\gamma$ -proteobacteria (Figure 3.3A, and Figure 3.5B), which are capable of the high growth rates in the freshwater, up to 3.0 to 4.2 d<sup>-1</sup>, were found in Harding Lake (Yokokawa et al. 2004). This is consistent with a rapid continuous shift in the distribution of dominant species observed in Harding Lake, according to the TRFLP, DGGE, and flow cytometry data (Figure 3.4, Figure 3.5A, and Figure 3.6).

Phylogenetic analyses of 16S rDNA clones provide an approach to assess bacterioplankton community composition. However, any sampling and analytical method has the potential for introducing some selectivity. Biased sample collection, differential DNA extraction efficiency and DNA amplification, and differential cloning of 16S rDNA are of significant concern in molecular ecological studies. We directly extracted DNA by using the freeze-and-thaw method (-20°C for 5 minutes, room temperature for 5 minutes, 5 cycles) (Bruns et al. 2002) and then amplified 16S rDNA. This reduced the bias from the traditional sample filtering collection and the DNA kit extraction, which cause the

loss of bacteria and DNA. Although we cannot completely rule out potential biases, these and other data (Giovannoni et al. 1990) suggest that a reasonable picture of bacterial composition in mixed populations can be obtained with 16S rDNA amplification and cloning approaches.

#### **4.2 Bacterial species changes**

To address how these bacterial populations in high-latitude lake adjust to seasonal differences while maintaining a rather constant biomass, we first used TRFLP and DGGE, which are valuable tools for assessing the diversity and the complexity of microbial communities (Scala et al. 2001, and Dunbar et al. 2001). We detected bands of genomic DNA (Figure 3.7A) and amplified the 16S rDNA fragments of about 1500 base pairs (Figure 3.7B) on agarose gels, confirming that bacterial genomic DNA was extracted and 16S rDNA was successfully amplified. To make comparisons between TRFLP profiles from different seasons, we calculated pair-wise similarity values by using Sorenson's index (Scala et al. 2001). Our results showed that most of the similarities were lower than 0.4 (Figure 3.4C) while only a value close to 1 indicates that species profiles are similar. The Sorenson index gives us direct and valid pair-wise comparisons of bacterial community compositions in these seasons. In addition, to test the accuracy of DGGE, we first amplified the human wild-type p53 gene and the mutant p53 gene. The mutant DNA is identical to the wild-type DNA, except for a single G to A mutation (PCR fragment base number 138) in exon 8 of the p53 gene. The PCR reaction produced a 191 bp fragment (Figure 3.8A). With a denaturing gradient of 25% to 65%, we successfully

separated amplified 191 bp fragments of the wild type and mutant p53 genes on 6.5% polyacrylamide gel (Figure 3.8B). This showed the validity and accuracy of DGGE for comparing the dominant bacterial community compositions of different seasons.

Comparative TRFLP or DGGE analysis of the bacterial 16S rDNAs of the three seasons revealed a small number of bacterial species in Harding Lake and a significant variability in the bacterial composition among the three seasons (Figure 3.4, and Figure 3.5A). Many of the DGGE bands of 16S rDNAs were faint (Figure 3.5A), suggesting low abundance of the template DNAs, but each one could represent one bacterial species in Harding Lake. Although DGGE only provided limited phylogenetic information, signature nucleotides of 16S rDNA allowed us to infer the phylogenetic affiliation of the sequenced dominant DGGE fragments. Sequence analysis of the DGGE bands revealed that 9 bands exhibited  $\alpha$ -proteobacteria,  $\gamma$ -proteobacteria, cyanobacteria, and actinobacteria signature sequences (Figure 3.5B).

The seasonal bacterial species change in Harding Lake might be due to the input of dissolved organic matter derived from terrestrial plants and soils and introduction of terrestrial bacteria. The marked shifts were due to the appearance of new populations of members of the bacteria. Crump (2003) reports that there are two bacterial community shifts in spring and in early summer, during the beginning and the end of dissolved organic matter influx, in an Arctic lake, and that bacterial community shifts are accompanied with change in terrestrial organic matter influx. In the Arctic, snow and ice

started to thaw in early spring, and melted snow carried a large amount of organics and nutrients into lakes with leaves, plants, and soils (Crump et al. 2003). More species of bacteria could take advantage of these nutrients or substrates than in winter. Similarly, in Harding Lake, runoff is estimated at 20 - 30% of the snowfall each year, and there is an obvious flow during snowmelt or heavy rainfall in spring and late summer (LaPerriere 2003). Therefore, the organic influx should also be obvious in Harding Lake. At the same time, terrestrial bacteria were also carried into the lake, consistent with the report by Crump (Crump et al. 2003). These bacteria changed the bacterioplankton structure and could be differentiated from the bacteria living in lakes based on 16S rDNA gene sequencing (Zwart et al. 2002). We identified total 22 bacterial species and confirmed that at least one species, *Knoellia sinensis* SAFR-013, playing an important role in decomposition of organic materials such as cellulose and chitin, was from soil or plants.

The causes for the seasonal bacterial species change also include some environmental factors involving in situ change in species succession, such as the availability of nutrients (HaldaAlija et al. 2001), temperature (HaldaAlija et al. 2001), phytoplankton blooms (Riemann et al. 2001), and signal molecules (Bruns et al. 2002). Among these factors the influence of dissolved organic matter and phytoplankton composition involved in the bacterial community shift are significant. For instance, bacterial communities of seven lakes in the Adirondack Mountains of New York State are affected by water chemistry (Hiorns et al. 1997). Lindstrom (2000) found that bacterioplankton community composition is indirectly influenced by the nutrient content

in five lakes. The nutrient structure changes the structure of the bacterioplankton community in these aquatic systems (Hofle 1992). As a consequence of spring and summer phytoplankton production, dissolved organic matter concentrations are higher and consist of a more complex structure of relatively labile organics in spring and summer than in winter; therefore, more species were found in spring and summer than in winter in Harding Lake. On the other hand, bacterial species could decompose dissolved organic matter in these aquatic environments and prevent the accumulation of large-scale dissolved organics despite high production rates during the peak of nutrient influx (Riemann et al. 2000, and Smith et al. 1995). When nutrients were substantially eliminated, these species of bacteria were likely to disappear after the depletion of certain types of nutrients, resulting in the shifts of bacterial species in Harding Lake. On the other hand, bacteria also released organic compounds so as to change the structures of lake chemistry and bacterioplankton in near polar lakes.

Based on the results of our study, it is difficult to accurately predict the future structure of the bacterial communities in Harding Lake. In general, together with other environmental factors, input of dissolved organic matter derived from terrestrial plants and soils, introduction of terrestrial bacteria, and bacteria themselves led to the bacterial species shifts with the seasonal change.

### 4.3 Effect of temperature on bacterial growth yield

Bacterial growth yield has been seriously underestimated in previous studies (Bratbak et al. 1985). The conversion efficiency of the substrates could not accurately reflect carbon and energy flow in aquatic systems based on these methods. Our *in situ* values for cell yield from amino acid mixtures were actually closer to 50% and 70% in active systems by using a modified, sensitive and accurate method (Button et al. 1981). Further, cell yield was found to increase with temperature according to a rate constant of  $0.93 \text{ g-S } ^\circ\text{C/g-cells}$  (Figure 3.10). Of significance was the maximum value for cell yield of  $0.70 \text{ g cell carbon produced per g of amino acid consumed}$ .

Theory presented provides formulations for expanding specific affinity theory to accommodate the effects of temperature on substrate distributions associated with nutrient-limited cell yield. It therefore appears that specific affinity theory has some advantage in formulating phenomena such as the effect of temperature on growth since yield functions are easily accommodated. All yields, including those from East Twin Lake during mid summer (not shown), were larger with warming. The large values compared with those published suggest that neither the effects of viral infection nor predation were significantly deleterious to cell yields. Thus, while bacteriophage infection is a clear part of microbial processes it seems not to affect general bacterial vigor as would be expected given the advantage of symbiosis.

Of course precise theoretical evaluations are impossible when system chemistry and microbiology varies over the experimental range of temperature, but temperature changes can never be associated with a particular process for a whole organism system. For example, the phenomenon of increased leakage associated with increased permeability at lower temperatures depends on the lipid structure of each species as adapted to prevailing conditions (Konings et al. 2002). Still, the trend of decreasing yield with decreasing temperature is clear (Figure 3.10). Furthermore, concepts are presented for partitioning metabolic efficiency into substrate for growth, for bioenergetics, and for endogenous processes, an approach that can deepen understanding of aquatic microbial processes.

#### **4.4 Bacterioplankton seasonal properties and multi-substrate use**

In our study, specific affinities for amino acids were only 20 to 1500 L/g-cells hr (Figure 3.9H) in near polar freshwater (in preparation) and seawater (Button et al. 2004), winter vs. summer, requiring simultaneous use of numerous substrates. Associated calculated growth rates were only months<sup>-1</sup> to years<sup>-1</sup> at measured ambient concentrations, but the simultaneous use of many substrates (Ideker et al. 2001) increased the rate to days<sup>-1</sup>, consistent with laboratory findings (Law et al. 1986).

Additionally, bacterial growth rate was 0.0045 hr<sup>-1</sup>, which was sufficient for complete population change within a few weeks while the bacterial content of Harding Lake water was relatively constant over the seasons (Figure 3.9B), even in winter when

the nutrient uptake rate was very small (Figure 3.9G). Therefore, winter populations were able to use many substrates simultaneously. The fast growth rates were consistent with a rapid continuous shift in the distribution of dominant species observed in Harding Lake, according to the TRFLP, DGGE, and flow cytometry data (Figure 3.4, and Figure 3.5A, and Figure 3.6).

Bacterial activity was observed to dramatically cycle over the year in Harding Lake near Fairbanks, Alaska (Figure 3.9). During springtime, warming increased specific affinities with activation energies that were larger than common values for substrate-sufficient cells and for isolated enzymes. Warming increased the rate of each step in the metabolism sequence to give larger concentrations of each intermediate thus enhancing the temperature effect. This exponentiation of rates with temperature helps explain the lag and subsequent bloom in bacterial activity observed during the spring bloom (in preparation).

The microbial systems in question appear to adapt to these rapidly changing conditions to provide a ready supply of minerals for rapid activity during the short summer (Karl et al. 1999, and Crump et al. 2003) while sustaining in a low energy state during winter, suggesting that the carbon cycle sustains ready activity, with capacity stored as a flywheel of sorts having metabolic inertia (Button et al. 2004). The large transitions in activity found in arctic waters are known to involve intermolecular properties of component macromolecules (van de Vossenberg et al. 1999), as well as



changes in microbial community composition. Both adaptations and species replacement are potential factors in an apparent transition between reliance on diffusion for the supply of intracellular nutrients in winter to conventional transport as the system warms from near 0°C. Because of the interdependent process of endergonic nutrient transport and energy derived from the transported nutrients, cold dark systems are hypothesized to rely on diffusion alone for nutrient acquisition.

#### **4.5 Experimental bias and future work**

TRFLP, DGGE, and recombinant DNA technique are powerful tools for assessing and comparing the diversity of complex microbial communities in aquatic systems (Liu et al. 1997, Macnaughton et al. 1999, and Bano et al. 2002). These techniques could be associated with possible biases introduced by PCR, such as chimera formation, (Kopezynski et al. 1994), heteroduplex formation (Ferris et al. 1997), template annealing (Suzuki et al. 1996), and differences in copy number of 16S rDNA (Farrelly et al. 1995). The result from possible effects was that the bacterial species number found with 16S rDNA sequences in the amplified products might not have reflected the real species number in the open-lake waters and original dilution cultures. Members of the bacterial community present in low abundance might still play an important role in the transformation of dissolved organic matter; furthermore, the bacterial species number in dilution cultures and the culturability values based on the bacterial species number might have been underestimated when we employed TRFLP, DGGE, and a clone library. Despite these disadvantages, PCR-based approaches have still provided valuable

information and are the most sensitive techniques available for describing and comparing the complex bacterial compositions.

Additionally, both epifluorescence microscopy and flow cytometry also have sensitivity limits for scoring positive and negative cultures, and counting populations. In this study, the sensitivity limit of epifluorescence microscopy was  $10^5$  cells per ml while flow cytometry's reached  $10^4$  cells per ml. However, flow cytometry, developed to give quantitative methods for dry cell mass (Robertson et al. 1998) and DNA content (Button et al. 2001), was sufficiently sensitive for aquatic bacteria. These demonstrated that flow cytometry could detect the small genome size, small dry mass, and low percentage of aquatic bacteria, and provided a supplement to microscopy data and genomic data for scoring positive and negative cultures. Using epifluorescence microscopy and flow cytometry, we scored culture as positive if there were a substantial number of bacteria ( $3.9 \times 10^4$  cells/ml) in it. However, using only these two approaches, several cultures could not be scored due to the inconsistency of their data. In this situation, TRFLP was used to score the cultures by comparing it with the data from epifluorescence microscopy and flow cytometry. In general, biases or errors were dramatically reduced for our investigation by combining these techniques.

Future studies with these techniques will be needed to understand the cell-cell interaction with pure cultures. We will also continue to improve the protocols of the techniques. Pure cultures were successfully produced with the dilution culture method

(Button et al. 1993). It will not be difficult for us to reproduce the pure dilution culture. However, it will be necessary to supply these dilution cultures with a more suitable nutritional environment; this can be done using dialysis bags or tubing dialyzed against a water community.

## Chapter 5

### Conclusions

The seasonal bacterial species change in Harding Lake resulted from input of organic matter derived from terrestrial plants and soils, an introduction of terrestrial bacteria, and bacteria themselves. Meanwhile, bacterial species were in turn responsible for decomposing and releasing the different types of dissolved organic matter; this changed the chemistry of the lake, and therefore also led to the seasonal bacterial species in the lake. Bacterial growth rate was sufficient for complete population change within weeks while the bacterial content of Harding Lake water was relatively constant over the seasons, even in winter when uptake nutrient rates were very small. Consequently, winter populations must have been able to use many substrates simultaneously.

Apparent culturability approached 10% in unamended lake water, and was inversely proportional to the number of cells inoculated from the mixed species from Harding Lake; this is consistent with antagonistic effect and quorum sensing. The dilution culture protocol used for seawater isolation and culturability determinations worked for freshwater as well. The concentration of added substrates in the study must have been higher than *Flexibacter sancti* and other species of bacteria could accept in these dilution cultures so that substrate addition could not improve bacterial culturability in the dilution cultures. Glucose and amino acid mix might inhibit the growth of *Flexibacter sancti*. Phylogenetic analyses based on 16S rDNA indicated close

relationships among the six bacterial divisions:  $\alpha$ -proteobacteria,  $\beta$ -proteobacteria,  $\gamma$ -proteobacteria, cytophaga/flexibacter/bacteriodes, acidobacteria, and cyanobacteria. This may provide insight into the recent evolution of the bacteria in near polar freshwaters. Additionally, the high abundances of  $\beta$ -proteobacteria and  $\gamma$ -proteobacteria suggested the high growth rates of these bacteria in the freshwater environments, consistent with a rapid continuous shift in the distribution of dominant species observed.

Lastly, our *in situ* values for bacterial growth yield from amino acid mix were actually closer to 50% and 70% in active systems by using a modified, sensitive and accurate method. Bacterial growth yield from amino acids increased with the increase of temperature between 1°C and 6°C.

**References:**

Alm, E.W., Oerther, D.B., and Larsen, N., 1996. The oligonucleotide probe database. *Appl. Environ. Microbiol.* 62: 3557-3559.

Amann, R., Ludwig, W., and Schleifer, K., 1995. Phylogenetic identification and *in situ* detection of individual microbial cells without cultivation. *Microbiol. Rev.* 59: 143-169.

Bano, N., and Hollibaugh, J.T., 2002. Phylogenetic composition of bacterioplankton assemblages from the Arctic Ocean. *Appl. Environ. Microbiol.* 68: 505-518.

Barer, M.R., and Harwood, C.R., 1999. Bacterial viability and culturability. *Adv. Microb. Physiol.* 41: 93-137.

Bartscht, K., Cypionka, H., and Overmann, J., 1999. Evaluation of cell activity and methods for the cultivation of bacteria from a natural lake community. *FEMS Microbiol. Ecol.* 28: 249-259.

Bratbak, G., and Dundas, I., 1985. Bacterial biovolume and biomass estimations. *Appl. Environ. Microbiol.* 49: 1488-1493.

Bruns, A., Cypionka, H., and Overmann, J., 2002. Cyclic AMP and acyl homoserine lactones increase the cultivation efficiency of heterotrophic bacteria from the central Baltic Sea. *Appl. Environ. Microbiol.* 68: 3978-3987.

Button, D.K., 2001. Isolation of oligobacteria, p. 164-173. *In* J. H. Paul (ed.), *Methods in Microbiology*, Vol. 30. Academic Press, New York.

Button, D.K., and Robertson, B.R., 1993. Use of high-resolution flow cytometry to determine the activity and distribution of aquatic bacteria, p. 163-173. *In* P. F. Kemp, B. F. Sherr, E. B. Sherr, and J. J. Cole (eds.), *Handbook of methods in aquatic microbial ecology*. Lewis, Ann Arbor, Michigan.

Button, D.K., and Robertson, B.R., 2001. Determination of DNA content of aquatic bacteria by flow cytometry. *Appl. Environ. Microbiol.* 67: 1636-1645.

Button, D.K., Robertson, B., Gustafson, E., and Zhao, X., 2004. The experimental and theoretical bases of specific affinity, a cytoarchitecture-based formulation of nutrient collection to supercede the Michaelis-Menten paradigm of microbial kinetics. *Appl. Environ. Microbiol.* 70: 5511-5521.

Button, D.K., Robertson, B.R., Jüttner, F., 1996. Microflora of a subalpine lake: bacterial populations, size, and DNA distributions, and their dependence on phosphate. *FEMS Microbiol. Ecol.* 21: 87-101.

Button, D.K., Schell, D.M., and Robertson, B.R., 1981. Sensitive and accurate methodology for measuring the kinetics of concentration-dependent hydrocarbon metabolism rates in seawater by microbial communities. *Appl. Environ. Microbiol.* 41: 936-941.

Button, D.K., Schut, F., Quang, P., Martin, R., and Robertson, B.R., 1993. Viability and isolation of marine bacteria by dilution culture: theory, procedures, and initial results. *Appl. and Environ. Microbiol.* 59: 881-891.

Calow, P., 1977. Conversion efficiencies in heterotrophic organisms. *Biol. Rev.* 52: 385-409.

Crump, B.C., Kling, G.W., Bahr, M., and Hobbie, J.E., 2003. Bacterioplankton community shifts in an Arctic lake correlate with seasonal changes in organic matter source. *Appl. Environ. Microbiol.* 69: 2253-2268.

De Giorgio, P.A., and Cole, J.J., and Cimblaris, A., 1997. Respiration rates in bacteria exceed phytoplankton production in unproductive aquatic systems. *Nature* 385: 148-150.



Ducklow, H.W., Quinby, H.L., and Carlson, C.A., 1995. Bacterioplankton dynamics in the equatorial Pacific during the 1992 El Niño. *Deep-Sea Res.* 42: 621-638.

Dunbar, J, Ticknor, L.O., and Kuske, C.R., 2001. Phylogenetic specificity and reproducibility and new method for analysis of terminal restriction fragment profiles of 16S rRNA genes from bacterial communities. *Appl. Environ. Microbiol.* 67: 190-197.

Farrelly, V., Rainey, F.A., and Stackebrandt, E., 1995. Effect of genomic size and *rrn* gene copy number on PCR amplification of 16S rRNA genes from a mixture of bacterial species. *Appl. Environ. Microbiol.* 61: 2798-2801.

Ferris, M.J., and Ward, D.M., 1997. Seasonal distributions of dominant 16S rRNA-defined populations in a hot spring microbial mat examined by denaturing gradient gel electrophoresis. *Appl. Environ. Microbiol.* 63: 1375-1381.

Giovannoni, S.J., Britschgi, T.B., Moyer, C.L. and Field, K.G., 1990. Genetic diversity in Sargasso Sea bacterioplankton. *Nature* 345: 60-63.

HaldaAlija, L, Hendricks, S.P., and Johnston, T.C., 2001. Spatial and temporal variation of enterobacter genotypes in sediments and the underlying hyporheic zone of an agricultural stream. *Microb. Ecol.* 42: 286-294.

Hiorns, W.D., Methe, B.A., and NierzwickiBauer, S.A., 1997. Bacterial diversity in Adirondack Mountain lakes as revealed by 16S rRNA gene sequences. *Appl. Environ. Microbiol.* 63: 2957-2960.

Hofle, M.G., 1992. Bacterioplankton community structure and dynamics after large-scale release of non-indigenous bacteria as revealed by low-molecular-weight-RNA analysis. *Appl. Environ. Microbiol.* 58: 3387-3394.

Ideker, T., Thorsson, V., Ranish, J.A., Christmas, R., Buhler, J., Eng, J.K., Bumgarner, R., Goodlett, D.R., Aebersold, R., Hood, L., 2001. Systematic perturbation and global analysis of galactose utilization in yeast. *Science* 292: 929.

Karl, D.M., Bird, D.F., Bjorkman, K., Houlihan, T., Shackelford, R., and Tupas, L., 1999. Microorganisms in the accreted ice of Lake Vostok, Antarctica. *Science* 286: 2144-2147.

Karner, M., and Fuhrman, J.A., 1997. Determination of active marine bacterioplankton: a comparison of universal 16S rRNA probes, autoradiography, and nucleoid staining. *Appl. Environ. Microbiol.* 63: 1208-1213.

Kleerebezem, M., Quadri, L.E., Kuipers, O.P., and de Vos, W.M., 1997. Quorum sensing by peptide pheromones and two-component signal-transduction systems in Gram-positive bacteria. *Mol. Microbiol.* 24: 895-904.

Kogure, K., Simidu, U., and Taga, N., 1979. A tentative direct microscopic method for counting living marine bacteria. *Can. J. Microbiol.* 25: 415-420.

Konings, W.N., Albers, S.V., Konings, S., and Driessen, A.J., 2002. The cell membrane plays a crucial role in survival of bacteria and archaea in extreme environments. *Antonie Van Leeuwenhoek* 81: 61-72.

Kopezynski, E.D., Bateson, M.M, and Ward, D.M, 1994. Recognition of chimetric small-sub-subunit ribosomal DNAs composed of genes from uncultivated microorganisms. *Appl. Environ. Microbiol.* 60: 746-748.

LaPerriere, J.D., 2003. Limnology of Harding Lake, Alaska: a deep, subarctic lake. *Lake and Reservoir Management.* 19: 93-107.

Law, A.T., and Button, D.K., 1986. Modulation of the affinity of a marine pseudomonad for toluene and benzene by hydrocarbon exposure. *Appl. Environ. Microbiol.* 51: 469-476.

Lindstrom, E. S., 2000. Bacterioplankton community composition in five lakes differing trophic status and humic content. *Microb. Ecol.* 40: 104-113.

Liu, W., Marsh, T.L., Cheng, H., and Forney, L.J., 1997. Characterization of microbial diversity by determining terminal restriction fragment length polymorphisms of genes encoding 16S rRNA. *63*: 4516-4522.

Macnaughton, S.J., Stephen, J.R., Venosa, A.D., Davis, G.A., Chang, Y., and White, D.C., 1999. Microbial population changes during bioremediation of an experimental oil spill. *Appl. Environ. Microbiol.* *65*: 3566-3574.

Muyzer, G, De Waal, E.C., and Uitterlinden, A.G., 1993. Profile of complex microbial population by denaturing gradient gel electrophoresis analysis of polymerase chain reaction-amplified genes coding for 16S rRNA. *Appl. Environ. Microbiol.* 1993. *59*: 695-700.

Quang, P.X., and Button D.K., 1998. Use of species distribution data in the determination of bacterial viability by extinction culture of aquatic bacteria. *J. Microb. Meth.* *33*: 203-210.

Ram, A.S.P., Nair, S., and Chandramohan, D., 2003. Bacterial growth efficiency in the tropical estuarine and coastal waters of Goa, southwest coast of India. *Microb Ecol.* *45*: 88-96.

Rappé, M.S., Connon, S.A., Vergin, K.L., and Giovannoni, S.J., 2002. Cultivation of the ubiquitous SAR11 marine bacterium clade. *Nature* 418: 630-632.

Reitner, B., Herziq, A., and Herndl, G.J., 1999. Dynamics in bacterioplankton production in a shallow, temperate lake (Lake Neusiedl, Austria): evidence for dependence on macrophyte production rather than on phytoplankton. *Aquatic Microbial Ecology* 19: 245-254.

Riemann, L., Steward, G.F., and Azam, F., 2000. Dynamics of bacterial community composition and activity during a mesocosm diatom bloom. *Appl. Environ. Microbiol.* 66: 578-587.

Riemann, L., and Winding, A., 2001. Community dynamics of free-living and particle-associated bacterial assemblages during a freshwater phytoplankton bloom. *Microb. Ecol.* 42: 274-285.

Robertson, B. R., Button, D. K., and Koch, A. L. 1998. Determination of the biomasses of small bacteria at low concentration in a mixture of species with forward light scatter measurements by flow cytometry. *Appl. Environ. Microbiol.* 64: 3900-3909.

Scala, D.J., and Kerkhof, L.J., 2001. Horizontal heterogeneity of denitrifying bacterial communities in marine sediments by terminal restriction fragment length polymorphism analysis. *Appl. Environ. Microbiol.* 66: 1980-1986.

Smith, D.C., Steward, G.F., Long, R.A., and Azam, F., 1995. Bacterial mediation of carbon fluxes during a diatom bloom in a mesocosm. *Deep Sea Res. II* 42:75-97.

Srinivasan, S., Ostling, J., Charlton, T., de Nys, R., Takayama, K. and Kjelleberg, S., 1998. Extracellular signal molecule(s) involved in the carbon starvation response of marine *Vibrio* sp. Strain S14. *J. Bacteriol.* 180: 201-209.

Suzuki, M.T., and Giovannoni, S.J., 1996. Bias caused by template annealing in the amplification of mixtures of 16S rRNA genes by PCR. *Appl. Environ. Microbiol.* 62: 625-630.

Swift, S., Throup, J.P., Williams, P., Salmond, G.P.C., and Stewart, G., 1996. The inner workings of a quorum sensing – a population-density component in the determination of bacterial phenotype. *Trends. Biochem. Sci.* 21: 214-219.

Taylor, G.T., 1982. The role of pelagic heterotrophic protozoa in nutrient recycling: a review. *Annls Inst. Oceanogr. Paris* 58: 227-241.

van de Vossenberg, J.L., Diessen, A.J., da Costa, M.S., and Konings, W.N., 1999.

Homeostasis of the membrane proton permeability in *Bacillus subtilis* grown at different temperature. *Biochim. Biophys. Acta*, 1419: 97–104.

Vetriani, C, Jannasch, H.W., Macgregor, B. J., Stahl, D.A., and Reysenbach, A., 1999.

Population structure and phylogenetic characterization of marine benthic archaea in deep-sea sediments. *Appl. Environ. Microbiol.* 65: 4375-4384.

Walker, G.C., 1996. The SOS response of *Escherichia coli*, p. 1400-1416. *In* F.C.

Neidhardt (ed.), *Escherichia coli* and *Salmonella*: cellular and molecular biology: 2nd ed., vol.1. ASM Press, Washington, D.C.

Williams, P.J., 1981. Incorporation of microheterotrophic processes into the classical paradigm of the marine food web. *Kieler Meeresforsch* 5: 1-28.

Yoch, D.C., 2002. Dimethylsulfoniopropionate: its sources, role in the marine food web, and biological degradation to dimethylsulfide. *Appl. Environ. Microbiol.* 68: 5804-5815.

Yokokawa, T., Nagata, T., and Cottrell, M.T., and Kirchman, D.L., 2004. Growth rate of the major phylogenetic bacterial groups in the Delaware estuary. *Limnol. Oceanogr.* 49: 1620-1629.

Zwart, G., Crump, B.C., Kamst-van Agterveld, M.P., Hagen, F., and Han, S.K., 2002.

Typical fresh bacteria: an analysis of available 16S rRNA gene sequences from plankton of freshwater lakes and rivers. *Aquat. Microb. Ecol.* 28: 141-155.



## APPENDICES

### Appendix A: Experimental and Theoretical Bases of Specific Affinity, a Cytoarchitecture-Based Formulation of Nutrient Collection Proposed To Supersede the Michaelis-Menten Paradigm of Microbial Kinetics \*

#### A.1 Abstract

A theory for solute uptake by whole cells was derived with a focus on the ability of oligobacteria to sequester nutrients. It provided a general relationship that was used to obtain the kinetic constants for *in situ* marine populations in the presence of naturally occurring substrates. *In situ* affinities of 0.9 to 400 liters g of cells<sup>-1</sup> h<sup>-1</sup> were up to 10<sup>3</sup> times smaller than those from a “*Marinobacter arcticus*” isolate, but springtime values were greatly increased by warming. Affinities of the isolate for usual polar substrates but not for hydrocarbons were diminished by ionophores. A kinetic curve or Monod plot was constructed from the best available data for cytoarchitectural components of the isolate by using the theory together with concepts and calculations from first principles. The order of effect of these components on specific affinity was membrane potential > cytoplasmic enzyme concentration > cytoplasmic enzyme affinity > permease concentration > area of the permease site > translation coefficient > porin concentration. Component balance was influential as well; a small increase in cytoplasmic enzyme

---

\* This paper was published in Applied and Environmental Microbiology, Sept. 2004. 70: 5511-5521.

Authors were Button, D.K., Robertson, B., Gustafson, E., and Zhao, X.

concentration gave a large increase in the effect of permease concentration. The effect of permease concentration on specific affinity was large, while the effect on  $K_m$  was small. These results are in contrast to the Michaelis-Menten theory as applied by Monod that has uptake kinetics dependent on the quality of the permease molecules, with  $K_m$  as an independent measure of affinity. Calculations demonstrated that most oligobacteria in the environment must use multiple substrates simultaneously to attain sufficient energy and material for growth, a requirement consistent with communities largely comprising few species.

## A.2 Introduction

The rate of nutrient transport into microorganisms is typically described by using the equations of Monod (Monod 1942). These formulations that are based on measurements of *in vitro* enzyme solutions and the theory described by Michaelis and Menten (Michaelis et al. 1913). Affinity for solute is usually taken as the Michaelis constant ( $K_m$ ), the concentration of substrate at half the maximal rate of uptake, and taken as an inherent property of both the population (White 2000) and its permeases (Radisky et al. 1999). However, the variation of  $10^{10}$  in  $K_m$  values was too great to be attributed to differences in proteins of common function and appears simply to reflect the concentration of proteins involved in substrate acquisition, metabolism, and biosynthesis. This concept was reinforced by equations that reflected the uptake rates from the number of permease molecules, the time required for each permease to translocate a molecule of substrate (Button 1998), and internal pool concentrations generated at the resulting

dynamic steady-state equilibrium (Button 1991). Specific affinity for substrate  $S$  ( $a_S$ ), a second-order rate constant for substrate sequestering that scales with nutrient acquisition power independently of the maximal rate (Robertson et al. 1979), could thus be related to cytoarchitectural composition, including permease abundance and properties. The purpose of this communication is to develop a relationship between the concentration-limited rate of nutrient transport and organism cytoarchitecture based on available theory, in situ and laboratory kinetic data, and derived concepts. These tools are used to describe the concentration-dependent nutrient flux into an isolate of “*Marinobacter arcticus*” from the content of various proteins and pools specified, in an attempt to understand the metabolic strategies of organisms that substantially maintain the nutrient chemistry of aquatic environments.

### A.3 Materials and Methods

***In situ* measurements.** Seawater samples were collected from either near the mouth of Resurrection Bay, Alaska, during an incoming tide or 10 km out into the Gulf of Alaska, all at a 10-m depth. Processing took place aboard the R/V *Alpha Helix*. Samples were sieved through 2.5- $\mu\text{m}$ -pore-size filters to remove phytoplankton when it was abundant, amended with radiolabeled substrate, and incubated at ambient temperatures. Uptake rates were calculated from four or five measurements of particle radioactivity retained on 0.08- $\mu\text{m}$ -pore-size filters from six 100-ml subsamples containing radiolabeled substrate at known concentrations over 2 to 12 h in random order to minimize systematic error. Activity was measured on shipboard, and incubation times

were adjusted to achieve the incorporation of about 100 dpm in the low-activity samples. Pyrolyzed prerinsed glassware was used throughout. Uptake was calculated from the ratio of filtered radioactivity to total radioactivity. Specific activities of radiolabeled substrates were calculated from known dilutions with unlabeled substrate and included a mixture of nine major amino acids (all at the highest specific activity available; ICN Pharmaceuticals, Inc.). Specific affinities ( $a_s$ ) were calculated from the incorporation rate of the labeled substrate as given by the radioactivity and specific activity of cell material retained on filters ( $v_R$ ) and cell yield ( $Y$ ) by using the equation

$$a_s = v_R / [S] Y \quad (1)$$

where  $[S]$  is the concentration of substrate  $S$ . (The derivation appears as equations 1 to 4 at the URL <http://www.ims.uaf.edu/fcm-kinetics-derivations.pdf>.) For abbreviations and symbol definitions, see Table 1, and for dimensional analyses see reference 6. Bacterial biomass ( $X$ ) was calculated from light scatter data by flow cytometry and the conversion factor of 5.5 g (wet weight)/g (dry weight) (Button et al. 2000). Uptake rates per unit biomass ( $v$ ) were obtained from apparent rates ( $v_a$ ) by correcting added substrate concentrations ( $[S_a]$ ) for *in situ* or naturally occurring amino acid concentrations ( $[S_n]$ ) using high performance liquid chromatography (Henrichs et al. 1987) data and a material balance according to the equation

$$v = v_a / \{([S_a] + [S_n]) / [S_a]\} \quad (2)$$

Rates were typically linear over time, with  $r^2$  values of 0.95 to 0.99. However, numerous replicates in parallel gave values that varied by as much as 20%, and variation was greatest when activity was low. Thus, while the measurements are taken as a best available reflection of absolute rates,  $r^2$  values overstate precision, and values here are insufficient to address the precise shape of kinetic curves. A similar large disparity was previously noted for phosphate kinetics and was minimized by reducing culture disturbance during sampling (Law et al. 1976). This topic will be further addressed in combination with freshwater kinetics.

**Laboratory measurements.** “*Marinobacter arcticus*,” a 0.3- $\mu\text{m}^3$  3.8-Mb gramnegative marine isolate (Button et al. 1981) was cultivated as previously described (Robertson, et al. 1987). Briefly, the isolate, was grown in artificial seawater amended with a 5-g/liter amino acid mixture and incubated on a shaker table at 22°C. For short-term uptake rates, populations of 400 to 900 mg/liter were harvested by centrifugation at 14,000 x g, resuspended by vortex mixer, washed twice with basal medium, diluted to a Coulter Counter wet biomass of 0.6 to 0.9 mg/liter computed from cell volume and a density of 1.04 g/cm<sup>3</sup>, incubated for 1 h to deplete substrate reserves, and amended with radiolabeled substrate in 6 ml of amino acid-free basal medium. Uptake was measured by collecting cells on 0.2- $\mu\text{m}$ -pore-size Nuclepore filters arranged in a manifold over 4 to 6 min. Uptake rates over 50 min were measured using populations of 1 to 5 mg/liter collected on filters. Respired <sup>14</sup>CO<sub>2</sub> was collected by a trap of phenethylamine

scintillation cocktail following purification by a train of H<sub>2</sub>SO<sub>4</sub> and Tenax traps at - 70°C (Button et al. 1981).

Metabolic inhibitors included 10 M carbonyl *m*-chlorophenylhydrazone (CCCP), 10 μM dicyclohexylcarbodiimide, and 20 μM monensin.

**Kinetics for whole cells.** Heterotrophic bacterial activity in aquatic systems depends on the rate at which organisms are able to accumulate organic solutes. This rate is the product of specific affinity and substrate concentration. Where several substrates are commonly used simultaneously, the total rate of uptake ( $v$ ) is given by the sum of the  $n$  individual rates according to the concentration and associated rate constant or specific affinity of each substrate, i.e.,

$$v = \sum a_i [S_i] \quad (3)$$

where  $i$  is a particular substrate and specific affinity is the ratio of rate to concentration ( $v/[S]$ ) at any specified  $[S]$ . Where each of the  $n$  substrates ( $S_i$ ) is accumulated at a rate ( $v_i$ ) according to hyperbolic or saturation kinetics, the contribution of the rate of one substrate to  $v$  is given by the equation (Button et al. 1989)

$$v_i = (V_{mi} a_{Si}^o [S_i]) / (V_{mi} + a_{Si}^o [S_i]) \quad (4)$$

This is the relationship described by Monod written in terms of the specific affinity ( $a^{\circ}_{Si}$ ), initial slope or maximal value of the slope of the rate versus concentration curve, and maximal velocity ( $V_{mi}$ ), the apparent upper limit of the transport rate. So written, this formulation separates processes of substrate collection and enzyme saturation to provide for the independent assignment of each. It also specifies the half-saturating concentrations for substrate collection ( $K_a$ ) according to the equation  $K_a = V_m / a^{\circ}_S$ . Since  $V_m$  often increases with  $[S]$ ,  $K_a$  is related to the maximal value of this rate constant ( $a^{\circ}_S$ ) to focus on nutrient collection. For hyperbolic kinetics,  $K_a$  equals  $K_m$ . Since both  $K_a$  and  $K_m$  depend on transport capacity, neither term, unlike  $a^{\circ}_S$ , adequately compares organismal kinetics in the absence of biomass-specific  $V_m$  data (Button 2000).

**Background substrate.** Values for  $a^{\circ}_{Si}$  and  $K_{ai}$  are of interest in the environment because they help anticipate the ambient concentrations of nutrients at which kinetic control is achieved, reflect the cytoarchitectural composition of the microflora, and suggest a cytoarchitecture that is distinct from that of most laboratory cultures (Button et al. 2001, and Robertson et al. 1998). However, values remain elusive because most aquatic dissolved organics remain unquantified. To address this difficulty, water samples are often amended with radiolabeled substrates as tracers of nutrient flux (Wright et al. 1965). Still, rates can remain indeterminate because added substrate increasingly dilutes the naturally occurring substrate as the small ambient concentrations are approached or exceeded. This result gives the appearance of hyperbolic saturation kinetics, but the background substrate decreases the apparent values of both the specific affinity and the

associated saturation constant,  $K_a$  (Button 2002). Absent isotope effect, when both added and incorporated radiolabeled substrates are equally diluted by the  $S_n$ , the specific affinity is given by the ratio  $v_a/[S_a]$  (equations 6 to 11 at <http://www.ims.uaf.edu/fcm-kinetics/kinetics-derivations.pdf>). Then, assuming hyperbolic kinetics, where  $a_S$  equals  $V_m/K_a$ , equation 4 linearized to affinity plot form becomes

$$v/[S] = -v (a^{\circ}_S/V_{\max}) + a^{\circ}_S \quad (5)$$

where  $a^{\circ}_S$ , the base value of the specific affinity, is given by the  $v/[S]$  intercept (hence the term affinity plot), the  $v$  intercept gives the maximal rate, and the slope is  $-1/K_a$  (equations 22 to 24 at <http://www.ims.uaf.edu/fcm-kinetics/kinetics-derivations.pdf>).

Additional substrates that may be cotransported again add equally to both  $v$  and  $[S]$ , so that the  $a^{\circ}_S$  intercept obtained was taken as the correct specific affinity, assuming that the kinetics were hyperbolic and that saturation and artifactual insults to the sample were insignificant.

**Cytoarchitectural model.** The diagram used for nutrient flow into a transthreptic (surface-feeding) cell is shown in Figure A.1. Periplasmic concentrations are reduced to a value that depends on the porin concentration in the outer membrane, the rate of diffusion through the membrane, and the rate of removal to the cytoplasm. These periplasmic concentrations specify the molecular collision rate with transporters having a specified density distribution within the inner cell membrane. The transport rate is controlled by collision success and affected by the transporter occupancy with substrate, availability of



energizing protons, and effective radius of the active site. Resulting substrate concentrations in the cytoplasmic pool concentration  $[S_c]$  reflect this transport rate together with metabolism and other losses. Metabolism is done by the enzyme sequence surrogate ( $E$ ) having a net specific affinity, catalytic constant, and molecular abundance that specify flow from the cytoplasmic pool to cell material (with a biomass of  $X$ ).

**Computational techniques.** Formulations describing nutrient flow through the nutrient sequestering process were solved in sequence. The substrate concentration for each step was calculated from the kinetics and concentrations associated with the preceding step as described below. The metabolic sequence was taken as at a unique set of steady states for each external  $[S]$ . Kinetic curves shown give only the final flux, i.e., the rate of formation of cell material, for each value of external  $[S]$ .

#### A.4 Results

***In situ* kinetics.** Since *in situ* kinetic constants are difficult to evaluate but essential to the description of oligobacterial activity, we explored their values. Figure A.2 shows Monod (Figure A.2A and C) and Scatchard or affinity plots (Figure A.2B and D) of amino acid uptake rates in the Gulf of Alaska. Plots using specific activities corrected for analytically determined leucine are shown in Figure A.2C and D. The hyperbolic nature of the Monod plot in Figure A.2A was ascribed to systematic dilution of added leucine by naturally occurring leucine because the apparent first-order region (when  $[S]$  was near 0) was eliminated by the correction of specific activities with analytical leucine.

This artifact was confirmed with computer simulations (Button 2002). However, as formulated above, both incorporated and added substrate were equally diluted by  $S_n$ , so that the ratio of  $v_a$  to  $[S_a]$  remained unaffected. This result was supported by the similar data patterns in Figure A.2B and D, where values for  $v/[S]$  were similar whether corrected for background substrate or not. The agreement, allowing for usual variation in uptake rate measurements among separate samples from a common source of low-activity populations, established that the specific affinity was near maximal, i.e., near the base value ( $a^{\circ}_S$ ), at 0.4 liters mg of cells<sup>-1</sup> h<sup>-1</sup> in the small  $S_a$  aliquots of this *in situ* sample and without imposing an unjustified extrapolation. Specific affinities shown were therefore taken to be reflective of the best available method for determining amino acid accumulation rates and therefore reflective of the ability of low-substrate-adapted bacteria to sequester substrate during steady state growth at the chosen site.

Additional kinetic data (Table A.2) show that mean values for specific affinity were small throughout the year, compared to those of laboratory cultures, but much larger during summer than winter. Looking for the active water necessary for autoradiographic determinations of substrate preferences, we sampled during a heavy spring bloom in the Gulf of Alaska associated with unusually warm 6°C El Niño waters in May 1998, but the smallness of the specific affinities was unexpected. Values for  $a_S$  were, however, increased within an hour by warming with an Arrhenius activation energy of 230 kJ/mol, consistent with recent reports (Yager et al. 1999). The large activation energy demonstrated ready capacity to achieve at least moderate values for specific affinity,

capacity not yet realized by these springtime populations. According to the largest specific affinity from Table A.2 and a cell yield of 2.5 g (wet weight) of cells/g of amino acids used from radioactive substrate incorporated versus that liberated as carbon dioxide (data not shown) by organisms that are 18% dry weight (Robertson et al. 1998), the growth rate with a single substrate was small by the equation  $\mu = a_S[S]Y = (400 \text{ liters/g of cells}^{-1} \text{ h}^{-1}) (8.5 \times 10^{-7} \text{ g of leucine liter}^{-1}) (2.5 \text{ g of cells/g of substrate used}) = 8.5 \times 10^{-4}/\text{h}$ , for a very long doubling time of 34 days.

**Uptake kinetics by oligobacterial isolates.** A membrane potential ( $\Delta\Psi$ ) provides the energy used in concentrative symport of many substrates (Paulsen et al. 1998). That specific affinities for the uptake of amino acids by bacterioplankton ranged from small in summer to nearly negligible in winter (Table A.2) brought into question the ability of the organisms to effect sufficient nutrient flux for a sustained membrane potential during periods of low productivity, given the costs of ion leakage (van de Vossenberg et al. 1999), substrate leakage (Robertson et al. 1979), molecule repair, and other endogenous processes (Nystrom et al. 1998). Glutamate collection at low temperature by “*M. arcticus*,” when it is washed and starved, was stimulated threefold by the addition of a mixture of amino acids (Table A.3), as reflected by the larger specific affinity. This result was consistent with a loss of membrane potential during the starvation step that was sufficiently replenished to enable scavenging of small concentrations of glutamate due to increased permease activity. Transport capacity, according to  $V_m$  values, was greatly stimulated as well. Further, glutamate addition stimulated the transport of leucine (Figure

A.3) according to the kinetic parameters shown in Table A.3. Rates were about the same as those from active waters (Figure A.2) but sustainable, as demonstrated by the concave-down curvature of the graphed values (Figure A.3A). Substrate use was insufficient to remove a significant portion of the leucine which would otherwise cause such curvature as well. The incubation time was too short and the curvature was in the opposite direction for the effect to be one of protein induction. The immediate stimulation of leucine uptake by glutamate, with a multisubstrate stimulation constant ( $K_S$ ) of 3  $\mu\text{g/liter}$  (Figure A.3B), agreed with a general finding of stimulation by auxiliary substrates in very-low-carbon and low-energy systems (Law et al. 1986, and Lendenmann et al. 1996). Larger additions of glutamate inhibited leucine transport, suggesting an indirect effect on the steady-state flux. Such uncompetitive inhibition is consistent with small maximal velocities that result from rate restriction at a point different from that of the initial reaction (Plowman 1972). This result was found for *in situ* rates as well; increasing substrate concentrations from 1 to 8  $\mu\text{g/liter}$  caused no increase in the December Gulf of Alaska rates shown in Table A.2 (data not shown), and the saturation constant for alanine in “*M. arcticus*” (Table A.3) was only 0.011 mg of alanine/liter (calculated by the equation  $K_m = V_m/a^{\circ}_S = 3.4 \text{ mg of alanine/g of cells} \cdot \text{h} [288 \text{ liters g of cells}^{-1} \text{ h}^{-1}]^{-1}$ ).

Leucine transport may be particularly facile among amino acids owing to both difficulty in biosynthesis (Simon et al. 1989) and lipophilicity; the highest specific affinity measured is for uptake of the nonpolar substrate toluene (Button et al. 1998). Transport of more-polar amino acids by “*M. arcticus*” was inhibited by protonophores,

such as CCCP (Table A.3), but not by the sodium ionophore monensin. The absence of inhibition by monensin, and a low 10% inhibition by the proton ejecting F1F0 ATPase-specific dicyclohexylcarbodiimide (data not shown), was consistent with organism dependence on the chemical potential of a proton gradient. Toluene transport was little inhibited by CCCP, and there was only minor inhibition of toluene metabolism as measured by carbon dioxide production. This hydrophilic substrate is thought to be accumulated by vectorial partitioning (Button 1985), which eliminates the energy requirement for a transmembrane concentration gradient of substrate (Robertson et al. 1987). These data indicated that polar substrate transport rather than metabolism was inhibited by the protonophores. While the data supported the absence of a chemical potential requirement for the accumulation of nonpolar substrates, they were also consistent with a need for a proton potential to transport polar substrates in the observed system, whether directly by symport or indirectly through ATP or other energy-transducing reserves (Paulsen et al. 2000). To further test whether membrane potential is a significant variable in polar solute transport by oligobacteria, alanine transport by washed but not starved cultures of "*M. arcticus*" was examined in the presence of protonophores (Table A.3). The specific affinity was low compared to that of usual enrichment culture isolates, and maximal rates of growth were still small compared with those expected. However, values were adequate for large mixtures of substrates due to the increased value of  $[S]$  in the calculation  $a_S = v/[S]$ . The addition of CCCP completely abolished transport, again consistent with a membrane potential requirement for transport.

**Cytoarchitecture and nutrient flux.** Available data were integrated into a formulation of concentration-dependent nutrient flux based on the cellular composition and catalytic activity of specified components beginning with membrane potential.

**Proton gradient.** Growth in low-nutrient systems requires concentrative transport, as described above, so that the many metabolic enzymes can operate efficiently. This “uphill” transport involves osmotic work. The increase in specific affinity with auxiliary substrate addition, the inhibition of the transport of polar substrates but not the transport of lipophilic substrates by protonophores, and the absence of sensitivity to sodium specific ionophores indicated that the energy for transport was from substrate metabolism as mediated by protons with a membrane potential ( $\Delta\Psi$ ). Membrane potential was formulated to increase in proportion to  $[S]$  at substrate concentrations near the affinity constant  $K_a$  by setting the membrane potential constant ( $K_{\Delta\Psi}$ ) at  $5 \mu\text{g}$  of alanine liter<sup>-1</sup>. Values were from sodium-ion-dependent transport of threonine (Dashper et al. 2001), with a maximal potential ( $\Delta\Psi_{\text{max}}$ ) of 150 mV, as often observed in microbial systems (Kashket et al. 1985). Binding of substrate to the permease complex must precede the active transport step. Completion of this step is also required to generate the energy necessary for solute accumulation so that the process is autocatalytic until permease-saturating potential is achieved. Transport was therefore formulated with positive cooperativity (Koshland et al. 2002) between protons produced from the metabolism of transported substrate and available substrate that can be

metabolized. The two substrates,  $H^+$  and  $S$ , were accommodated with an  $n$  of 2 in the sigmoidal relationship for proton gradient by the equation

$$\Delta\Psi = \Delta\Psi_{\max}[S]^n/(K_{\Delta\Psi}^n + [S]^n) \quad (6)$$

**Permease concentration.** The dependence of substrate-permease collision success on membrane potential was formulated from positive cooperativity theory because permeases both require and produce the membrane potential needed to activate the transporters (equation 7).

$$N_a = N \Delta\Psi^n/(K_{HS}^n + \Delta\Psi^n) \quad (7)$$

$N_a$  is the number of active transporters among  $N$  total permeases. It is specified by the proton-substrate interaction constant  $K_{HS}^n$ , where  $n$  is the number of interacting species ( $H^+ + N = 2$ ), and by  $N$  at large values of  $\Delta\Psi$ , where all permeases are activated.  $N$  was set at 2,400 molecules/cell from “*Cycloclasticus oligotrophus*” dimensions, kinetics, collision frequency calculations, and the dioxygenase concentration associated with toluene uptake (Button et al. 1998) by assuming transport by vectorial partitioning (Button 1985).  $K_{HS}$  was set at 20 to specify that half the permease molecules were active at the observed affinity constant for alanine transport of 1.4  $\mu\text{g/liter}$  in substrate-deficient “*M. arcticus*.”  $n$  was set at 2 to reflect the interactive effect of electrical gradient and transporter concentration. The linear increase in  $N_a$  with  $[S]$  is then preceded by a region

without energized permeases at low values of  $[S]$  and truncated at a maximal value of  $N_a$  (equal to  $N$ ) when the value of  $[S]$  is large (Figure A.4B).

**Transport.** A theoretical value for  $a^{\circ}_S$  can be obtained from the per-site rate constant for bimolecular collisions ( $k$ , equal to  $4Dr_s/1,000$ , where  $D$  is a molecular diffusion constant and  $r_s$  is the effective radius of an active site) according to the number of permeases, the diffusion constant, the areas of the permease sites, and substrate mass (Berg 1988). Dividing by cell mass and using a spherical cell of density  $\rho$  (1.03 g of cell material  $\text{cm}^{-3}$ ) gives an equation for determining  $a^{\circ}_S$  of

$$a^{\circ}_S = R_m \{ (N_a 4 D r_s M) / [(4/3) \pi r^3 \rho] \} \quad (8)$$

so that the rate of transport from the exterior at values of  $[S]$  large enough to maintain membrane potential but too small to saturate the permeases remains calculable by the equation  $v = a^{\circ}_S [S]$ . The resistance of the outer cell membrane to substrate diffusion into the periplasmic space ( $R_m$ ) depends on the concentration and properties of porins in the outer membrane. It is taken as the ratio of observed rate in the presence of an outer membrane to the expected rate in the absence of an outer membrane, as discussed below. Some of the permeases will be occupied and unable to collect substrate. Where saturation is hyperbolic, the rate decreases with  $[S]$  according to equation 4, and the specific affinity is equal to  $v/[S]$  at any  $[S]$ . For membrane potential sufficient cells, the maximal rate of transport ( $V_m$ ) is given by the rate or velocity ( $v$ ) asymptote of the  $v$ -versus- $[S]$  Monod



plot. Neglecting interactive enhancement, the value of  $V_m$  depends on the number of molecules of the  $S_i$ -compatible transporters per gram of cell material and the associated catalytic constant ( $k_{cat}$ ). Again converting from cell volume to mass, the maximal rate of transport is given by the equation

$$V_m = k_{cat}NM/[\frac{4}{3}\pi r^3 \rho] \quad (9)$$

Calculations included a small additional term ( $k_{ind}[S]$ ) to describe the effects of large substrate concentrations that induce additional proteins usually observed in systems over a range of steady states (Robertson et al. 1979). This induction results in additional capacity that increases the value of  $V_m$ . Substituting equations 8 and 9 for affinity and maximal velocity in equation 4 gives the concentration-dependent rate of transport in a way that depends on the number of transporters together with their catalytic properties and bioenergetic requirements but neglects the downstream constraints considered below.

**Cytoplasmic substrate.** Unregulated cytoplasmic concentrations of substrate ( $[S_c]$ ) depend on the rates of import and use of the substrates. When use is proportional to concentration, i.e., saturation is insignificant,  $[S_c]$  becomes a function of active transport rate alone. Since transport through a porous medium depends on the pressure gradient across the medium (Darcy's law) (Morse 1963), and pressure at constant volume is proportional to concentration (Boyle's law),  $[S_c]$  is a linear function of transport rate over the relevant values of  $[S]$ , as documented below. The value of  $[S_c]$  is then equal to  $L_v$ ,

where  $L$  is the translation coefficient (equations 5 and 33 to 37 at <http://www.ims.uaf.edu/fcm-kinetics/kinetics-derivations.pdf>) and  $v$  is the rate of transport. Support for the relationship together with the value of  $L$  was taken from measurements of external  $[S]$  in phosphate-limited continuously cultivated *Rhodotorula rubra* samples. There, the concentrations of phosphate in the metabolic pools were proportional to the rates at which phosphate was transported (Robertson et al. 1979). Absolute concentrations were taken from glutamic acid in the pools of arginine-limited continuous cultures of marine isolate 198, which ranged from 5 to 16 mg/liter with growth rate (Law et al. 1977). The present calculations assumed that transport capacity and restriction to substrate flow by the outer membrane in “*M. arcticus*” were similar to those in the two pelagic isolates.

**Rate of metabolism.** The use of accumulated substrate in the metabolic pools depends on the concentration and catalytic properties of the associated catabolic and anabolic enzymes operating in their intracellular environment beginning with  $S_c$ . For Michaelian or hyperbolic kinetics, the rate is given by the maximal velocity and specific affinity associated with the cytoplasmic enzyme assemblage according to the equation

$$V = V_m a^o_c [S_c] / \{V_m + a^o_c [S_c]\} \quad (10)$$

where  $a^{\circ}_c$  is the affinity of metabolic enzyme for cytoplasmic substrate. Maximal velocity was taken from observed rates and converted to numbers of enzyme molecules per cell by using the value for cell mass used above and typical  $k_{\text{cat}}$  values for metabolic enzymes in the cytoplasm (Amdur et al. 1966). The specific affinity for this enzyme assemblage was calculated from typical values for  $K_m$  and the relationship  $a^{\circ}_c = V_m/K_m$  for hyperbolic kinetics (Button et al. 1989, and Cleland 1975).

**Solutions of the rate equation.** The kinetics specified by equations 6 through 10 together with the cytoarchitectural and kinetic properties specified in Table A.1 are shown as the Monod plot given by the central curve in Figure A.4A. The size of the threshold in substrate concentration was affected by the extent of cooperativity in the absence of an auxiliary energy source in this experimental single-substrate environment as specified by  $n$  in equation 6. The change in curve shape and properties effected by a 10-fold increase or reduction in porin concentration is shown as well. Shown in Figure A.4B through G are changes in this concentration-velocity relationship at steady state by the following additional cytoarchitectural parameters: permease cooperativity, permease concentration, size of the active site, value for the translation coefficient, concentration of metabolic enzymes in the cytoplasm, and mean kinetic properties of cytoplasmic enzymes.

**Quantitative effects.** The effect of changing cytoarchitectural parameters by specific amounts can be seen by comparing the broken lines in Figure A.4 with the

central curves. These were used to obtain the change in kinetic parameters with respect to the change in cytoarchitecture (Table A.4).

The porin concentration influences nutrient flux into the periplasm and depends on the species examined. A change from a ratio of 0.002 between measured flux and that calculated for an organism without outer membrane resistance (Martinez et al. 1992) had only a moderate effect on the specific affinity ( $v/[S]$ ) at particular concentrations of substrate (Figure A.4A and Table A.4). The maximal affinity was little affected by porin concentration because rates were metabolism-limited, as discussed below.

Changes in substrate-proton cooperativity with departure from the theoretical Hill constant value of 2 had a major effect Table A.4. Proportional change in kinetic parameters for whole cells by quantitative change in isolated cytoarchitectural properties calculated as an effect on both specific affinity and the size of the substrate threshold, i.e., the substrate concentration necessary for endergonic transport (Figure A.4B; Table A.4). Maximal velocity remained constant (Figure A.4C) as rates became dependent on substrate processing time ( $1/k_{\text{cat}}$  for cytoplasmic enzyme concentration,  $[E]$ ) at the larger concentrations of substrate.

Permease concentration affected the specific affinity only marginally (Figure A.4B) because flux was again largely controlled by enzyme concentration. Specific affinity increased with the active-site area below a diameter of 6 Å ( $r_s = 0.3$  nm). Larger

permease sites shifted limitation to enzyme concentration, and there was no effect on the value of  $V_m$  (Figure A.4D) due to flux control by the limited amounts of  $E$ .

An increase in the translation coefficient effected an increase in specific affinity, particularly with an  $L$  of  $<2.5$  g of cells  $\cdot$  h liter<sup>-1</sup> (Figure A.4E), due to the increase in the internal substrate concentration-driving force with increases in the intercellular concentration of substrate. At higher concentrations, rates again were truncated due to limitation by the metabolic enzyme concentration of the cell.

Additional metabolic enzymes had a moderate effect on specific affinity because of an improved balance between permease and enzyme concentrations over the base calculation when  $[S]$  was large, but there was a greater effect on maximal rate as the constraint to substrate flow was reduced (Figure A.4F). When the affinity of the enzymes changed, so did that of the organisms, while  $V_m$ , set by the number of enzyme molecules and their catalytic constants, was unaffected (Figure A.4G). In Figure A.4H, the effect of permease concentration on specific affinity is shown together with a 3.7-fold increase in enzyme concentration over that in Figure A.4F. This effect alleviated much of the constraint of enzyme concentration on specific affinity, so that changes in permease concentration became 12-fold more effective in generating nutrient flux.

## A.5 Discussion

**Specific affinity measurements.** The comparison of specific affinities obtained from affinity plots of *in situ* data showed that these data (calculated by  $v/[S]$ ) remained only lightly affected by background substrate, as predicted by the theory. Thus, improved values for the specific affinities of both natural and defined populations can be obtained from rates of radiolabeled substrate uptake where nutrient concentrations are too low for accurate measurement. In the absence of a substrate threshold, the effect of background substrate on the specific affinity becomes significant only when the total concentration is near or above the affinity constant ( $K_a$ ). For example, if  $[S_n]$  is 1  $\mu\text{g/liter}$  and  $K_a$  is only 2  $\mu\text{g/liter}$ , the computed underestimate in the base specific affinity ( $a^\circ_s$ ) is 45%. However, if  $K_m$  is taken as a measure of organism affinity, the error may be many powers of 10 because the variation in  $V_m$  is so large (Button 1998). When other energy-yielding substrates are present and used by the population but do not compete with  $S_a$ , the effect will be to decrease the size of the substrate threshold. The shape of the kinetic curve cannot be determined when the concentration of background substrate approaches that of  $S_a$ , because  $S_n$  is particularly effective in reducing apparent flux at small values of  $[S]$  (cf. Figure A.2A and C). Because the hyperbolic nature of the curve (Figure A.2A) is due to isotope dilution rather than saturation, scatter in the data due to a systematical change in apparent  $[S]$  is also minimized, which could lead to false confidence in the kinetics. *In situ* specific affinities (Table A.2) were similar to those of the isolate measured under conditions of starvation. The absolute flux of a particular nutrient, as calculated from specific affinity, can be determined only to the accuracy that the concentration of

substrate and population size or mass are known. Ambient concentrations for many substrates have been measured, such as the amino acids here, and flow cytometry reduces error in biomass measurements (Robertson et al. 1998). *In situ* microbial activities toward a particular substrate can therefore now be accurately compared from apparent specific affinity data. Also, reasonable estimates of nutrient fluxes can be obtained for substrates that can be chemically measured from the specific affinity of the population.

**Interpretations of kinetic data.** The calculated doubling time for “*M. arcticus*” of 34 days with a single substrate at 1  $\mu\text{g/liter}$  together with stimulation by auxiliary substrate, and inhibition of transport at only 17  $\mu\text{g/liter}$ , was consistent with low-capacity systems that necessarily saturate at very small concentrations. Thus, the number of substrates ( $n$ ) in equation 3 must be large; 34 substrates at 1  $\mu\text{g/liter}$  are needed for a doubling time of 1 day. This large number of necessary substrates is consistent with the appearance of more than 100 transport-associated genes in many species of aquatic bacteria (<http://www.tigr.org/~ipaulsen/>). Upper estimates of *in situ* growth rates exceed 1 per day (Paulsen et al. 2000), while many substrate concentrations are likely to be smaller than 1  $\mu\text{g/liter}$ . This fact suggests that even more different utilizable substrates are present and used by most bacteria. That the affinity constant ( $K_a$ ) is small can be due either to the ability to collect, transport, and process substrate so that  $V_m$  is approached at low  $[S]$  or to low downstream enzyme capacity so that product inhibition limits the effective catalytic constants (cf. Figure A.4C and F). The increase in both specific affinity and maximal velocity by auxiliary substrates in the laboratory system (Figure A.3) was

attributed to an increase in the membrane potential produced by the multiple substrate-adapted species. That natural populations were not stimulated by cosubstrate addition is consistent with a strong barrier to active transport from both the low temperature and the low membrane potential associated with small concentrations of substrate. Saturating concentrations for both the oligobacterial isolate and *in situ* activity were exceedingly small compared to most determinations (Button 1998), with  $K_a$  values in the microgram per liter range. Specific affinities were very small as well. In contrast to kinetic data from common laboratory cultures (Button 1985, and Button 1998), these data show limited ability to transport substrate at growth-sustaining rates, particularly when a single substrate is supplied as the sole carbon and energy source. Further, a membrane potential is needed, and the need may remain unsatisfied when there are few substrates at small concentrations unless an energy reserve has been stored and sustained. Preferences for tested substrates, according to  $a^{\circ}_s$ , were rather similar. This similarity was also evident for the mixture, interpreted as use through separate pathways, with the overall value remaining constant due to division by the sum of the concentrations of the number of substrates supplied. The net flux should increase in accord with equation 3, consistent with a necessity for most environmental bacteria to use numerous substrates simultaneously. This need for multiple substrates decreases the number of available metabolic niches, leading to the single-digit number of dominant species in common samples according to terminal restriction fragment length polymorphism (unpublished data).



**Flux calculations.** Use of a sequential solution for calculating flux through a multistep process was rationalized by the apparent unidirectional nature of several steps in the metabolic sequence, such as intermediate and macromolecule biosynthesis, steps that are either strongly exergonic or mechanistically irreversible due to physical partitioning. Effects of such irreversible steps on the associated rate constants may be anticipated from the Haldane relationship (Haldane 1930) that relates the equilibrium constant of a reaction ( $K_{eq}$ ) to its kinetic constants. Simplifying, the active transport step to a bimolecular reaction between periplasmic substrate and permease molecules with instantaneous movement to the cytoplasm gives the following equation (Figure A.1):  $K_{eq} = V_1K_c/V_2K_m$ , where  $V_1$  and  $V_2$  are the maximal forward and reverse rates and  $K_m$  and  $K_c$  are the associated Michaelis constants. Converting the kinetic constants to rate constants (Plowman 1972) and setting the collection rate of cytoplasmic protons by permease in the alkaline electronegative environment at 0 to render the rate irreversible gives the following equation (equations 49 to 51 at <http://www.ims.uaf.edu/fcm-kinetics/kinetics-derivations.pdf>):  $K_{eq} \approx k_1^{2k_3}$ , where  $k_1$  and  $k_3$  are rate constants for reaction steps. This equation formalizes the situation where, for irreversible sequences, flow depends on the concentrations and catalytic constants of the enzymes together with the concentrations of the reactants. Resistances of downstream concentrations to forward rates were taken as integral components of the associated kinetic constants because hyperbolic kinetics remain hyperbolic even in the presence of product inhibition (Plowman 1972). The magnitude of the back reaction rate constant  $k_2$  is essential to the calculation of  $K_m$  from the Michaelis-Menten equation, but it does not necessarily mean that there is formation of

substrates and uncombined permease from the ternary complex. Hyperbolic kinetics may also be derived from the residence time needed to move substrate through the permease, time during which an additional substrate molecule may not be accepted (6; equations 12 to 30 at <http://www.ims.uaf.edu/fcm-kinetics/kinetics-derivations.pdf>). Thus, the absence of a back reaction does not preclude saturation kinetics.

**Cytoarchitectural effects.** Among the major calculated influences was the effect of the Hill constant on the substrate threshold and thus the specific affinity at small concentrations of substrate. Because of the interactive effects of transporter concentration and membrane potential, this effect should be diminished by auxiliary chemical potential-generating substrates. In low-activity systems, such as winter seawater or starved cultures, the magnitude of the Hill constant should be important, since small values can increase the concentrations of substrate necessary for transport.

A unique kinetic theory for microbial growth, as opposed to one borrowed from enzyme kinetics, was further supported by temperature studies. Large *in situ* activation energies for transport of 211 kJ/mol during the onset of the spring bloom in the Gulf of Alaska and 70 to 90 kJ/mol during various seasons in Harding Lake, Alaska, were observed (unpublished data). These activation energies were well above the 40 kJ/mol usually observed for either isolated enzymes (Haldane 1930) or nutrient-sufficient microbial growth (Felip et al. 1996). Acceleration of each step due to warming increases pool concentrations for the succeeding enzymatic reaction, which is temperature

accelerated, and increases the temperature effect according to the number of steps in the sequence. And all steps in a metabolic sequence, according to the flux control theorem (Brown et al. 1994), participate in rate control so that control is spread among fast as well as slow steps (de Vienne et al. 2001). During nutrient limitation, the temperature effect can be large because several steps can influence the rate, while the change of the flux associated with a single component, such as porin concentration, is small; a doubling of the porin concentration resulted in only a 1.6% change in the organism's specific affinity (Table A.4). The concentration of transporters in bacteria and other cells remains unmeasured; however, estimates from electrophoretically separated inducible membrane proteins gave specific affinities near values reported here, assuming specified resistance from the outer membrane and more from steps downstream. This result supports the formulations of molecular collision frequency incorporated into equation 8. The formulations describe far faster movement of dissolved substrates to active sites than does traditional Fickian diffusion. This effect had been observed much earlier from the weight loss of leaves due to the diffusion of water through stomata (A. Koch, personal communication) and is also expressed as the cage effect that enhances calculated rates of enzymatic reaction (Amdur et al. 1966). The calculation of maximal velocity from equation 9 also depends on the effective residence time of the substrate in the permease (the reciprocal of  $k_{\text{cat}}$ ) together with permease concentration. Catalytic constants for permeases are unknown, so values for complex enzymatic reactions were used. That different cellular components are required to specify specific affinity and maximal velocity (equations 8 and 9) demonstrates that effectors of flux control in a multistep

pathway need not be the same step at different concentrations. This is an advantage of equation 4 for describing nutrient flux. For example, the effect of variable permease concentration among species on specific affinity or the effect of additional substrate on maximal velocity through induction of additional enzyme is easily accommodated, as demonstrated in Figure A.4. The diameter of the active site was estimated from the diameter of the substrate molecule; however, the effective value remains unknown. The diameter had a major effect on specific affinity, but its effectiveness was truncated here on the large side by the limitation of flux due to a small downstream  $[E]$  (Figure A.4D). Transport involves the collision of protons as well as substrate with the active site, increasing the order of reaction from second to third, depending on the residence time of protons in the permease following collision. While low ( $10^{-8}$  M) external concentrations of  $H^+$  might be expected to reduce the specific affinity, a fourfold increase in  $a_s$  was observed with an increase in pH (data not shown). Neglecting pH effects on the permease, proton limitation alone should have produced the opposite effect. The  $[S_e]$  at steady state depends on saturable input from transport (equation 4), product inhibition of transport that was taken as an inherent component of the kinetic constants in the forward direction, and losses due to  $Sc$  metabolism and leakage. Given the likely limited permease concentration for any specific substrate ( $[S_i]$ ) together with the environmentally small values of  $[S_i]$ , the resulting transport rate will be low. Therefore, translation to pool concentration is likely to result in much smaller concentrations than are measured in commonly cultivated organisms. When the resulting pool concentrations are less than  $K_m$  for the enzymes,  $L$  should strongly affect the whole-cell affinity, as the calculations

showed (Figure A.4E). The use of cytoplasmic substrate was formulated with Michaelis-Menten kinetics and recast to specify the unsaturated and saturated rates with independent parameters (equation 10). The cytoplasmic enzymes were assumed to be a solution of enzymes whose catalytic rates could be approximated by hyperbolic kinetics, i.e., without threshold.

**Component balance.** The relative effectiveness ( $\epsilon$ ) of model components on the specific affinity in this metabolic enzymerestricted system (Table A.4) in decreasing order was as follows: membrane potential > cytoplasmic enzyme concentration > metabolic enzyme affinity > permease concentration > effective permease site diameter > translation coefficient > porin concentration. Decreasing the permease concentration 10-fold to 50 molecules per cell allowed permease content to become dominant in affinity control (cf. Figure A.4H and C). Oligobacteria have special need for biochemical conservation, due to limited resources. Increasing the permease concentration is of greater advantage than increasing the enzyme concentration because the sequences of unique enzymes are longer in the catabolic and anabolic pathways than in the transport process, and their dilute cytoarchitecture (Robertson et al. 1998) is thus explained. The permease concentration was particularly effective in reducing the substrate threshold when metabolic enzymes were restricted because of the additional membrane potential generated for transport. The substrate threshold became far less significant in the absence of a requirement for cooperativity with a cosubstrate, such as hydrogen ions, and the kinetic curve became more nearly hyperbolic. This large threshold resulted from model

conditions of limitation by a single substrate. It will decrease in proportion to additional utilizable substrates at microgram per liter concentrations. But the thresholds may be significant even in multisubstrate systems, such as those of dormant cold-seawater organisms during warming (Table A.1). There, the large activation energies associated with small specific affinities observed were consistent with sufficient transport being generated by warming both to form a membrane potential and to load pools that contain temperature-affected enzymes. The membrane potential necessary to prime active transport may also be generated in mixotrophic organisms by the proteorhodopsin system, as indicated by a wide distribution of the related genes (de la Torre 2003).

The specific affinity for the model organism over a range of concentrations (Figure A.5) was calculated from the central distribution of cytoarchitectural components of Figure A.4 as a function of nutrient concentration to suggest changes in factors controlling the rates. Energy levels dominate at low substrate concentrations because nutrient accumulation is thermodynamically impossible without energy. This result suggests that the delay in bacterial activity during springtime could be due to the need of a membrane potential for substrate transport together with the need for transported substrate to generate a membrane potential. At intermediate concentrations of substrate, both the permease concentration and the enzyme concentration of the cell help to control organism affinity. At high nutrient concentrations, unspecified and uninvestigated macromolecular processes, such as cell wall formation, may limit net rates of growth at values characteristic of the species. Alternatively, the dominant small-genome forms may

lack efflux pumps that prevent inhibition by common substrates such as amino acids at high concentrations (I. Paulsen, personal communication). Specific affinities calculated from Monod kinetics are also shown to demonstrate limitations imposed by linking the kinetics of a heterogeneous system to a single step. Thus, one might use the Michaelis constant to suggest concentrations where substrates become limiting but not to indicate the ability of a culture, population, or permease to transport and collect that substrate, as indicated by the disparity between specific affinity and  $K_m$  values in Table A.4. Instead, the data argue that the ability to sequester substrates can be reported with the least ambiguity by a specific affinity. Transport capacity is then independently expressed by maximal velocity, since the two kinetic constants can be controlled at different points in the transport-metabolism sequence. A result of the kinetics calculated for Figure A.4 was that, with the assumptions and data specified, they matched measurements from whole cells reasonably well (cf. Table A.2 and A.3 and Figure A.4) without adjustments. This agreement was by chance due to the large uncertainty in kinetic and cytoarchitectural parameters, such as those of equation 8. However, the effect of any enzyme-catalyzed step on the flux through a metabolic sequence decreases inversely with the number of steps in that sequence (Brown et al. 1994), so error in formulating any single step is minimized. This may be seen here, where the change in specific affinity was only 1.6% of the change in porin concentration (Table A.4). Yet the data demonstrated satisfactory model function, considering the good agreement between theoretical and measured rates. These data and calculations demonstrate that bacterial proteomes are mosaics whose cross-species differences affect nutrient utilization through variation in protein

concentration as well as identity. Minimal size increases the optimal surface-to-mass ratio and decreases susceptibility to predation, but small size limits both the abundance of each protein and the number of different biochemical components as set in turn by space requirements for the encoding DNA. The result is a distribution of major cytoarchitectural components that is hypothesized to approach those specified.

#### **A.6 Acknowledgements**

Support was provided by the Ocean Sciences Life in Extreme Environments program and the Arctic Sciences section of Polar Programs, both components of the National Science Foundation.



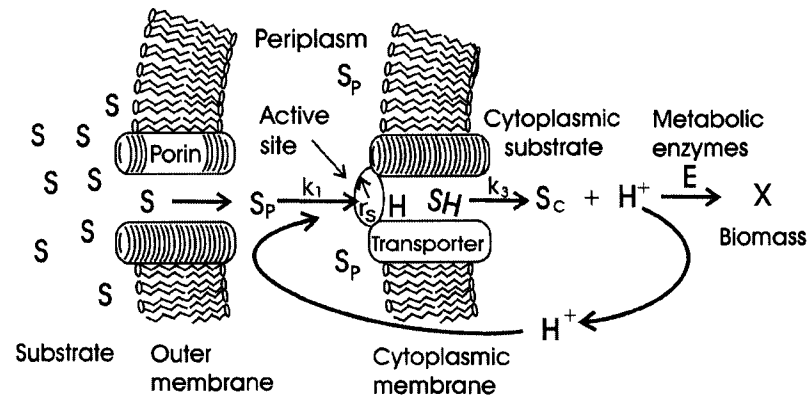


Figure A.1. Cytoarchitectural model of nutrient kinetics. Ambient nutrient  $S$  diffuses through a porin to periplasmic concentration ( $[S_p]$ ), where it combines with a proton-empowered permease having an active-site radius of  $r_s$ . Transport produces a  $[S_c]$  that generates both a proton potential and a concentration-driving force that facilitates substrate flow through an enzyme sequence ( $E$ ) to produce cell material ( $X$ ).

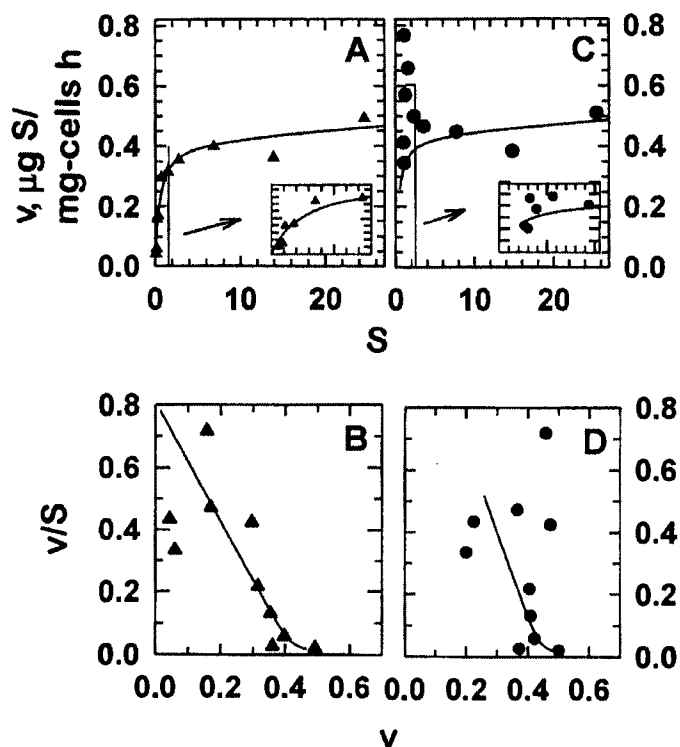


Figure A.2. Monod (A and C) and affinity (B and D) plots of leucine uptake from Resurrection Bay, Alaska, seawater at a 10-m depth in Thumb Cove during June. Panels A and B show apparent rates from the specific activity of the [ $^3\text{H}$ ]leucine added; panels C and D show rates corrected for an ambient leucine concentration ( $[S_n]$ ) of 0.85  $\mu\text{g/liter}$ . Insets expand data near the origin. Both rates were corrected for an incorporation-to-uptake ratio of cell yields ( $Y$ ) using a value of 0.45 from  $^{14}\text{CO}_2$  liberation and  $^3\text{H}$  incorporation rate data. When fit to the equation  $v = V_m[S]/(K_a + [S]) + k_{\text{ind}}[S]$ , the parameters for observed (A and B) and  $S_n$ -corrected (C and D) rates ( $V_m$ ) were 0.42 and 0.50  $\mu\text{g}$  of leucine  $\text{mg}$  of cells $^{-1}\text{h}^{-1}$ , and  $k_{\text{ind}}$  was 0.002 and 0.003 liters  $\text{g}$  of cells $^{-1}\text{h}^{-1}$ . The affinity constants ( $K_a$ ) obtained from  $[S]$  at the half-maximal value of  $v/[S]$  and the rate  $v$  (the affinity plot abscissa) were 1.5 and 1.9  $\mu\text{g/liter}$  from panels B and D, respectively.

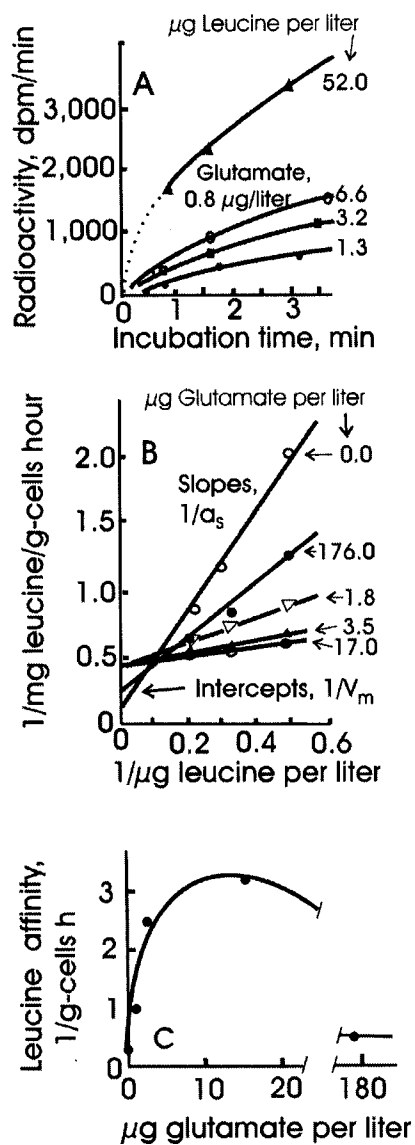


Figure A.3. Uptake of [<sup>14</sup>C]leucine by "*M. arcticus*" in the presence of glutamate. (A) Time course showing effect of leucine concentration on incorporated radioactivity. (B) Lineweaver-Burk plot based on the equation  $1/v = a^{\circ}_s(1/[S]) + 1/V_m$ , with leucine as the variable substrate and glutamate as the auxiliary substrate. Rates were taken from the best line through the data points independent of the origin. (C) Dependence of the specific affinity for leucine on the concentration of glutamate.

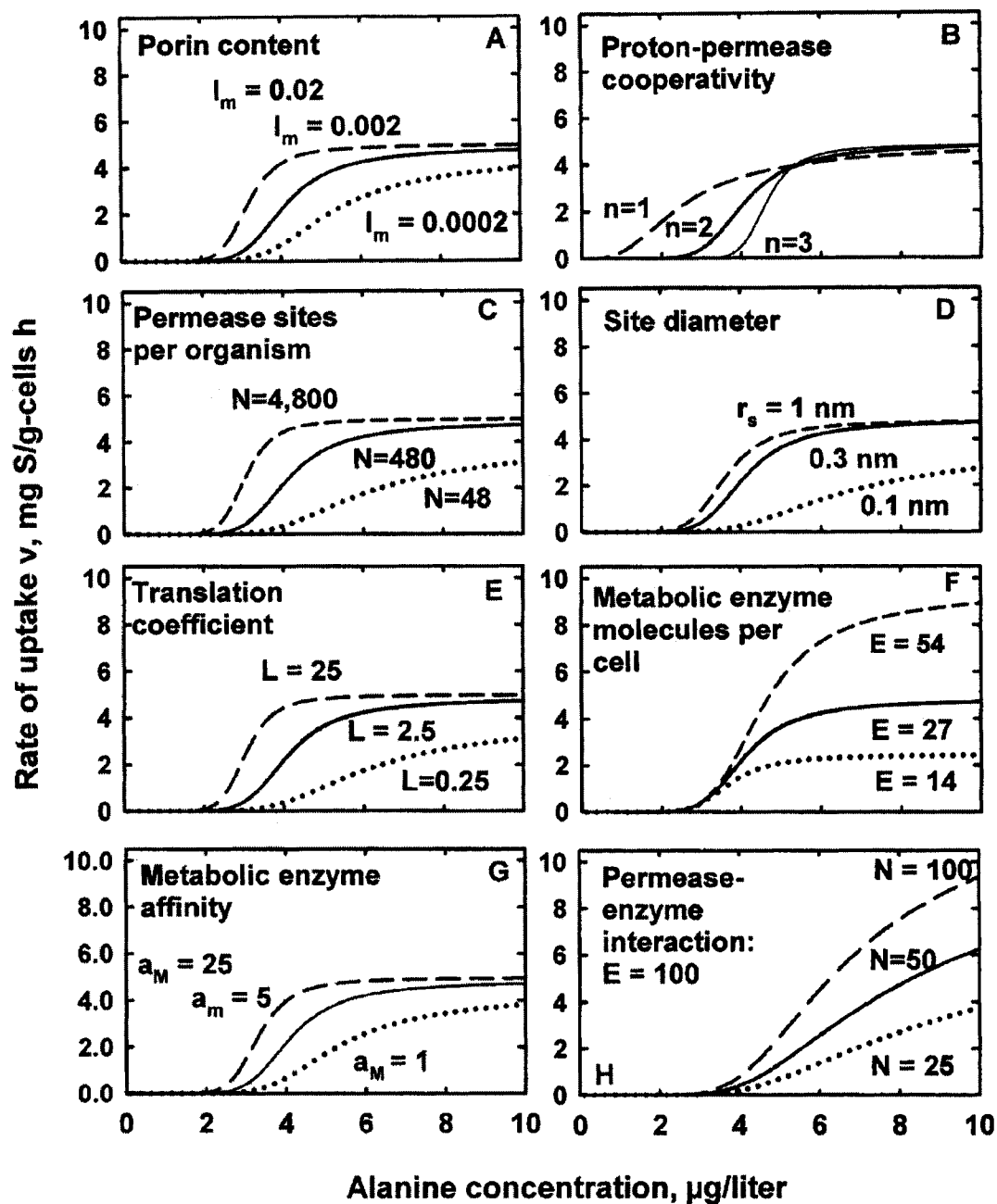


Figure A.4. Kinetics of alanine uptake by “*M. arcticus*” to 10  $\mu\text{g/liter}$ . The solid line in each panel shows the base calculation. The effects of changing each parameter by the amounts indicated are shown by the broken lines.

Table A.1. Nomenclature

Term	Definition	Examples of value(s) used
$\bar{A}$	Avogadro's number	$6.02 \times 10^{23}$ molecules/mol
$a$	$a_c$ , affinity of metabolic enzyme for cytoplasmic substrate; $a_s$ , affinity of organism for substrate ( $v/[S]$ at ambient $[S]$ and associated saturation); $a_s^0$ , base or maximal specific affinity assuming hyperbolic kinetics; $a_{smax}$ , maximal value of the affinity for nonhyperbolic kinetics	$a_c = 5$ liters g of cells <sup>-1</sup> h <sup>-1</sup> from $V_m/K_m$ , where $K_m = 10^{-3}$ M and $V_m = 5$ mg of S g of cells <sup>-1</sup> h <sup>-1</sup>
$D$	Molecular diffusion constant for $[S]$	$9 \times 10^{-6}$ cm <sup>2</sup> /s for alanine
$[E]$	Concentration of cytoplasmic enzymes	Defined by $V_m$ and $k_{cat}$ for the conversion of cytoplasmic alanine to cell material
$e$	Effectiveness factor	Change in kinetic parameter/change in cytoarchitectural parameter
$i$	A particular $S$ among $n$ total	Near 1 $\mu$ g/liter for many aquatic substrates
$k$	Rate constant for reaction steps (odd, forward; even, back); $k_{cat}$ , catalytic constant; $k_{ind}$ , induction constant for increased metabolic capacity with the concentration of ambient substrate	$k_{cat} = 86$ mol of substrate transformed mol of protein <sup>-1</sup> s <sup>-1</sup> (20); $k_{ind} = 60$ liters g of cells <sup>-1</sup> h <sup>-1</sup> gives a threshold concentration of 2 $\mu$ g liter <sup>-1</sup>
$K$	$K_a$ (affinity constant), $[S]$ at $a_s^0/2$ ; $K_{eq}$ , equilibrium constant; $K_{ind}$ , induction or stimulation constant of added substrate; $K_m$ , (Michaelis constant), $[S]$ at $V_m/2$ ; $K_{\Delta\psi}$ , membrane potential constant; $K_{\Sigma S}$ , multisubstrate stimulation constant, concentration for half maximal increase; $K_{HS}$ , proton-substrate cooperativity constant	$K_a = 4$ $\mu$ g of S liter <sup>-1</sup> for alanine; $K_m = 890$ mg of $[S_c]$ /liter for alanine; $K_{\Delta\psi}$ (value of $\Delta\psi$ at $[S] = 5$ $\mu$ g liter <sup>-1</sup> in Hill equation with $n = 2$ )
$L$	Translation coefficient from flux to concentration of cytoplasmic substrate	2.5 g of cells $\cdot$ h/liter to give $[S_c]$ in mg/liter
$M$	Molecular weight	89 Da for alanine
$\mu$	Specific rate of growth	$8.5 \times 10^{-4}$ h <sup>-1</sup> for in situ limitation by leucine
$N$	Number of molecules of a particular permease; $N_a$ , number of $\Delta\psi$ -activated molecules	Molecules cell <sup>-1</sup> , 480 from a 60,000-molecular-weight protein (43) when 1% of the membrane protein mass is the permease in question and cell membrane comprises 1% of the dry cell mass
$n$	Hill constant for positive cooperativity	Dimensionless; $n = 2$ from cooperativity between protons and S
$\Delta\psi$	Chemical potential of ions that can be involved in permease activity for solute transport	Maximal value, 150 mV (22)
$\rho$	Organism density	1.03 g of cell material cm <sup>-3</sup> (39)
$Q_{10}$	Factor change in rate with a change in temperature of 10°C	Dimensionless; 2.8
$R_m$	Resistance of outer membrane to molecular diffusion of substrate as ameliorated by porins	$2 \times 10^{-3}$ times the expected rate in the absence of resistance to porins (28)
$r$	Radius; $r_s$ , radius of a spherical cell; $r_a$ , effective radius of an active site	$r_s$ , $0.4 \times 10^{-4}$ cm; $r_a$ , $3 \times 10^{-8}$ cm
$[S]$	Concn of a particular substrate such as alanine; $[S_a]$ , concn of added substrate; $[S_c]$ , concn of cytoplasmic substrate; $[S_e]$ , concn of natural or background substrate; $[S_p]$ , concn of periplasmic substrate	$[S] = 0$ to $1 \times 10^{-5}$ g of alanine liter <sup>-1</sup> in kinetic curves for whole cells
$v$	Rate of S uptake by a cell population with biomass $X$ ; $v_R$ , rate of uptake of labeled $S_a$ retained in the presence of $S_m$ at the prevailing yield ( $Y$ ); $v_a$ , apparent rate of labeled substrate uptake in the presence of $S_m$	g of substrate g of cells <sup>-1</sup> h <sup>-1</sup>
$V$	Maximal rate for a reaction step (odd, forward; even, back); $V_m$ , maximal net rate	$V_m = 5$ mg of S g of cells <sup>-1</sup> (wet weight) h <sup>-1</sup> from initial uptake experiments
$X$	Biomass	g of cells (wet weight) liter <sup>-1</sup>
$Y$	Cell yield	g of cells produced/g of substrate consumed

Table A.2. Specific affinities for bacterioplankton in Gulf of Alaska coastal water. a. Until 19 October, substrates were at trace levels. On 13 December and thereafter, levels were at 1  $\mu\text{g/liter}$  and below. All substrates were radiolabeled. b. Affinity after the temperature was raised from 6 to 15°C over 2 h. c. Range over 24 h.

Date (1998)	Substrate <sup>a</sup>	Biomass ( $\mu\text{g/liter}$ )	Affinity (liters g of cells <sup>-1</sup> h <sup>-1</sup> )
3 May	Leucine	400	6.0 (110 <sup>b</sup> )
22 July	Leucine	340	400
10 August	Leucine	270	50-140 <sup>c</sup>
27 August	Amino acid mix	74	48
19 October	Leucine	140	30
13 December	Amino acid mix	27	4.3
13 December	Glucose	27	0.9
14 December	Glutamate	25	4.4
14 December	Leucine	25	7.4

Table A.3. Effect of cosubstrates and inhibitors on amino acid uptake by *Marinobacter arcticus*

Substrate	Unamended culture		Unique addition	Amended culture	
	Specific affinity (liters g of cells <sup>-1</sup> h <sup>-1</sup> )	$V_m$ (mg of <i>S</i> g of cells <sup>-1</sup> h <sup>-1</sup> )		Specific affinity (liters g of cells <sup>-1</sup> h <sup>-1</sup> )	$V_m$ (mg of <i>S</i> g of cells <sup>-1</sup> h <sup>-1</sup> )
Glutamate	373	0.58	Acid mix <sup>a</sup>	1,150	17
Leucine	270	7	Glutamate <sup>b</sup>	3,100	2.2
Leucine	5,900	ND <sup>e</sup>	CCCP	27	ND
Toluene	290	0.52	CCCP <sup>c</sup>	260	ND
Alanine <sup>d</sup>	288	3.4	CCCP	0.0	ND

- a. Kinetic constants were calculated from the sum of nine added amino acids.
- b.  $K_a = 3.0 \mu\text{g/liter}$ ;  $K_{\Sigma S} = 3 \mu\text{g of glutamate/liter}$  for glutamate stimulation of leucine uptake by glutamate with maximal increase in leucine specific affinity at  $17 \mu\text{g of glutamate/liter}$  (Figure A.3).
- c. Forty-five percent of the toluene uptake into cell material and  $\text{CO}_2$  was diverted to acid-nonvolatile products.
- d. Affinity was measured at  $3.9 \mu\text{g of alanine/liter}$ ; the sodium motive force affecting ionophore monensin had no effect.
- e. ND, not determined.

Table A.4. Proportional change in kinetic parameters for whole cells by quantitative change in isolated cytoarchitectural properties calculated as an effectiveness factor<sup>a</sup>.

<b>Structural property</b>	<b>Specific affinity</b>	<b>Maximal velocity</b>	<b>Michaelis constant</b>	<b>Substrate threshold</b>
Porin concentration	2	0	-3	-2
Hill constant	-100	0	17	66
Permease concentration <sup>b</sup>	2	0	-3	-3
Permease concentration <sup>c</sup>	25	7	-3	-3
Site diameter	11	0	-33	-19
Translation coefficient	2	2	-2	-3
Enzyme concentration	31	100	-20	-3
Enzyme affinity	15	0	-10	-2.6

- a. All table values are percent changes in effectiveness factor,  $\epsilon$ .
- b. Variation in permease-dependent transport rates, where rates are further constrained by a limited concentration of cytoplasmic enzymes (Figure A.4C).
- c. Rates with additional cytoplasmic enzymes (Figure A.4H).



**References**

- Amdur, I., and G. G. Hammes. 1966. *Chemical kinetics, principles and selected topics*. McGraw-Hill, New York, N.Y.
- Berg, H. C. 1988. A physicist looks at bacterial chemotaxis. *Cold Spring Harbor Symp. Quant. Biol.* 53:1–9.
- Brown, G. C., and C. E. Cooper. 1994. The analysis of rate limitation within enzymes: relations between flux control coefficients of rate constants and unidirectional rates, rate constants and thermodynamic parameters of single isolated enzymes. *Biochem. J.* 300:159–164.
- Button, D. K. 1985. Kinetics of nutrient-limited transport and microbial growth. *Microbiol. Rev.* 49:270–297.
- Button, D. K. 1991. Biochemical basis for whole-cell uptake kinetics: specific affinity, oligotrophic capacity, and the meaning of the Michaelis constant. *Appl. Environ. Microbiol.* 57:2033–2038.
- Button, D. K. 1998. Nutrient uptake by microorganisms according to kinetic parameters from theory as related to cytoarchitecture. *Microbiol. Mol. Biol. Rev.* 62:636–645.

Button, D. K. 2000. Abandon Michaelis-Menten? ASM News 66:510.

Button, D. K. 2002. Kinetics (microbial): theory and applications, p. 1738–1747. *In* G. Bitton (ed.), The encyclopedia of environmental microbiology. John Wiley & Sons, New York, N.Y.

Button, D. K., and B. R. Robertson. 1989. Kinetics of bacterial processes in natural aquatic systems based on biomass as determined by high-resolution flow cytometry. Cytometry 10:558–563.

Button, D. K., and B. R. Robertson. 2000. Effect of nutrient kinetics and cytoarchitecture on bacterioplankton size. Limnol. Oceanogr. 45:499–505.

Button, D. K., and B. R. Robertson. 2001. The distribution of DNA among bacterioplankton and among *Cycloclasticus oligotrophus* cells growing at various rates by flow cytometry of DAPI-stained organisms. Appl. Environ. Microbiol. 67:1636–1645.

Button, D. K., B. R. Robertson, and K. S. Craig. 1981. Dissolved hydrocarbons and related microflora in a fjordal seaport: sources, sinks, concentrations, and kinetics. Appl. Environ. Microbiol. 42:708–719.

Button, D. K., B. R. Robertson, P. W. Lepp, and T. M. Schmidt. 1998. A small, dilute-cytoplasm, high-affinity, novel bacterium isolated by extinction culture and having kinetic constants compatible with growth at ambient concentrations of dissolved nutrients in seawater. *Appl. Environ. Microbiol.* 64:4467–4476.

Button, D. K., D. M. Schell, and B. R. Robertson. 1981. Sensitive and accurate methodology for measuring the kinetics of concentration-dependent hydrocarbon metabolism rates in seawater. *Appl. Environ. Microbiol.* 41:936–941.

Cleland, W. W. 1975. Partition analysis and the concept of net rate constants as tools in enzyme kinetics. *Biochemistry* 14:3220–3224.

Dashper, S. G., L. Brownfield, N. Slakeski, P. S. Zilm, A. H. Rogers, and E. C. Reynolds. 2001. Sodium ion-driven threonine transport in *Porphyromonas gingivalis*. *J. Bacteriol.* 183:4142–4148.

de la Torre, J. R., L. M. Christianson, O. Béjà, J. Heidelberg, D. M. Karl, and E. F. DeLong. 2003. Proteorhodopsin genes are distributed among divergent marine bacterial taxa. *Proc. Natl. Acad. Sci.* 100: 12830-12835.

de Vienne, D., B. Bost, J. Fievet, and C. Dillmann. 2001. Optimization of enzyme concentrations for unbranched reaction chains: the concept of combined response coefficient. *Acta Biotheor.* 49:341–350.

Dunbar, J., Takala, S., Barns, S.M., Davis, J.A, and Kuske, C.R., 1999. Levels of bacterial community diversity in four arid soils compared by cultivation and 16S rRNA gene cloning. *Appl. Environ. Microbiol.* 65: 1662-1669.

Felip, M., M. L. Pace, and J. J. Cole. 1996. Regulation of planktonic bacterial growth rates: the effects of temperature and resources. *Microb. Ecol.* 31:15–28.

Haldane, J. B. S. 1930. *Enzymes*. Longmans, Green and Co., London, United Kingdom.

Hatanaka, T., T. Negishi, M. Kubota-Akizawa, and T. Hagishita. 2002. Purification, characterization, cloning and sequencing of phospholipase D from *Streptomyces septatus* TH-2. *Enzyme Microb. Technol.* 31:233–241.

Henrichs, S., and J. Farrington. 1987. Early diagenesis of amino acids and organic matter in two coastal marine sediments. *Geochim. Cosmochim. Acta* 51:1–15.

Kashket, E. R. 1985. Effects of  $K^+$  and  $Na^+$  on the proton motive force of respiring *Escherichia coli* at alkaline pH. *J. Bacteriol.* 163:423–429.

Koshland, D. E. J., and H. Kambiz. 2002. Proteomics and models for enzyme cooperativity. *J. Biol. Chem.* 277:46841–46843.

Law, A. T., and D. K. Button. 1977. Multiple-carbon-source-limited growth kinetics of a marine coryneform bacterium. *J. Bacteriol.* 129:115–123.

Law, A. T., and D. K. Button. 1986. Modulation of the affinity of a marine pseudomonad for toluene and benzene by hydrocarbon exposure. *Appl. Environ. Microbiol.* 51:469–476.

Law, A. T., B. R. Robertson, S. S. Dunker, and D. K. Button. 1976. On describing microbial growth kinetics from continuous culture data: some general considerations, observations, and concepts. *Microb. Ecol.* 2:261–283.

Lendenmann, U., M. Snozzi, and T. Egli. 1996. Kinetics of the simultaneous utilization of sugar mixtures by *Escherichia coli* in continuous culture. *Appl. Environ. Microbiol.* 62:1493–1499.

Martinez, M. B., F. J. Schendel, M. C. Flickinger, and G. L. Nelsestuen. 1992. Kinetic properties of enzyme populations *in vivo*: alkaline phosphatase of the *E. coli* periplasm. *Biochemistry* 31:11500–11509.

Michaelis, L., and M. M. Menten. 1913. Die Kinetik der Invertinwirkung. *Biochem. Z.* 49:333–369.

Monod, J. 1942. *Recherches sur la croissance des cultures bacteriennes*. Hermann, Paris, France.

Morse, R. W. 1963. Fluid-flow properties of porous media and viscosity of suspensions, p. 2–194. *In* D. E. Gray (ed.), *American Institute of Physics handbook*, 2nd ed. McGraw Hill, New York, N.Y.

Nystrom, T., and N. Gustavsson. 1998. Maintenance energy requirement: what is required for stasis survival of *Escherichia coli*? *Biochim. Biophys. Acta* 1365:225–231.

Paulsen, I. T., L. Nguyen, M. K. Sliwinski, R. Rabus, and M. H. Saier, Jr. 2000. Microbial genome analyses: comparative transport capabilities in eighteen prokaryotes. *J. Mol. Biol.* 301:75–100.

Paulsen, I. T., M. K. Sliwinski, and M. H. Saier. 1998. Microbial genome analysis: global comparisons of transport capabilities based on phylogenies, bioenergetics and substrate specificities. *J. Mol. Biol.* 277:573–592.

Plowman, K. M. 1972. Enzyme kinetics. McGraw-Hill, New York, N.Y.

Radisky, D., and J. Kaplan. 1999. Regulation of transition metal transport across the yeast plasma membrane. *J. Biol. Chem.* 274:4481–4484.

Robertson, B. R., and D. K. Button. 1979. Phosphate-limited continuous culture of *Rhodotorula rubra*: kinetics of transport, leakage, and growth. *J. Bacteriol.* 138:884–895.

Robertson, B. R., and D. K. Button. 1987. Toluene induction and uptake kinetics and their inclusion in the specific-affinity relationship for describing rates of hydrocarbon metabolism. *Appl. Environ. Microbiol.* 53:2193–2205.

Robertson, B. R., D. K. Button, and A. L. Koch. 1998. Determination of the biomasses of small bacteria at low concentration in a mixture of species with forward light scatter measurements by flow cytometry. *Appl. Environ. Microbiol.* 64:3900–3909.

Scarrett, M.G., Levasseur, M., Schultes, S., Michaud, S., Cantin, G., Vezina, A., Gosselin, M., and Mora, S.J. de., 2000. Production and consumption of dimethylsulfide (DMS) in North Atlantic waters. *Mar. Ecol. Prog. Ser.* 204: 13-26.

Simon, M., and F. Azam. 1989. Protein content and protein synthesis rates of planktonic bacteria. *Mar. Ecol. Prog. Ser.* 51:201–213.

van de Vossenberg, J. L. C. M., A. J. M. Driessen, M. S. da Costa, and W. N. Konings. 1999. Homeostasis of the membrane proton permeability in *Bacillus subtilis* grown at different temperatures. *Biochim. Biophys. Acta* 1419: 97–104.

Strom, S.L., 2000. Bacterivory: interactions between bacteria and their grazers, p. 351-386. *In* D. L. Kirchman (ed.). *Microbial ecology of the oceans*. John Wiley, New York.

Taylor, G.T., 1982. The role of pelagic heterotrophic protozoa in nutrient recycling: a review. *Annls Inst. Oceanogr. Paris* 58: 227-241.

Thurman, E.M., 1985. *Organic geochemistry of natural waters*. Martinus/Dr. W. Junk. Publishers. Dordrecht. The Netherlands.

Watanabe, K., and Baker, P.W., 2000. Environmentally relevant microorganisms. *Journal of Bioscience and Bioengineering* 89: 1-11.

White, D. (ed.). 2000. *The physiology and biochemistry of prokaryotes*. Oxford University Press, New York, N.Y.

Wright, C. A., R. Seckler, and P. Overath. 1986. Molecular aspects of sugar: ion cotransport. *Annu. Rev. Biochem.* 55:225–249.



Wright, R. T., and J. E. Hobbie. 1965. The uptake of organic solutes in lake water. *Limnol. Oceanogr.* 10:22–28.

Yager, P. L., and J. W. Deming. 1999. Pelagic microbial activity in an arctic polynya: testing for temperature and substrate interactions using a kinetic approach. *Limnol. Oceanogr.* 44:1882–1893.

**Appendix B: The Effect of Temperature on Nutrient Limited Cell Yield**  
**(in preparation)**

**Abstract**

Bacterial growth efficiencies, 11 to 39%, are reported for aquatic systems. These are significantly less than those for bacterial cultures, which are more than twice as large. However, these efficiencies bring into questions previous assumptions about cellular biomass and special routes of substrate processing. Using *in situ* measurements cell yields from amino acid mixtures were actually closer to 50% and 70%, and were found to increase with temperature. The maximum value for cell yield was 0.70 g cell carbon per g amino acid carbon consumed. Our exploratory measurements of secondary productivity were even higher which, if correct, could affect concepts of carbon cycling. Moreover, specific affinity theory, which describes nutrient flux as a linked sequence of diffusion, transport, bioenergetic, and enzymatic steps, appears able to accommodate the observed temperature effect. Theoretical treatments of microbial function show major effects of temperature on biochemically effected flux. However, the environmentally relevant condition of nutrient limitation is less well developed. The effects of temperature on Michaelis constants have been previously described; however, ambiguities in the dependency of  $K_m$  on  $V_{max}$  exist. A theory is presented that expands specific affinity theory to accommodate the effects of temperature on substrate distributions associated with nutrient limited cell yield.

**Appendix C: Annual Dynamic of Microbial Processes in a Near-arctic Lake  
(in preparation)**

**Abstract**

Organic and mineral aquatic nutrients are metabolized at the expense of solar energy, which is subsequently dissipated in the carbon cycle. Polar regions are subject to large annual variation in this energy input, resulting in large variations in aquatic microbial activity. This activity supports secondary productivity and helps control climate affecting greenhouse gases. Microbial systems in question appear to adapt to rapidly changing conditions to provide a ready supply of minerals for rapid activity during the short summer, while maintaining in a low energy state during winter. This suggests that the carbon cycle acts like a flywheel; it maintains metabolic inertia, by storing metabolic intermediates and the related enzymes. Analytical and theoretical advancements have identified significant constraints to carbon cycling during the annual light cycle at high latitudes. Specific affinity theory predicts that in vast marine and freshwater systems, previously undescribed nutrient's thresholds for microbial activity become significant during winter. The existence of such thresholds is corroborated by large biannual changes in *in situ* specific affinities, which are alleviated during springtime with a surge in microbial activity. During springtime, warming increased specific affinities with activation energies that were larger than common values for substrate-sufficient cells and for isolated enzymes. This was attributed to a threshold in the concentration of substrate, which is dependent on external source energy. Warming

then increases the rate of each step in the metabolic sequence to give larger concentrations of each intermediate, which amplifies the temperature effect. This exponentiation of rates with temperature helps explain the lag and subsequent bloom in bacterial activity observed during the spring bloom.

### Appendix D: PCR Protocol with Promega PCR Core Systems

1. Combine the following components, as listed in Table 1, in sterile, 0.5–0.6ml microcentrifuge tubes. Amplification reactions may be scaled up or down as necessary.

Table D.1. Reaction Volumes and Final Concentrations of the PCR Components.

Component	Component Volume	Final Concentration
MgCl <sub>2</sub> , 25mM Solution	3μl	1.5mM
Thermophilic DNA Polymerase		
10X Reaction Buffer, MgCl <sub>2</sub> -Free	5μl	1.0X
PCR Nucleotide Mix, 10mM each	1μl	200μM each
Upstream Control Primer	5–50pmol	0.1–1.0μM
Downstream Control Primer	5–50pmol	0.1–1.0μM
<i>Taq</i> DNA Polymerase, 5u/μl	0.25μl	1.25u/50pl
template DNA	variable	<0.5pg/50μl
Nuclease-Free Water to a final volume of	50μl	

2. If using a thermal cycler without a heated lid, overlay the reaction mix with 1–2 drops (approximately 50μl) of mineral oil to prevent evaporation during thermal cycling. Centrifuge the reaction mix in a microcentrifuge for 5 seconds.

Step	Temperature	Time	Number of Cycles
Initial Denaturation:	95°C	2 minutes	1 cycle
	↓		
Denaturation:	95°C	0.5–1 minute	25–35 cycles
Annealing:	42–65°C	1 minute	
Extension:	72–74°C	1–2 minutes	
	↓		
Final Extension:	72–74°C	5 minutes	1 cycle
	↓		
Soak:	4°C	indefinite	1 cycle

Figure D.1. Thermal cycling conditions for PCR amplification. These guidelines apply to target sequences between 200 and 2,000bp and are optimal for the Perkin-Elmer thermal cycler model 480 or comparable thermal cyclers.

- Place the reactions in a thermal cycler that has been preheated to 95°C. We recommend heating the samples at 95°C for 2 minutes to ensure that the target DNA is completely denatured. Incubation longer than 2 minutes at 95°C is unnecessary and may reduce the yield.
- Start the thermal cycling program. The cycling profile given in Figure 1 may be used as a guideline. Optimize the amplification profile for each primer/target combination.

**Reference:**

Technique Bulletin No.254 for Promega PCR Core Systems.

## Appendix E: Purification of Genomic DNA from Bacteria with Qiagen Tissue Kit

Buffer for enzymatic lysis:

- 20 mM Tris·Cl, pH 8.0
- 2 mM sodium EDTA
- 1.2% Triton® X-100
- 20 mg/ml lysozyme; add lysozyme just before use

1. Harvest cells (maximum  $2 \times 10^9$  cells) in a microcentrifuge tube by centrifuging for 10 min at  $5000 \times g$  (7500 rpm). Discard supernatant.
2. Resuspend bacterial pellet in 180  $\mu$ l enzymatic lysis buffer.
3. Incubate for at least 30 min at 37°C.
4. Add 25  $\mu$ l proteinase K and 200  $\mu$ l Buffer AL. Mix by vortexing.

Note: Do not add proteinase K directly to Buffer AL.

5. Incubate at 70°C for 30 min.
6. Add 200  $\mu$ l ethanol (96–100%) to the sample, and mix thoroughly by vortexing.

It is important that the sample and the ethanol are mixed thoroughly to yield a homogeneous solution. A white precipitate may form on addition of ethanol. It is essential to apply all of the precipitate to the DNeasy Mini spin column.

6. Pipet the mixture from step 4 into the DNeasy Mini spin column placed in a 2 ml collection tube (provided). Centrifuge at  $\geq 6000 \times g$  (8000 rpm) for 1 min. Discard flow-through and collection tube.

7. Place the DNeasy Mini spin column in a new 2 ml collection tube (provided), add

500  $\mu$ l Buffer AW1, and centrifuge for 1 min at  $\geq 6000 \times g$  (8000 rpm). Discard flow-through and collection tube.

8. Place the DNeasy Mini spin column in a 2 ml collection tube (provided), add 500  $\mu$ l Buffer AW2, and centrifuge for 3 min at  $20,000 \times g$  (14,000 rpm) to dry the DNeasy membrane. Discard flow-through and collection tube. This centrifugation step ensures that no residual ethanol is carried over during the following elution. Following the centrifugation step, remove the DNeasy Mini spin column carefully so that the column does not come into contact with the flow-through, since this will result in carryover of ethanol. If carryover of ethanol occurs, empty the collection tube and reuse it in another centrifugation step for 1 min at  $20,000 \times g$  (14,000 rpm).

9. Place the DNeasy Mini spin column in a clean 1.5 ml or 2 ml microcentrifuge tube (not provided), and pipet 200  $\mu$ l Buffer AE directly onto the DNeasy membrane. Incubate at room temperature for 1 min, and then centrifuge for 1 min at  $\geq 6000 \times g$  (8000 rpm) to elute. Elution with 100  $\mu$ l (instead of 200  $\mu$ l) increases the final DNA concentration in the elute, but also decreases the overall DNA yield.

10. Repeat elution once as described in step 9.

**Reference:**

Qiagen DNeasy Tissue Handbook.



**Appendix F: Purification of PCR Products with Amicon Microcon-PCR Centrifugal  
Filter Devices**

1. Insert the Micron-PCR sample reservoir into one of the two vials provided.
2. Pipette 400  $\mu\text{L}$  distilled water or TE buffer into sample reservoir. Add 100  $\mu\text{L}$  PCR reaction to the reservoir (0.5 ml maximum volume). Seal with attached cap. Note: smaller volumes of PCR product may be used, but the volume in the sample reservoir should always be adjusted to a final volume of 500  $\mu\text{L}$ .
3. Place assembly in a compatible centrifuge and counterbalance with a similar device.
4. Spin the Micron-PCR unit at 1000 x g for 15 minutes. Note: For optimal recovery, do not centrifuge longer than the specified 15-minutes or greater than 1000 x g.
5. Remove assembly from centrifuge. Separate vial from sample reservoir. Save filtrate until sample has been analyzed.
6. Place sample reservoir upright into a clean vial and add 20  $\mu\text{L}$  distilled water or TE buffer carefully to the end of the reservoir (Avoid touching the membrane surface).
7. Invert the reservoir into a clean vial and spin at 1000 x g for 2 minutes.

**Reference:**

Instruction Manual of Amicon Microcon-PCR Centrifugal Filter Devices.

## **Appendix G: DGGE Protocol with the Dcode™ System and Model 475 Gradient Delivery System**

### **Pre-heating the Running Buffer**

1. Fill the electrophoresis tank with 7 L of 1x TAE running buffer.

**Note:** It is recommended that the running buffer not be reused. Reusing the running buffer may affect the migration rate and band resolution.

2. Place the temperature control module on top of the electrophoresis tank. Attach the power cord to the temperature control module and turn the power, pump, and heater on. The clear loading lid should be on the temperature control module during preheating.

3. Set the temperature controller to the desired temperature: 60°C.

4. Preheat the buffer to the set temperature. It can take 1 to 1.5 hours for the system to heat the buffer up to the set temperature. Heating the buffer in a microwave helps reduce the preheating time.

### **Assembling the Parallel Gradient Gel Sandwich**

1. Assemble the gel sandwich on a clean surface. Lay the large rectangular plate down first, then place the left and right spacers of equal thickness along the short edges of the larger rectangular plate. To assemble parallel gradient gels, place the spacers so that the grooved opening of the spacers faces the sandwich clamps. When properly placed, the grooved side of the spacers and the notches will face the sandwich clamps, and the hole is located near the top of the plates.

2. Place the short glass plate on top of the spacers so that it is flush with the bottom edge of the long plate.
3. Loosen the single screw of each sandwich clamp by turning each screw counterclockwise. Place each clamp by the appropriate side of the gel sandwich with the locating arrows facing up and toward the glass plates
4. Grasp the gel sandwich firmly. Guide the left and right clamps onto the sandwich so that the long and short plates fit the appropriate notches in the clamp. Tighten the screws enough to hold the plates in place.
5. Place the sandwich assembly in the alignment slot (the slot without cams) of the casting stands with the short glass plate forward. Loosen the sandwich clamps and insert an alignment card to keep the spacers parallel to the clamps. Note: Always use the alignment slot and alignment card to set the spacers in place. Failure to use these can result in gel leakage while casting, as well as buffer leakage during the run.
6. Align the plates and spacers by simultaneously pushing inward on both clamps at the locating arrows while at the same time pushing down on the spacers with your thumbs; tighten both clamps just enough to hold the sandwich in place. Pushing inward on both clamps at the locating arrows will insure that the spacers and glass plates are flush against the sides of the clamps.
7. Remove the alignment card. Remove the sandwich assembly from the casting stand and check that the plates and spacers are flush at the bottom. If the spacers and glass plates are not flush, realign the sandwich and spacers to obtain a good seal. (Repeat steps 5–7).

8. When a good alignment and seal are obtained, tighten the clamp screws until it is finger-tight.

### **Casting Parallel Denaturing Gradient Gels**

1. Place the gray sponge onto the front casting slot. The camshafts on the casting stand should have the handles pointing up and pulled out. Place the sandwich assembly on the sponge with the shorter plate facing you. When the sandwich is placed correctly, press down on the sandwich and turn the handles of the camshaft down so that the cams lock the sandwich in place. Position the gel sandwich assembly by standing it upright.
2. One length of Tygon tubing is provided and should be cut into two 15.5 cm lengths and one 9 cm length. The longer pieces of Tygon tubing will be used to conduct the gel solution from the syringes into the Y-fitting. The short piece of Tygon tubing will conduct the gel solution from the Y-fitting to the gel sandwich. Connect one end of the 9 cm Tygon tubing to the Y-fitting and connect a luer coupling to the other end of the 9 cm tubing. Connect luer fittings onto the two long pieces of tubing. Connect the luer fittings to 30 ml syringes. Do not connect the long Tygon tubing to the Y-fitting at this time.
3. Label one of the syringes LO (for the low density solution) and one HI (for the high density solution). Attach a plunger cap onto each syringe plunger "head." Position the plunger "head" in the middle of the plunger cap and tighten enough to hold the plunger in place. Position the cap in the middle for proper alignment with the lever on the gradient delivery system. Slide each syringe into a syringe sleeve. Move the sleeve to the middle of the syringe, keeping the volume gradations visible. Make sure that the lever

attachment screw is in the same plane as the flat or back side of the sleeve. This is very important for proper attachment of the syringe to the lever. Note: Insure that the tubing is free of any gel material by pushing water through the tubing with the syringe. The tubing should be free of material before casting, remove any remaining water from the tubing.

4. Rotate the cam wheel counterclockwise to the vertical or start position. To set the desired delivery volume, loosen the volume adjustment screw. Place the volume setting indicator located on the syringe holder to the desired volume setting. Tighten the volume adjustment screw. For 16 x 16 cm gels (1 mm thick), set the volume setting indicator to 14.5.

5. From the stock solutions, pipette out the desired amounts of the high and low density gel solutions into two disposable test tubes. Optional: To visually check the formation of the gradient, add 100  $\mu$ l of DCode dye solution per 5 ml high density solution. The steps below are time-sensitive (about 7–10 minutes). Insure that steps 2 through 5 are done before proceeding further. Be thoroughly familiar with the following steps before casting the gel.

6. Add the final concentration of 0.09% (v/v) each of ammonium persulfate and TEMED solutions. The 0.09% (v/v) concentrations allow about 5–7 minutes to finish casting the gel before polymerization. Cap and mix by inverting several times. With the syringe connected to the tubing, withdraw all of the high density solution into the HI syringe. Do the same for the low density solution into the LO syringe. Note: Acrylamide is a very hazardous substance. Use caution: wear gloves and eye protection at all times. Avoid skin contact.

7. Carefully remove air bubbles from the LO syringe by turning the syringe upside down (plunger cap towards the bench) and gently tapping the syringe. Push the gel solution to the end of the tubing. Do not push it out of the tubing as loss of solution will disturb the volume required to cast the desired gel. Note: The gel solution volume should be greater than the amount set on the volume adjustment lever. For example, if the indicator setting is set at 14.5, the syringe should contain 15 ml of solution. This extra solution is needed to deliver the correct amount for casting.
8. Place the LO syringe into the gradient delivery system syringe holder (LO density side) by holding the syringe by the plunger and inserting the lever attachment screw into the lever groove. Do not handle the syringe. It will dispense the gel solution out of the syringe. Casting a parallel gel is referred to as a top filling method, so place the LO syringe on the correct side of the gradient system.
9. Carefully remove the air bubbles from the HI syringe by turning the syringe upside down (plunger cap towards the bench) and gently tapping the syringe. Push the solution to the end of the tubing. Do not push it out of the tubing as loss of solution will disturb the volume required to cast the desired gel.
10. Place the HI syringe into the gradient delivery system syringe holder (HI density side) by holding the syringe by the plunger and inserting the lever attachment screw into the lever. Do not handle the syringe. It will dispense the gel solution out of the syringe.
11. Slide the tubing from the low-density syringe over one end on the Y-fitting. Do the same for the high-density syringe.
12. Attach a 19-gauge needle to the coupling. Hold the beveled side of the needle at the

top-center of the gel sandwich and cast. For convenience, the needle can be taped in place.

13. Rotate the cam wheel slowly and steadily to deliver the gel solution. It is important to cast the gel solution at a steady pace to avoid any disturbances between the gel solutions within the gel sandwich.

14. Carefully insert the comb to the desired well depth and straighten. Let the gel polymerize for about 60 minutes.

15. Place the tubing and needle into a beaker of water and reverse the cam on the Gradient Delivery System. This will rinse the tubing and Y-fitting. Remove both syringes from the syringe holder on the gradient delivery system. Detach the syringe tubing from the Y-fitting. Run or push water out through the syringe, tubing, and Y-fitting several times to get rid of any residual gel solution. It is very important that this is done quickly after casting to avoid premature gel polymerization.

16. After polymerization, remove the comb by pulling it straight up slowly and gently.

17. Continue with Section 8 for electrophoresis.

### **Assembling the Upper Buffer Chamber**

1. Lay the inner core flat on a bench. Make sure the white U-shaped gasket on the inner core is seated properly and clear of any particles that may cause leakage, such as residual gel material.

2. After the gel has polymerized, release the gel sandwich from the casting stand by turning the camshafts 180°, to the up position, and pulling them outward. Remove the

sandwich and the comb. Note: To easily visualize the wells when loading the samples, use a permanent marker to mark the wells.

3. With the short glass plate facing the core, position the gel sandwich so that the locating pins on the core are fitted into the grooves on the outside surface of the sandwich clamps. The gel sandwich should be positioned at an angle of  $20^\circ$  with the core. Keeping this angle to a minimum will prevent distortion of the gasket while the sandwich slides into place. Note: To help insure a good buffer seal, lubricate the entire front of the core gaskets with water or running buffer prior to attaching the gel sandwich to the core. This will allow the glass plate sandwich to slide onto the gasket properly.

4. With your fingers below the latch on the core and your thumbs resting on the bottom of the sandwich clamps, gently push the gel sandwich down onto the core with one simple motion. The upper edge of the short inner glass plate should be seated against the notches of the U-shaped gasket and the tabs of each clamp should be held securely against the latch assemblies on both sides of the core

5. Turn the core to its other side and repeat steps 1–4 to attach the second gel sandwich. Note: When the gel sandwich has been properly installed, the shorter inside glass plate will be forced against the notch in the U-shaped gasket to create a leak-proof seal.

Always inspect the contact between the gasket and glass plate to make sure the glass plate is seated against the notch in the gasket and is not resting above or below this notch. Improper installation of the gel sandwich can result in buffer leakage during the run.

6. If only one gel is to be run, assemble a set of glass plates without the spacers. Place the short glass plate on top of the long glass plate. Guide the left and right clamps onto the



sandwich so that the plates fit the appropriate notches in the clamp. Insure that the bottom of the glass plates is flush. Tighten the screws enough to hold the plates in place. No further alignment is necessary. Attach it to the other side of the core to form an upper chamber dam.

7. Pour 350 ml of running buffer into the upper buffer chamber. At this point, check the integrity of the upper buffer seal. If the buffer appears to be leaking, pour the running buffer into a beaker, remove the gel sandwich assemblies (Section 8.4), re-lubricate the gasket, and repeat steps 1–4.

### **Sample Loading**

1. Remove the clear loading lid. Wash the wells with running buffer to remove any unpolymerized gel material or denaturants in the wells.
2. Load the samples using a pipetman and a sequencing-loading tip. Be careful not to pierce the wells during sample delivery.
3. Place the clear loading lid on top of the temperature control module.

### **Running DGGE**

1. For DGGE run the gel at 130 volts. Apply power to the DCode system and begin electrophoresis. As a precaution, always set the voltage, current, and power limits when possible. Note: The voltage should not exceed 180 V otherwise electrophoretic heating may affect results.
2. The run time should be determined empirically for each fragment being analyzed. As a

reference during electrophoresis, two marker dyes in the 2x gel loading dye can be used to determine when to stop a DGGE run. The dyes are bromophenol blue (dark blue) and Xylene cyanol (light blue).

### **Removing the Gel**

1. After electrophoresis is complete, turn the power supply and system (heater, pump, and power) off. Disconnect the power cord and electrical leads. Allow the heater to cool for approximately 1 minute in the buffer.

2. Remove the temperature control module and place it on the DCode lid stand.

Caution: The heater is still hot. Do not touch. Carefully pull the core out of the electrophoresis tank. Pour off the upper buffer into the tank by tilting the core above and over the chamber.

3. Lay the core and gel sandwiches on a padded surface to absorb buffer spills.

a. For 16 x 10 cm and 7.5 x 10 cm gels, remove the sandwich assembly with your thumb, pushing on the latches on the core outward and your index finger pushing on the sandwich clamp. Pull the sandwich assembly off the locating pins on the top of the core.

b. For 16 x 16 cm and 16 x 20 cm gels, remove the sandwich assembly with your index fingers below the sandwich clamps and your thumbs resting on the latches on the core.

Gently remove the assembly by pulling up (in a manner opposite to the way it was attached). Pull the sandwich assembly off the locating pins on the top of the core.

4. Loosen the single screw of each clamp and remove the clamps from the sandwich.

Carefully pry off the shorter glass plate. Do not use a metal spatula to remove the glass

plate. This may chip or crack the plate.

5. Remove the spacers and cut one corner of the gel to distinguish between gels.

Note: If different buffers are used between runs it is advisable to rinse the pump with distilled water. Place the DCode module on the DCode stand. Fill a 500 ml beaker with distilled water and place it under the pump inlet tube. Place an empty beaker under the pump outlet tube. Turn the pump on for 1–2 minutes.

### **Staining and Photographing the DGGE Gel**

1. Remove the gel from the glass plate.

2. Place the gel into a dish containing 250 ml of running buffer and 25  $\mu$ l of 10 mg/ml ethidium bromide (50  $\mu$ g/ml). Stain for 5–15 minutes.

2. After staining, carefully transfer the gel into a dish containing 250 ml of 1x running buffer. Destain for 5–20 minutes.

3. Place the gel on a UV transilluminator and photograph.

### **Reference:**

Instruction Manual of Bio-Rad Dcode Universal Mutation Detection System.

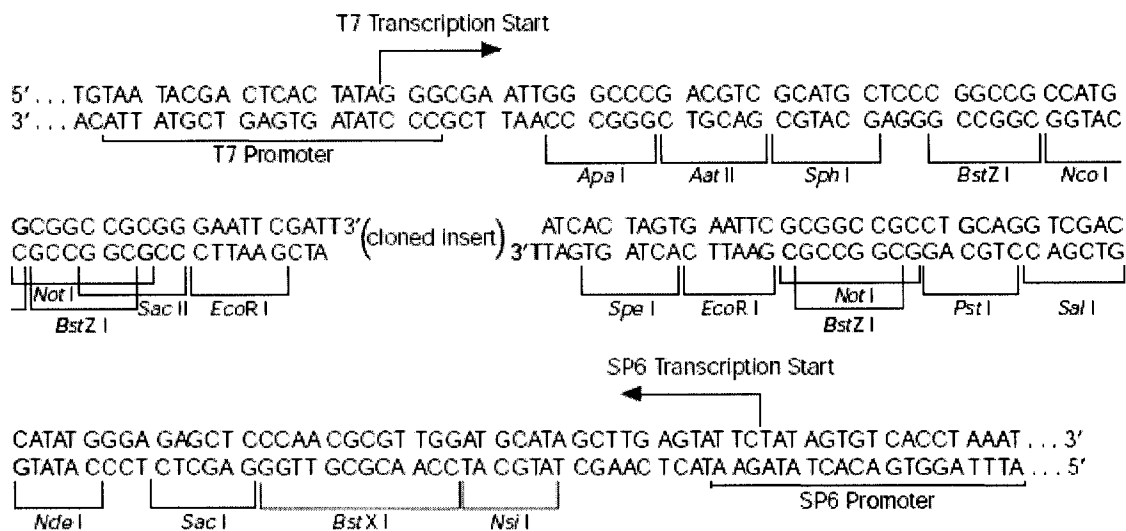
## **Appendix H: DNA Gel Purification Protocol with Bio-Rad Quantum Prep™ ‘N Squeeze DNA Gel Extraction Spin Columns**

1. Electrophorese the DNA sample in an agarose gel or polyacrylamide gel, then stain with an appropriate reagent, e.g., ethidium bromide or SYBR Green I.
2. Using a clean razor blade, carefully excise the band of interest. Trim excess agarose or polyacrylamide from all six sides of the DNA band to maximize recovery and purity.
3. Chop the trimmed gel slice and place the pieces into the filter cup of the Quantum Prep Freeze ‘N Squeeze DNA Gel Extraction Spin Column. Place the filter cup into the dolphin tube. If the volume of your trimmed gel slice is too great to fit into one filter cup, then use two or more and pool the recovered samples at the end of the protocol.
4. Place the Quantum Prep Freeze ‘N Squeeze DNA Gel Extraction Spin Column (filter cup nested within dolphin tube) in a -20° C freezer for 5 minutes.
5. Spin the sample at 13,000 x g for 3 minutes at room temperature.
6. Collect the purified DNA from the collection tube; the agarose or polyacrylamide debris will be retained within the filter cup of the Quantum Prep Freeze ‘N Squeeze DNA Gel Extraction Spin Column. The DNA is ready to use for PCR, ligations, labeling or other enzymatic reactions.

### **Reference:**

The Protocol of Bio-Rad Quantum Prep™ ‘N Squeeze DNA Gel Extraction Spin Columns.

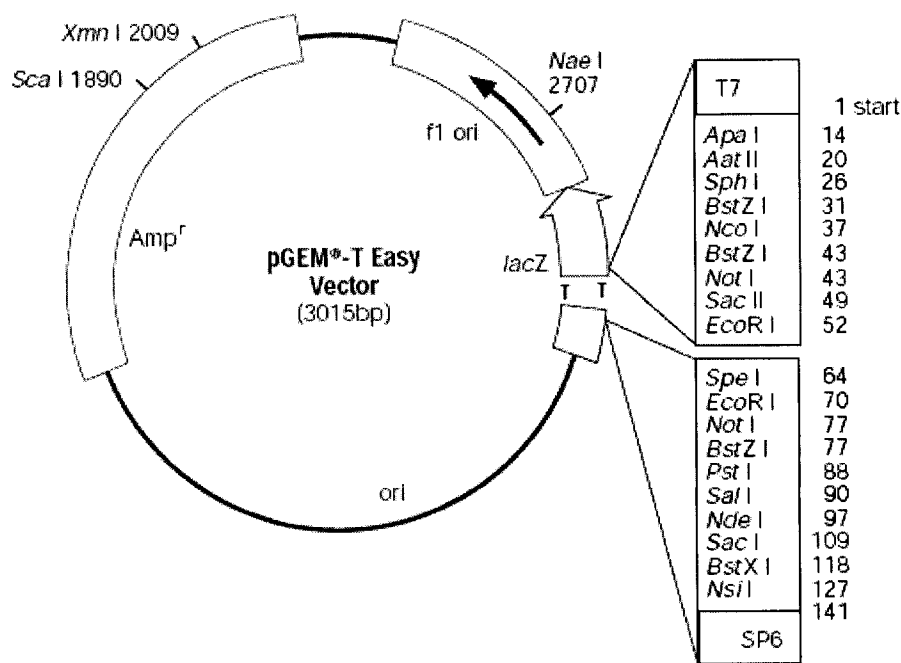
## Appendix I: pGEM-T Easy Vector Multiple Cloning Sequences



### Reference:

Technical Manual No. 42 for Promega pGEM-T and pGEM-T Easy Vector Systems.

## Appendix J: pGEM-T Easy Vector Map and Sequence Reference Points



### pGEM<sup>®</sup>-T Easy Vector sequence reference points:

T7 RNA polymerase transcription initiation site	1
multiple cloning region	10–128
SP6 RNA polymerase promoter (–17 to +3)	139–158
SP6 RNA polymerase transcription initiation site	141
pUC/M13 Reverse Sequencing Primer binding site	176–197
<i>lacZ</i> start codon	180
<i>lac</i> operator	200–216
$\beta$ -lactamase coding region	1337–2197
phage f1 region	2380–2835
<i>lac</i> operon sequences	2836–2996, 166–395
pUC/M13 Forward Sequencing Primer binding site	2949–2972
T7 RNA polymerase promoter (–17 to +3)	2999–3

### Reference:

Technical Manual No. 42 for Promega pGEM-T and pGEM-T Easy Vector Systems.

### Appendix K: Protocol for Ligations Using the pGEM®-T Easy Vectors

1. Briefly centrifuge pGEM®-T Easy Vector and Control Insert DNA tubes to collect contents at the bottom of the tubes.
2. Set up ligation reactions as described below.
3. Vortex the 2X Rapid Ligation Buffer vigorously before each use.

	Standard Reaction	Positive Control	Background Control
2X Rapid Ligation Buffer, T4 DNA Ligase	5µl	5µl	5µl
pGEM®-T or pGEM®-T Easy Vector (50ng)	1µl	1µl	1µl
PCR product	Xµl*	–	–
Control Insert DNA	–	2µl	–
T4 DNA Ligase (3 Weiss units/µl)	1µl	1µl	1µl
deionized water to a final volume of	10µl	10µl	10µl

4. Incubate the reactions overnight at 4°C.

Notes: 1. Use only Promega T4 DNA Ligase supplied with this system in performing pGEM®-T Easy Vector ligations. Other commercial preparations of T4 DNA ligase may contain exonuclease activities that may remove the terminal deoxythymidines from the vector. 2. 2X Rapid Ligation Buffer contains ATP, which degrades during temperature fluctuations. Avoid multiple freeze-thaw cycles and exposure to frequent temperature changes by making single-use aliquots of the buffer. 3. It is important to vortex the 2X Rapid Ligation Buffer before each use. 4. Longer incubation times will increase the number of transformants. Generally, incubation overnight at 4°C will produce the maximum number of transformants.

#### Reference:

Technical Manual No. 42 for Promega pGEM-T and pGEM-T Easy Vector Systems.

### **Appendix L: Protocol for Transformation Using pGEM®-T Easy Vector Ligation Reactions**

1. Prepare 2 LB/ampicillin/IPTG/X-Gal plates for each ligation reaction, plus two plates for determining transformation efficiency. Equilibrate the plates to room temperature prior to plating.
2. Centrifuge the tubes containing the ligation reactions to collect contents at the bottom of the tube. Add 2 $\mu$ l of each ligation reaction to a sterile 1.5ml microcentrifuge tube on ice. Set up another tube on ice with 0.1ng uncut plasmid for determination of the transformation efficiency of the competent cells.
3. Remove tube(s) of frozen JM109 High Efficiency Competent Cells from -70°C storage and place in an ice bath until just thawed (about 5 minutes). Mix the cells by gently flicking the tube.
4. Carefully transfer 50 $\mu$ l of cells into each tube prepared in Step 2 (100 $\mu$ l cells for determination of transformation efficiency).
5. Gently flick the tubes to mix and place them on ice for 20 minutes.
6. Heat-shock the cells for 45–50 seconds in a water bath at exactly 42°C (Do Not Shake).
7. Immediately return the tubes to ice for 2 minutes.
8. Add 950 $\mu$ l room temperature SOC medium to the tubes containing cells transformed with ligation reactions and 900 $\mu$ l to the tube containing cells transformed with uncut plasmid.
9. Incubate for 1.5 hours at 37°C with shaking (~150rpm).



10. Plate 100 $\mu$ l of each transformation culture onto duplicate LB/ampicillin/IPTG/X-Gal plates. For the transformation control, a 1:10 dilution with SOC medium is recommended for plating. If a higher number of colonies is desired, the cells may be pelleted by centrifugation at 1,000  $\times$  g for 10 minutes, resuspended in 200 $\mu$ l of SOC medium, and 100 $\mu$ l plated on each of 2 plates.

11. Incubate the plates overnight (16–24 hours) at 37°C. Longer incubations or storage of plates at 4°C (after 37°C overnight incubation) may be used to facilitate blue color development. White colonies generally contain inserts.

Notes: Colonies containing  $\beta$ -galactosidase activity may grow poorly relative to cells lacking this activity. After overnight growth, the blue colonies may be smaller than the white colonies, which are approximately one millimeter in diameter.

**Reference:**

Technical Manual No. 42 for Promega pGEM-T and pGEM-T Easy Vector Systems.

**Appendix M: Plasmid Purification with Promega Vac-Man Laboratory Vacuum  
Manifold and Wizard Plus Minipreps DNA Purification System**

1. Pellet 3–5ml of cells by centrifugation at  $10,000 \times g$  for 10 minutes. Pour off the supernatant and blot the tube upside-down on a paper towel to remove excess media.
2. Completely resuspend the cell pellet in  $300\mu\text{l}$  of Cell Resuspension Solution. Transfer the resuspended cells to a 1.5ml microcentrifuge tube.
3. Add  $300\mu\text{l}$  of Cell Lysis Solution and mix by inverting the tube 4 times. The cell suspension should clear immediately.
4. Add  $300\mu\text{l}$  of Neutralization Solution and mix by inverting the tube several times.
5. Centrifuge the lysate at  $10,000 \times g$  in a microcentrifuge for 5 minutes. If a pellet has not formed by the end of the centrifugation, centrifuge an additional 15 minutes.
6. Pipet 1ml of the resuspended resin into each barrel of the Minicolumn/syringe assembly.
7. Carefully remove all of the cleared lysate from each miniprep and transfer it to the barrel of the Minicolumn/syringe assembly containing the resin. No mixing is required.
8. Open the stopcocks and apply a vacuum of at least 15 inches of Hg to pull the resin/lysate mix into the Minicolumn. When all of the sample has completely passed through the column, break the vacuum at the source. Apply a vacuum and continue it for 30 seconds after all of the solution has flowed through the columns. Note that this solution will flow through the column more slowly than the standard Column Wash Solution.

9. Add 2ml of the Column Wash Solution to the Syringe Barrel and reapply the vacuum to draw the solution through the Minicolumn.
10. Dry the resin by continuing to draw a vacuum for 30 seconds after the solution has been pulled through the column. Do not dry the resin for more than 30 seconds. Remove the Syringe Barrel and transfer the Minicolumn to a 1.5ml microcentrifuge tube. Centrifuge the Minicolumn at  $10,000 \times g$  in a microcentrifuge for 2 minutes to remove any residual Column Wash Solution.
11. Transfer the Minicolumn to a new microcentrifuge tube. Add  $50\mu\text{l}$  of nuclease-free water to the Minicolumn and wait 1 minute. Centrifuge the tube at  $10,000 \times g$  in a microcentrifuge for 20 seconds to elute the DNA. The DNA will remain intact on the Minicolumn for up to 30 minutes; however, prompt elution will minimize nicking of plasmids in the range of 20kb.
12. Remove and discard the Minicolumn. Follow these storage recommendations: DNA is stable in water without addition of buffer if stored at  $-20^{\circ}\text{C}$  or below. DNA is stable at  $4^{\circ}\text{C}$  in TE buffer. To store the DNA in TE buffer, add  $5\mu\text{l}$  of 10X TE buffer to the  $50\mu\text{l}$  of eluted DNA.

**Reference:**

Technical Bulletin No. 114 for Promega Wizard *Plus* Minipreps DNA Purification System.

**Appendix N: Protocol for Culturability Experiment 1**

1. Fire all the glassware and wash culture tube caps with 10% HCL.
2. Take 8 L soak water from Harding Lake.
3. Soak 70 culture tubes and ten 0.2  $\mu\text{m}$  polyester filters.
4. Autoclave these filters for 40 minutes.
5. Store them at 5°C after cooling down.
6. Take 8 L of Harding Lake water for preparing medium with glass sampler.
7. Put 250  $\mu\text{l}$  of 37% formalin filtered with 0.22  $\mu\text{m}$  Millex-GP filter into three 20 ml of Harding Lake water.
8. Examine the cell count with flow cytometer when convenient.
9. Filter 4 L of Harding Lake water with GF/B glass microfibre filters.
10. Filter the filtrate with autoclaved 0.2  $\mu\text{m}$  polyester filters.
11. Pour out soak water from 62 culture tubes.
12. Rinse them with the filtered filtrate.
13. Add 50 ml of the filtrate to each of the 62 culture tubes.
14. Autoclave them for 40 minutes.
15. Store them at 5°C after cooling down.
16. Take 4 L of Harding Lake water for inoculums on April 9, 2002.
17. Check the cell count with epifluorescence microscope.
18. Calculate the cell count:  $(\# / 10,000 \mu\text{m}^2 / 2) (\pi r^2 / 3 \text{ ml})$ . The concentration is  $2.79 \times 10^6$  cells/ml.

19. Put 250  $\mu\text{l}$  of 37% formalin filtered with 0.22  $\mu\text{m}$  Millex-GP filter into three 20 ml of Harding Lake water.

20. Examine the cell count with flow cytometer when convenient.

21. Dilute the Harding Lake water to get inoculums. The concentration of the field sample is  $2.79 \times 10^6$  cells/ml. Accurately transfer 1 ml of the field sample into a 18 ml glass test tube with a 1 ml graduated pipette. Then accurately add 9 ml of the medium to it with a 1 ml graduated pipette and mix it. The concentration is 2790 cells/10  $\mu\text{l}$ . Accurately transfer 1 ml of the field sample into the second 18 ml glass test tube with a 1 ml graduated pipette. Then accurately add 9 ml of the medium to it with a 1 ml graduated pipette and mix it. The concentration is 279 cells/10  $\mu\text{l}$ . Accurately transfer 1 ml of the field sample into the third 18 ml glass test tube with a 1 ml graduated pipette. Then accurately add 9 ml of the medium to it with a 1 ml graduated pipette and mix it. The concentration is 27.9 cells/10  $\mu\text{l}$ . Accurately transfer 1 ml of the field sample into the fourth 18 ml glass test tube with a 1 ml graduated pipette. Then accurately add 9 ml of the medium to it with a 1 ml graduated pipette and mix it. The concentration is 2.79 cells/10  $\mu\text{l}$ . So we have the 4 diluted samples and the concentrations are 2790 cells/10  $\mu\text{l}$ , 279 cells/10  $\mu\text{l}$ , 27.9 cells/10  $\mu\text{l}$ , and 2.79 cells/10  $\mu\text{l}$  respectively.

22. Sterilely put the right number of cells from these diluted samples into the 60 culture tubes to acquire inoculums. First, using 10  $\mu\text{l}$  micropipettes, accurately transfer 2  $\times$  10  $\mu\text{l}$  of the diluted sample (2.79 cells/10  $\mu\text{l}$ ) into 10 culture tubes containing 50 ml of the medium respectively. With 10  $\mu\text{l}$  micropipettes, accurately transfer 10  $\mu\text{l}$  of the diluted sample (27.9 cells/10  $\mu\text{l}$ ) into 10 culture tubes containing 50 ml of the medium

respectively. Using 25  $\mu\text{l}$  micropipettes, accurately transfer 25  $\mu\text{l}$  of the diluted sample (27.9 cells/10  $\mu\text{l}$ ) into 10 culture tubes containing 50 ml of the medium respectively.

With 25  $\mu\text{l}$  micropipettes, accurately transfer 3x25  $\mu\text{l}$  of the diluted sample (27.9 cells/10  $\mu\text{l}$ ) into 10 culture tubes containing 50 ml of the medium respectively. With 10  $\mu\text{l}$  micropipettes, accurately transfer 2x10  $\mu\text{l}$  of the diluted sample (279 cells/10  $\mu\text{l}$ ) into 10 culture tubes containing 50 ml of the medium respectively. Lastly, use the last 10 culture tubes containing 50 ml of the medium without bacteria as control. Please see the table below:

2 x 10  $\mu\text{l}$  (2.79 cells/10  $\mu\text{l}$ ) --- 5.58 cells

10  $\mu\text{l}$  (27.9 cells/10  $\mu\text{l}$ ) --- 27.9 cells

25  $\mu\text{l}$  (27.9 cells/10  $\mu\text{l}$ ) --- 69.75 cells

3 x 25  $\mu\text{l}$  (27.9 cells/10  $\mu\text{l}$ ) --- 209.25 cells

2 x 10  $\mu\text{l}$  (279 cells/10  $\mu\text{l}$ ) --- 558 cells

23. After growing the 60 cultures at 5°C for 4 weeks, put 25  $\mu\text{l}$  of 37% formalin filtered with 0.22 micron Millex-GP filter into 2 ml of each culture in 4 ml vial respectively on May 21, 2002.

24. Check positive or negative with flow cytometer and epifluorescence microscope when convenient.

25. If positive, determine the species number of bacteria with TRFLP.

### Appendix O: Protocol for Culturability Experiment 2

1. Fire all the glassware and wash culture tube caps with 10% HCL.
2. Take 8 L soak water from Harding Lake.
3. Soak 70 culture tubes and ten 0.2  $\mu\text{m}$  polyester filters.
4. Autoclave these filters for 40 minutes.
5. Store them at 8°C after cooling down.
6. Take 8 L of Harding Lake water for preparing medium with glass sampler.
7. Put 250  $\mu\text{l}$  of 37% formalin filtered with 0.22  $\mu\text{m}$  Millex-GP filter into three 20 ml of Harding Lake water.
8. Examine the cell count with flow cytometer when convenient.
9. Filter 4 L of Harding Lake water with GF/B glass microfibre filters.
10. Filter the filtrate with autoclaved 0.2  $\mu\text{m}$  polyester filters.
11. Pour out soak water from 62 culture tubes.
12. Rinse them with the filtered filtrate.
13. Add 50 ml of the filtrate to each of the 62 culture tubes.
14. Autoclave them for 40 minutes.
15. Store them at 8°C after cooling down.
16. Take 4 L of Harding Lake water for inoculums on May 17, 2002.
17. Check the cell count with epifluorescence microscope.
18. Calculate the cell count:  $(\# / 10,000 \mu\text{m}^2 / 2) (\pi r^2 / 3 \text{ ml})$ . The concentration is  $3.02 \times 10^6$  cells/ml.

19. Put 250  $\mu\text{l}$  of 37% formalin filtered with 0.22  $\mu\text{m}$  Millex-GP filter into three 20 ml of Harding Lake water.

20. Examine the cell count with flow cytometer when convenient.

21. Dilute the Harding Lake water to get inocula. The concentration of the field sample is  $3.02 \times 10^6$  cells/ml. Accurately transfer 1 ml of the field sample into a 18 ml glass test tube with a 1 ml graduated pipette. Then accurately add 9 ml of the medium to it with a 1 ml graduated pipette and mix it. The concentration is 3020 cells/10  $\mu\text{l}$ . Accurately transfer 1 ml of the field sample into the second 18 ml glass test tube with a 1 ml graduated pipette. Then accurately add 9 ml of the medium to it with a 1 ml graduated pipette and mix it. The concentration is 302 cells/10  $\mu\text{l}$ . Accurately transfer 1 ml of the field sample into the third 18 ml glass test tube with a 1 ml graduated pipette. Then accurately add 9 ml of the medium to it with a 1 ml graduated pipette and mix it. The concentration is 30.2 cells/10  $\mu\text{l}$ . Accurately transfer 1 ml of the field sample into the fourth 18 ml glass test tube with a 1 ml graduated pipette. Then accurately add 9 ml of the medium to it with a 1 ml graduated pipette and mix it. The concentration is 3.02 cells/10  $\mu\text{l}$ . So we have the 4 diluted samples and the concentrations are 3020 cells/10  $\mu\text{l}$ , 302 cells/10  $\mu\text{l}$ , 30.2 cells/10  $\mu\text{l}$ , and 3.02 cells/10  $\mu\text{l}$  respectively.

22. Sterilely put the right number of cells from these diluted samples into the 60 culture tubes to acquire inoculums. First, using 10  $\mu\text{l}$  micropipettes, accurately transfer 2  $\times$  10  $\mu\text{l}$  of the diluted sample (3.02 cells/10  $\mu\text{l}$ ) into 10 culture tubes containing 50 ml of the medium respectively. With 10  $\mu\text{l}$  micropipettes, accurately transfer 10  $\mu\text{l}$  of the diluted sample (30.2 cells/10  $\mu\text{l}$ ) into 10 culture tubes containing 50 ml of the medium



respectively. Using 25  $\mu\text{l}$  micropipettes, accurately transfer 25  $\mu\text{l}$  of the diluted sample (30.2 cells/10  $\mu\text{l}$ ) into 10 culture tubes containing 50 ml of the medium respectively.

With 25  $\mu\text{l}$  micropipettes, accurately transfer 3x25  $\mu\text{l}$  of the diluted sample (30.2 cells/10  $\mu\text{l}$ ) into 10 culture tubes containing 50 ml of the medium respectively. With 10  $\mu\text{l}$  micropipettes, accurately transfer 2x10  $\mu\text{l}$  of the diluted sample (302 cells/10  $\mu\text{l}$ ) into 10 culture tubes containing 50 ml of the medium respectively. Lastly, use the last 10 culture tubes containing 50 ml of the medium without bacteria as control. Please see the table below:

2 x 10  $\mu\text{l}$  (3.02 cells/10  $\mu\text{l}$ ) --- 6.04 cells

10  $\mu\text{l}$  (30.2 cells/10  $\mu\text{l}$ ) --- 30.2 cells

25  $\mu\text{l}$  (30.2 cells/10  $\mu\text{l}$ ) --- 75.5 cells

3 x 25  $\mu\text{l}$  (30.2 cells/10  $\mu\text{l}$ ) --- 226.5 cells

2 x 10  $\mu\text{l}$  (302 cells/10  $\mu\text{l}$ ) --- 604 cells

23. After growing the 60 cultures at 8 °C for 4 weeks, put 25  $\mu\text{l}$  of 37% formalin filtered with 0.22 micron Millex-GP filter into 2 ml of each culture in 4 ml vial respectively on June 17, 2002.

24. Check positive or negative with flow cytometer and epifluorescence microscope when convenient.

25. If positive, determine the species number of bacteria with TRFLP.

**Appendix P: Protocol for Culturability Experiment 3 with Species Distribution**

1. Fire all the glassware.
2. Take 8 L soak water from Harding Lake.
3. Soak 120 culture tubes and fourteen 0.2  $\mu\text{m}$  polyester filters.
4. Autoclave these filters for 40 minutes.
5. Store them at 12°C after cooling down.
6. Take 8 L of Harding Lake water for preparing medium with glass sampler.
7. Put 250  $\mu\text{l}$  of 37% formalin filtered with 0.22  $\mu\text{m}$  Millex-GP filter into two 20 ml of Harding Lake water.
8. Examine the cell count with flow cytometer when convenient.
9. Filter 8 L of Harding Lake water with GF/B glass microfibre filters.
10. Filter the filtrate with autoclaved 0.2  $\mu\text{m}$  polyester filters.
11. Pour out soak water from 120 culture tubes.
12. Rinse them with the filtered filtrate.
13. Add 50 ml of the filtrate to each of the 120 culture tubes.
14. Autoclave them for 40 minutes.
15. Make the mixture of glucose and amino acid at 0.5  $\mu\text{g}$ , 1.25  $\mu\text{g}$ , 2.5  $\mu\text{g}$ , 5.0  $\mu\text{g}/\text{ml}$  and put them into 4x120 tubes respectively and autoclave them.
16. Store them at 12°C after cooling down.
16. Take 4 L of Harding Lake water for inoculums on Oct. 11, 2004.
17. Check the cell count with epifluorescence microscope.

18. Calculate the cell count:  $(\# / 10,000 \mu\text{m}^2 / 2) (\pi r^2 / 3 \text{ ml})$ . The concentration is 3.14 cells/ml.

19. Put 250  $\mu\text{l}$  of 37% formalin filtered with 0.22  $\mu\text{m}$  Millex-GP filter into 220 ml of Harding Lake water.

20. Examine the cell count with flow cytometer when convenient.

21. Dilute the Harding Lake water to get inoculums. The concentration of the field sample is  $3.03 \times 10^6$  cells/ml. Accurately transfer 1 ml of the field sample into a 18 ml glass test tube with a 1 ml graduated pipette. Then accurately add 9 ml of the medium to it with a 1 ml graduated pipette and mix it. The concentration is 3030 cells/10  $\mu\text{l}$ . Accurately transfer 1 ml of the field sample into the second 18 ml glass test tube with a 1 ml graduated pipette. Then accurately add 9 ml of the medium to it with a 1 ml graduated pipette and mix it. The concentration is 303 cells/10  $\mu\text{l}$ . Accurately transfer 1 ml of the field sample into the third 18 ml glass test tube with a 1 ml graduated pipette. Then accurately add 9 ml of the medium to it with a 1 ml graduated pipette and mix it. The concentration is 30.3 cells/10  $\mu\text{l}$ . Accurately transfer 1 ml of the field sample into the fourth 18 ml glass test tube with a 1 ml graduated pipette. Then accurately add 9 ml of the medium to it with a 1 ml graduated pipette and mix it. The concentration is 3.03 cells/10  $\mu\text{l}$ . So we have the 4 diluted samples and the concentrations are 3030 cells/10  $\mu\text{l}$ , 303 cells/10  $\mu\text{l}$ , 30.3 cells/10  $\mu\text{l}$ , and 3.03 cells/10  $\mu\text{l}$  respectively.

22. Put the right number of cells from these diluted samples into the 120 culture tubes to acquire inoculums. The 60 culture tubes are prepared for glucose and amino acid mixture addition and the other 60 culture tubes for without substrate addition. The final

concentration of the substrate mixture is 5  $\mu\text{g/L}$  (0.25  $\mu\text{g}/50\text{ml}$ ). First, using 10  $\mu\text{l}$  micropipettes, accurately transfer 2x10  $\mu\text{l}$  of the diluted sample (3.03 cells/10  $\mu\text{l}$ ) into 10 culture tubes containing 50 ml of the medium respectively. Using 25  $\mu\text{l}$  micropipettes, accurately transfer 25  $\mu\text{l}$  of the diluted sample (30.3 cells/10  $\mu\text{l}$ ) into 10 culture tubes containing 50 ml of the medium respectively. With 25  $\mu\text{l}$  micropipettes, accurately transfer 3x25  $\mu\text{l}$  of the diluted sample (30.3 cells/10  $\mu\text{l}$ ) into 10 culture tubes containing 50 ml of the medium respectively. With 10  $\mu\text{l}$  micropipettes, accurately transfer 2x10  $\mu\text{l}$  of the diluted sample (303 cells/10  $\mu\text{l}$ ) into 10 culture tubes containing 50 ml of the medium respectively. Lastly, use the last 10 culture tubes containing 50 ml of the medium without bacteria as control. Please see the table below:

2 x 10  $\mu\text{l}$  (1.6 cells/10  $\mu\text{l}$ ) --- 3.2 cells

25  $\mu\text{l}$  (16.0 cells/10  $\mu\text{l}$ ) --- 40 cells

3 x 25  $\mu\text{l}$  (30.3 cells/10  $\mu\text{l}$ ) --- 120 cells

2 x 10  $\mu\text{l}$  (303 cells/10  $\mu\text{l}$ ) --- 320 cells

23. During incubation, add the four different concentrations of the glucose and amino acid mixture into the cultures at day 1, day 7, day 14, and day 21 respectively. After growing the 120 cultures at 12°C for 4 weeks, put 25  $\mu\text{l}$  of 37% formalin filtered with 0.22  $\mu\text{m}$  Millex-GP filter into 2 ml of each culture in 4 ml vial respectively on Nov. 5, 2004. The population is  $3.3 \times 10^6$  cells/ml by the flow cytometer.

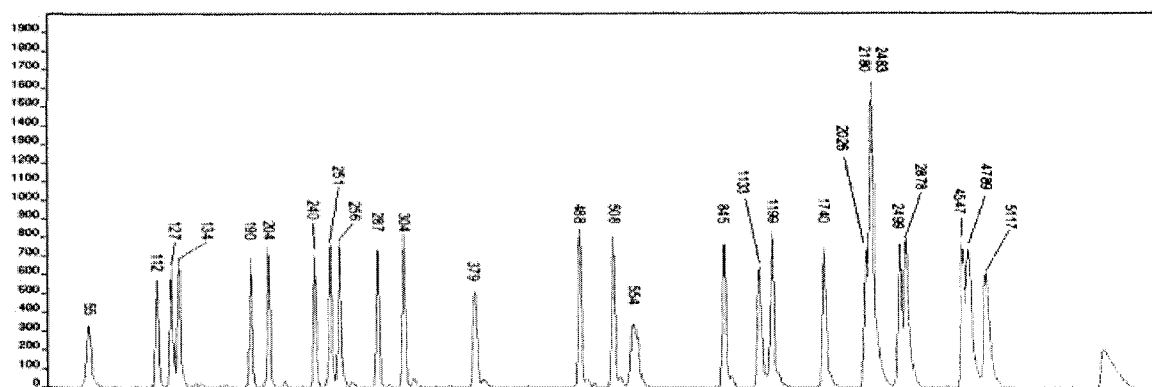
24. Check positive or negative with flow cytometer and epifluorescence microscope when convenient.

25.If positive, determine the species number of bacteria with TRFLP.

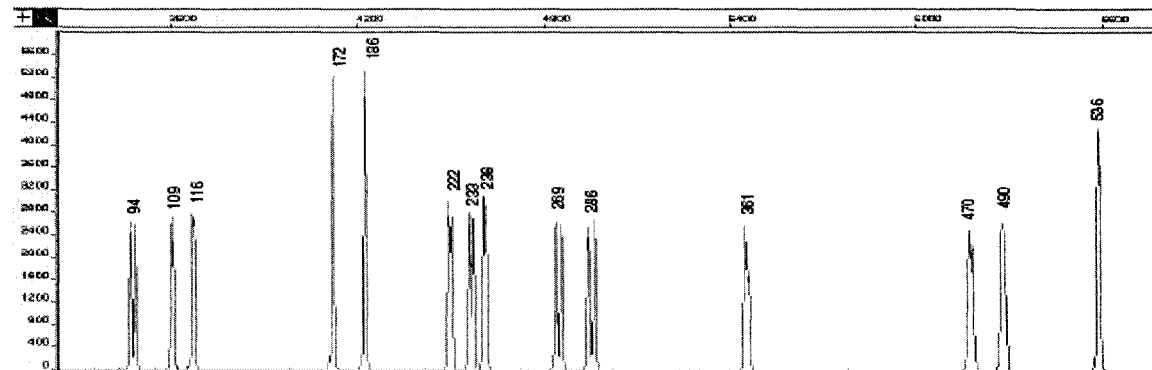
26.Identify the bacteria by recombinant DNA technique.

**Appendix Q: ABI Internal DNA Standard GeneScan TAMRA 2500 and GeneScan  
ROX 2500**

1. GeneScan TAMRA 2500:

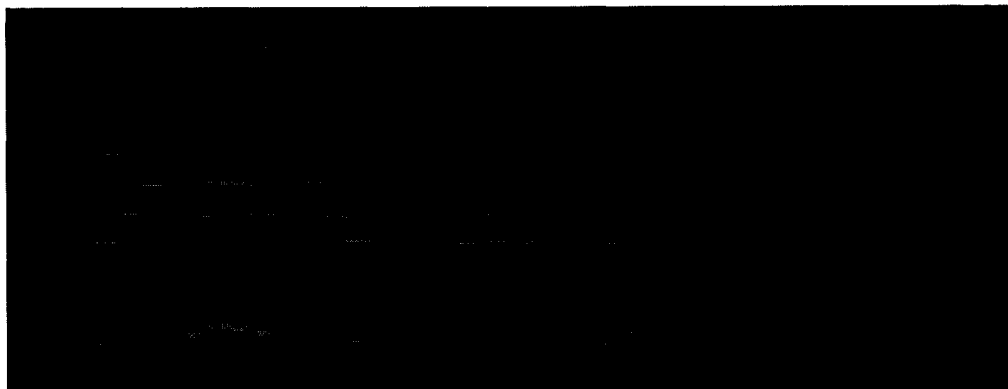


2. GeneScan ROX 2500:



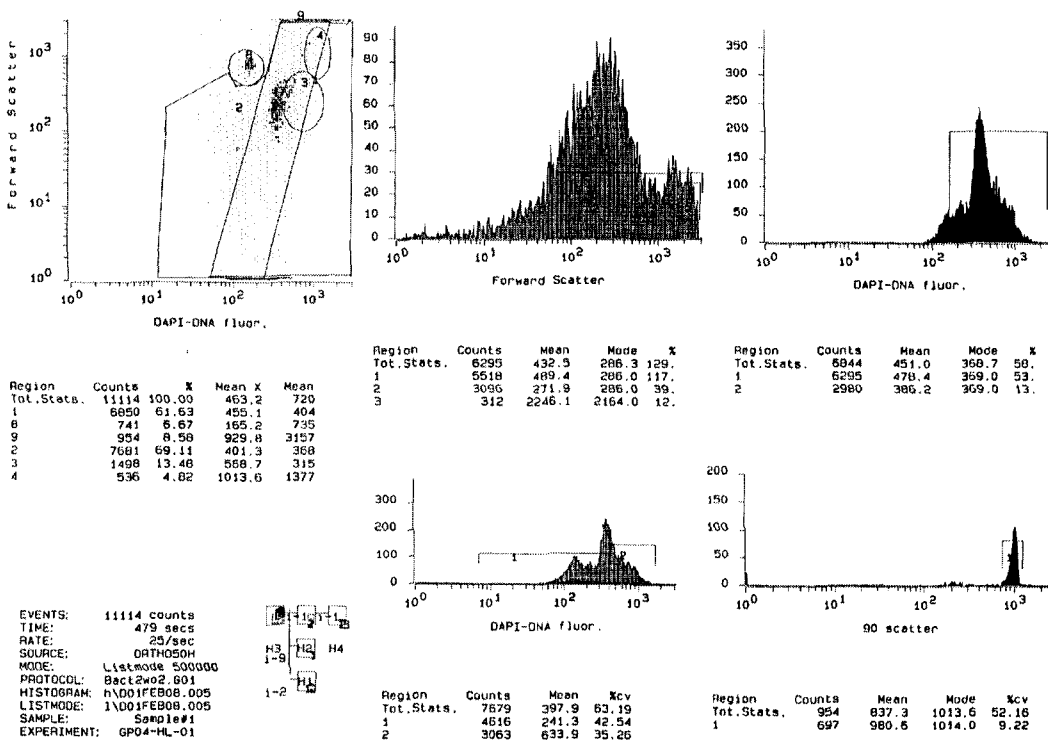
**Reference:**

Applied Biosystems GeneScan Reference Guide.

**Appendix R: The Image from ABI 373XL DNA Sequencer**

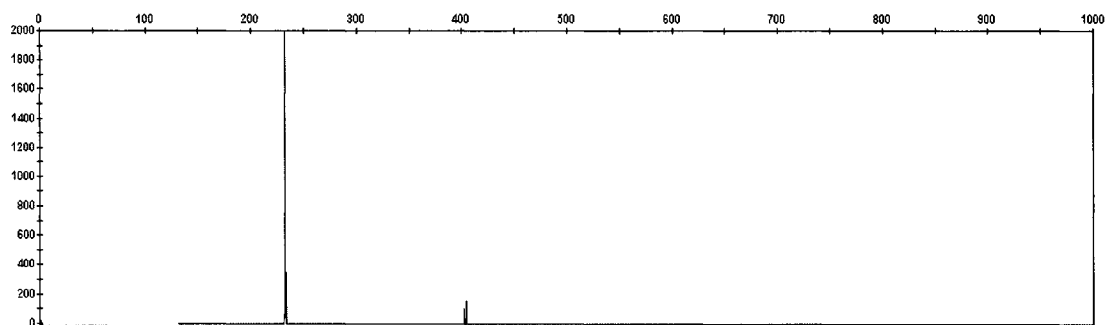
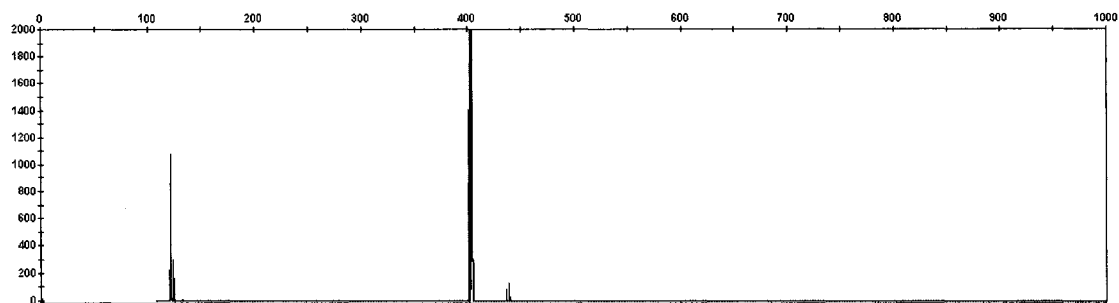
Note: Fainter bands-internal DNA standard; brighter bands-sample DNA.

### Appendix S: Flow Cytometry Cytographs of Positive Dilution Culture





**Appendix T: Electropherograms of the 5' T-RFLP of *Msp* I-digested bacterial 16S  
rDNAs from Positive Dilution Cultures**



**Appendix U: The Quantification of Some Purified Recombinant Plasmid DNA by  
NanoDrop ND-1000 Spectrophotometer**

Sample ID	Date	Time	ng/ul	260/280
	4/21/2005	11:00 AM	0.00	NaN
water	4/21/2005	11:01 AM	-0.24	0.48
1	4/21/2005	11:02 AM	124.10	1.91
2	4/21/2005	11:04 AM	397.29	1.92
3	4/21/2005	11:07 AM	296.40	1.94
4	4/21/2005	11:08 AM	283.13	1.93
5	4/21/2005	11:09 AM	173.15	1.91
6	4/21/2005	11:10 AM	288.46	1.92
7	4/21/2005	11:12 AM	271.25	1.94
water	4/21/2005	11:13 AM	-0.01	-0.02
	4/21/2005	11:21 AM	0.00	NaN
water	4/21/2005	11:21 AM	0.27	0.71
8	4/21/2005	11:22 AM	NaN	NaN
8	4/21/2005	11:23 AM	233.76	1.92
9	4/21/2005	11:24 AM	263.90	1.92
10	4/21/2005	11:25 AM	152.16	1.94
11	4/21/2005	11:26 AM	365.78	1.92
12	4/21/2005	11:27 AM	226.42	1.95
13	4/21/2005	11:29 AM	363.02	1.92
14	4/21/2005	11:30 AM	264.22	1.93
15	4/21/2005	11:31 AM	275.98	1.92
16	4/21/2005	11:32 AM	327.67	1.92
17	4/21/2005	11:34 AM	336.28	1.94
18	4/21/2005	11:35 AM	213.30	1.90
19	4/21/2005	11:36 AM	226.07	1.95
20	4/21/2005	11:37 AM	220.53	1.93
21	4/21/2005	11:38 AM	261.44	1.95
22	4/21/2005	11:39 AM	289.75	1.94
23	4/21/2005	11:39 AM	303.83	1.94
24	4/21/2005	11:40 AM	359.25	1.93

**Appendix V: ABI 3100 Genetic Analyzer Sequencing of Uncultured Bacterium****Clone KM94**